Fenton Oxidation Initiated by FeOCl Pre-Coat for Cleaning Persistent Gel-Like Fouling of Ceramic Nanofiltration

Lu Yao (4783859)

to be defended publicly on August 31, 2020 at 1:30 PM

TU Delft

Fenton Oxidation Initiated by FeOCl Pre-Coat for Cleaning Persistent Gel-Like Fouling of Ceramic Nanofiltration

by

Lu YAO (4783859)

in partial fulfilment of the requirements for the degree of

Master of Science
in Civil Engineering

at the Delft University of Technology,
to be defended publicly on Monday August 31, 2020 at 1:30 PM.

Assessment Committee:

TU Delft	Prof.dr.ir. L.C. (Luuk) Rietveld (Chair)
TU Delft	Prof. dr. Evgeny A. Pidko
TU Delft	Dr. ir. S.G.J. Heijman
TU Delft	Dr. ir. Ralph Lindeboom
TU Delft	Ir. Bin Lin

TU Delft

ABSTRACT

Ceramic nanofiltration (NF) is a newly developed technology for municipal sewage reclamation for drinking water production, agricultural and industrial utilisation, but organic fouling limits it to pilot-scale application. Herein, Fenton-based cleaning catalysed by FeOCl pre-coat was performed on ceramic NF membrane to clean persistent gel-like fouling. FeOCl pre-coating on ceramic NF membrane was conducted by pressure-driven filtration. Gel-like fouling was simulated by Ca-alginate. The compact fouling layer was proposed to impede the diffusion of H_2O_2; therefore, NaCl was introduced to perform Na-Ca ion exchange to relax the fouling layer and improve the mass transfer in Fenton-based cleaning. The cleaning efficiency of Fenton cleaning and NaCl treatment were evaluated individually, and their synergistic effect was determined by a mixture of NaCl/H_2O_2.

In pre-coating, the iron loading could be controlled by permeate flux. Moreover, the iron loading on the membrane had a linear relationship with FeOCl dosage. The pre-coated FeOCl layer slightly decreased membrane permeability (by 4%), presumably because the porous FeOCl pre-coat provided abundant channels for water permeation. NaCl pre-treatment displayed high efficiency in the removal of the reversible fouling layer, which contributed to 50% of flux decline. The FeOCl pre-coat catalysed Fenton-based cleaning, which achieved a complete flux recovery in 1 hour. The addition of tert-butanol (an ·OH scavenger) in Fenton-based cleaning system decreased the cleaning efficiency, which confirmed the participation of ·OH in Fenton-based cleaning. No remarkable synergistic effect was observed between NaCl induced fouling layer swelling and Fenton oxidation. It was likely due to the effect of turbulent flush on improving the diffusion of H_2O_2 in Fenton-based cleaning, which surpassed the effect of fouling layer swelling induced by NaCl treatment.

ACKNOWLEDGEMENTS

The two-year study life at the Delft University of Technology was the most challenging experience I have ever had in the past 24 years. I can still remember the freshness that I felt for the culture and the loneliness that I suffered from for being away from friends and family at the beginning of the study. Language has become the biggest obstacle that each lesson was like the IELTS listening test during the first month. Fortunately, I have adjusted myself to the intensive learning schedule and reached the final stage of obtaining the master's degree, MSc thesis. However, as a beginner in scientific research, I felt stressful for completing the thesis, and further challenges arose due to the unanticipated outbreak of COVID-19. In retrospect, this work would never have been done without the help of many supporters.

First and foremost, I would like to express my sincere appreciation to the assessment committee. Prof. Luuk Rietveld, as the chair of the committee, provided me with valuable suggestions in building critical thinking in data analysis and report writing. Dr. Bas Heijman extended a significant amount of assistance throughout this project in designing the experiments, analysing the experimental results, and preparing presentations. He was always supportive and helped me to explain the results in a scientific way. Prof. Evgeny Pidko, as an external member of the committee, gave me helpful advice, especially in the Fenton-related data analysis, with his extensive knowledge in catalysis. Dr. Ralph Lindeboom provided me with constructive suggestions in experimental design and gave detailed comments in report writing. I would also like to thank my daily supervisor, Bin Lin. The completion of my thesis would not have been possible without the continuous help and support of him.

I would like to extend my thanks to Armand Middeldorp and Patricia van den Bos, who have endeavoured to maintain a good and safe experimental environment under the coronavirus situation. Ruud Hendrikx at the Department of Materials Science and Engineering of the Delft University of Technology is acknowledged for the X-ray analysis. Dustin Laur at the Faculty of Applied Science of the Delft University of Technology is acknowledged for the SEM and EDS analysis.

I would also like to thank my lovely friends in Delft, who also experienced a tough time due to the outbreak of COVID-19 and MSc thesis. The warm encouragements we shared accompanied me through the past ten months, and the tasty food they served healed me from struggling with the report. Besides, many special thanks go to my boyfriend Kuisheng, who is always supportive and willing to listen to me whenever I encounter any difficulty. His encouragements always help me to rebuild my confidence.

Last but not least, I would like to express my deepest love and gratitude to my parents, who always respect my choice and support from behind. 爸爸妈妈谢谢你们，我爱你们！

I always believe that adversity brings out the best in a person. The experience in Delft is a treasure which built up my strength and would encourage me to brave the difficulties in the future.

CONTENT

LIST OF FIGURES

LIST OF TABLES

LIST OF ABBREVIATIONS

AFM	Atomic Force Microscopy
AOP	Advanced Oxidation Process
AOX	Absorbable Organic Halogen
BEOP	Biofilm-Enhanced Osmotic Pressure
BSA	Bovine Serum Albumin
CEOP	Cake-Enhanced Osmotic Pressure
DLVO	Derjaguin-Landau-Verwey-Overbeek Theory
DOM	Dissolved Organic Matter
EDL	Electrical Double Layer
EDS	Energy-Dispersive X-Ray Spectroscopy
EDTA	Ethylene Diamine Tetraacetic Acid
EPS	Extracellular Polymeric Substrate
ESR	Electron Spin Resonance
HPLC	High-Performance Liquid Chromatography
MF	Microfiltration Membrane
MWCO	Molecular Weight Cut-Off
NF	Nanofiltration Membrane
NOM	Natural Organic Matter
PA	Polyamide
PE	Polypropylene
PEG	Poly(Ethylene Glycol)
PES	Polyethersulfone
PVDF	Polyvilidenefluoride
RO	Reverse Osmosis
ROS	Reactive Oxygen Species
SDS	Sodium Dodecyl Sulphate
SEM	Scanning Electron Microscope
THM	Trihalomethane
TMP	Transmembrane Pressure
TOC	Total Organic Carbon
UF	Ultrafiltration Membrane
VDW	van der Waals
XRD	X-ray Diffraction

1 INTRODUCTION

1.1. BACKGROUND

Due to the ever-increasing water demand, municipal wastewater is proposed to be a promising alternative water source for drinking water supply, agricultural and industrial uses (Kramer et al. 2020, Rietveld et al. 2011). Ceramic nanofiltration (NF) has emerged as an attractive new technology for water reclamation, given its superior separation capability upon various organic molecules and small colloids (Shams Ashaghi et al. 2007, Weber et al. 2003). Besides, it displays outstanding robustness in harsh chemical, thermal and mechanical conditions (Lee et al. 2013, Shams Ashaghi et al. 2007, Weber et al. 2003). With the breakthrough of the manufacturing technology, ceramic NF membrane with good quality has been commercially available (Fujioka et al., 2014). However, organic fouling is a major obstacle that limits the up-scaling application of ceramic NF membrane in wastewater reuse. Extracellular polymeric substrate (EPS) in municipal sewage is of high fouling tendency due to its sticky nature and high gelling property, which contributes remarkably to the organic fouling of ceramic NF membrane (Kramer et al. 2020).

Appropriate membrane cleaning strategies are necessary to remove the attached fouling layer and restore membrane permeability. Generally, membrane cleaning is classified into physical and chemical cleaning (Wang et al. 2014, Zhao et al. 2000). Physical cleaning, such as backwash and forward flush, aims at detaching the reversible fouling layer. The backwash is inapplicable to the ceramic NF membrane due to the low permeability of the NF membrane and the potential physical damage to the end-sealing of the ceramic membrane at high transmembrane pressure (TMP). The forward flush is ineffective in removing the sticky gel-like fouling layer (Chang and Judd 2002, Huang et al. 2008, Soesanto et al. 2019). Chemical cleaning by acid, base and/or hypochlorite is frequently required (Wang et al. 2014), which leads to large consumption of chemicals and deteriorates the integrity and life span of the membrane. Furthermore, the consequent oxidation by-products and the overdosage of chemicals might cause secondary pollution (Wang et al. 2014). Hence, a green and efficient cleaning strategy without deteriorating membrane integrity and the environment is urged to be explored.

Fenton oxidation is an advanced oxidation process (AOP) in which Fenton(like) catalyst decomposes H_2O_2 and generates nonselective, highly reactive radicals, i.e. hydroxyl radicals (·OH). It is environmentally friendly and harmless to membrane integrity. Iron-based catalysts outstand due to their high catalytic activity, accessibility, recyclability and low toxicity (He et al. 2016). Iron oxychloride (FeOCl) is a novel, heterogeneous Fenton-like catalyst that performs exceptional Fenton activity and catalytic durability (Yang et al. 2013, Zhang et al. 2017). Sun et al. (2018) performed bovine serum albumin (BSA) fouling and Fenton-based cleaning on FeOCl immobilised polymeric UF membranes. The almost complete flux recovery confirmed the high efficiency of the membrane-based FeOCl catalysed Fenton oxidative cleaning. However, the FeOCl catalysed Fenton oxidation for cleaning persistent gel-like fouling

of ceramic NF membrane is still lack of knowledge, regarding the approaches for coating Fenton catalysts on ceramic NF membranes and the efficiency and influencing factors of Fenton-based cleaning on the membrane surface. Besides, preliminary experiments in our lab proposed the hindrance of mass transfer by the compact gel-like fouling layer. Lee and Elimelech (2007) applied salt cleaning on polymeric RO membrane fouled by Ca-alginate to clean the gel-like fouling layer via salt-Ca ion exchange. Nevertheless, no previous study has investigated the synergistic effect between NaCl and Fenton oxidation for persistent gel-like fouling of ceramic NF membrane.

In this study, the FeOCl particles were deposited onto the membrane surface by a pressure-driven filtration. Sodium alginate, a kind of polysaccharide, was selected as the model organic foulant to mimic EPS in municipal sewage. Calcium ions were dosed to the fouling solution to enhance membrane fouling by forming interchain among alginate molecules and ceramic NF membrane (Lee et al. 2006a, You et al. 2020). The efficiency of NaCl pre-treatment and Fenton-based cleaning for persistent gel-like fouling of ceramic NF membrane were investigated respectively, and the synergistic effect between NaCl and Fenton oxidation were examined by a mixture of NaCl/H_2O_2.

1.2. KNOWLEDGE GAPS AND RESEARCH OBJECTIVES

Based on state of the art demonstrated in *Section 1.1*, several knowledge gaps are still to be investigated:

1) Membrane modification by pressure-driven pre-filtration of FeOCl on ceramic NF membrane as a Fenton-based catalytic layer is lack of researches.
2) Heterogeneous Fenton oxidation processes induced by a pre-coated FeOCl layer on membrane surface for cleaning persistent gel-like fouling of ceramic NF membrane is seldom studied.
3) Uncertainties still exist concerning the synergistic effect between NaCl and Fenton oxidation in a membrane-based cleaning.

The objective of this research is to determine the effectiveness, efficiency, and the underlying mechanism of FeOCl catalysed Fenton-based cleaning for Ca-alginate fouled FeOCl pre-coated ceramic NF membrane. This information is essential to develop a green cleaning strategy to achieve effective and efficient cleaning for persistent gel-like fouled ceramic membrane without compromising membrane quality.

1.3. RESEARCH QUESTIONS AND APPROACHES

According to the background information and knowledge gaps summarised in *Section 1.1* and *Section 1.2*, three research questions were proposed to achieve the research objectives mentioned in *Section 1.2*. These research questions are:

1) What are the main factors affecting the pre-coating (i.e., iron loading) of FeOCl catalysts on top of ceramic NF membrane by the pressure-driven pre-filtration method?
2) What are the efficiency, influencing factors and mechanisms of using the NaCl pre-treatment and FeOCl catalysed Fenton oxidation for cleaning gel-like fouling of ceramic NF membrane?
3) What are the efficiency and underlying synergistic mechanisms of the NaCl/Fenton-based cleaning for gel-like fouling on ceramic NF membrane?

Literature review and laboratory research were two approaches applied to answer these research questions.

Literature review:

A literature review, which is presented in *Chapter 2*, acts at an introduction of the basic mechanisms regarding the topic and the preparation of the laboratory experiments. The collected experimental raw data were analysed and interpreted based on the experimental phenomenon and literature to ensure the agreement between the laboratory result and the scientific theory. Due to the closure of WaterLab in 2020, the literature review was extended to compromise the workload.

Laboratory research:

Laboratory experiments were divided into three stages corresponding to the three research questions:

Stage I: *Investigate the factors that influence the catalytic activity of the synthesised FeOCl.*

In this stage, a synthetic condition to generate a highly active FeOCl catalyst was explored. According to the literature, three synthetic conditions were focused, including, 1) heating rate, 2) heating duration, and 3) the participation of oxygen. Fenton activity of the corresponding synthesised catalyst was determined by the Fenton-based decolouration rate of methylene blue. The effect of chloride ion on the Fenton activity of FeOCl was explored by adding a certain amount of NaCl to the Fenton reaction system.

Stage II: *Examine the factors that affect the iron loading and coating efficiency of FeOCl pre-coating on ceramic NF membrane.*

In this stage, the effects of membrane permeability and FeOCl dosage on the iron loading on ceramic NF membrane were explored. Regarding each aspect, FeOCl pre-coating was conducted under identical condition except for the targeted factor. The pre-coating was evaluated in terms of the iron loading, pre-coating efficiency and the consequent permeability decline. Research question 1) was solved in this stage.

Stage III: *Determine the efficiency of NaCl pre-treatment, Fenton-based cleaning and NaCl/Fenton synergistic cleaning, respectively, and study the corresponding underlying mechanisms.*

In NaCl pre-treatment, three factors were investigated, including 1) treatment hydrodynamics, 2) treatment duration, and 3) Na^+ concentration. In this stage, the

hydrodynamic condition indicated a turbulent forward flush or a soaking mode. The performance of NaCl pre-treatment was assessed by determining the flux recovery after the treatment. In Fenton-based cleaning, the effects of three factors, including 1) cleaning hydrodynamics, 2) H_2O_2 concentration, and 3) cleaning duration, were explored. The cleaning efficiency was evaluated by measuring the flux recovery after Fenton-based cleaning. Besides, the underlying mechanism of Fenton-based cleaning was explored. The effect of ·OH was evaluated by comparing the flux recoveries of Fenton-based cleaning with/without the addition of tert-butanol, an ·OH scavenger. Research question 2) was answered at this stage.

In addition, the synergistic effect between NaCl and Fenton-based cleaning was evaluated by measuring the flux recovery of a Ca-alginate fouled ceramic NF membrane cleaned by a mixture of NaCl/H_2O_2. Research question 3) was answered at this stage. The hypothetical mechanism of the synergistic effect of NaCl/Fenton is explained in *Section 2.5*.

The detailed experimental setup, laboratory materials and methods are elucidated in *Chapter 3*.

2 LITERATURE REVIEW

2.1. CERAMIC NANOFILTRATION MEMBRANES

A membrane filtration process separates a feed stream into permeate and concentrate, with transmembrane pressure (TMP) as a driving force. Membrane processes perform high efficiency in water purification and water reclamation. Due to the current concerns such as water scarcity and increasingly rigorous wastewater discharge criterion, it has been widely implemented in the wastewater treatment process (Fujioka et al. 2014, van der Bruggen et al. 2003).

According to the fabricated material, membrane is generally classified into polymeric membrane and ceramic membrane. Most commercial polymeric membranes are fabricated by hydrophobic polymers such as polyvilidenefluoride (PVDF), polyethersulfone (PES), polypropylene (PE) and polyamide (PA) (Ashfaq et al. 2020, Chu et al. 2016, Hilal et al. 2004, Kochkodan and Hilal 2015, Soesanto et al. 2019, Sun et al. 2018). Ceramic membrane is much less studied compared to the polymeric membrane, yet an increasing amount of corresponding research is conducted in recent times. Typically, ceramic membranes consist of several sublayers, including a support layer which is fabricated by macro-porous alumina (α-Al_2O_3), intermediate sublayers which narrow the water path, and an active layer which is composed of titania (TiO_2) (Shams Ashaghi et al. 2007). Ceramic membranes are distinguished by its outstanding chemical, thermal and mechanical durability as well as stable performance (Lee et al. 2013, Shams Ashaghi et al. 2007, Weber et al. 2003). The exceptional advantages extend its application in harsh conditions such as aggressive chemical (strong acids and bases) and high temperature. Additionally, it is experimentally demonstrated to be less susceptible to organic fouling due to its hydrophilic property (Fujioka et al. 2014, Lee et al. 2013, Lee and Kim 2014). Thus, it has been applied in the treatment of landfill leachate, food and beverage industry, and chemical production process (Fujioka et al. 2014, van der Bruggen and Vandecasteele 2003).

Based on pore size, membranes can be divided into two categories: micro- and ultrafiltration membranes (MF and UF), and nanofiltration and reverse osmosis (NF and RO) membranes. MF and UF membranes aim at larger organic compounds and microorganisms. In comparison, NF and RO membranes are applied to retain micropollutants and ions. NF is originated from RO, and it is distinguished by its relatively higher water permeability, lower operating pressure and, lower salt rejection (van der Bruggen and Vandecasteele 2003). A typical pore size of the polymeric NF membrane is around 1 nm (Fujioka et al. 2014). Despite a relatively slower development, the manufacture technologies for ceramic membrane has achieved a breakthrough, and ceramic NF membrane with molecular weight cut-off (MWCO) of 200 Da was commercially obtained (Fujioka et al. 2014, van der Bruggen et al. 2003). Fujioka et al. (2014) suggested that ceramic NF membrane is negatively charged and performed higher rejection to negatively charged trace organic compounds due to electrostatic repulsion. As the rapid development of membrane filtration process, NF membranes have been widely applied in seawater desalination,

drinking water purification, oilfield produced water treatment and wastewater reclamation (Mohammad et al. 2015, Shams Ashaghi et al. 2007, Zhao and Yu 2015).

2.2. FOULING OF NANOFILTRATION MEMBRANE

Membrane fouling is a phenomenon that includes physical and chemical interactions. It occurs at the surface or in the pores of a membrane due to the accumulation or trapping of foulants during mass transfer across the membrane (Kochkodan and Hilal 2015, Tang et al. 2011). To date, fouling of NF membranes was mainly caused by colloidal or dissolved organic matter (DOM) (Hilal et al. 2004, Li and Elimelech 2004, Lin et al. 2014, Mohammad et al. 2015, Shams Ashaghi et al. 2007, van der Bruggen et al. 2003). Moreover, organic compounds in the feedwater serve as a nutrient source for bacteria which could lead to membrane biofouling (Baker and Dudley 1998, Zhao and Yu 2015). Membrane fouling causes several detrimental impacts on a membrane process, including reduction of permeate flux, deterioration of permeate quality, and decrease of membrane lifespan. Additionally, high frequency of chemical cleaning increases the energy consumption and operational cost of the process (Elimelech et al. 1997, Hilal et al. 2004, Mohammad et al. 2015, Vrijenhoek et al. 2001, Zhao and Yu 2015, Zhu et al. 1997). Eventually, the accumulation of irreversible requires a replacement of membrane elements which imposes a substantial economic burden on the plant (up to 50% of the total cost) (Matin et al. 2011).

2.2.1. Organic Fouling

1) Type of organic foulants

Organic fouling is a major cause of the deterioration of permeate productivity and quality which brings up the energy consumption and operational cost in ceramic NF membrane (Soesanto et al. 2019). Organic foulants can be classified into rigid biopolymers, fulvic compounds and flexible biopolymers (Tang et al. 2011). Rigid biopolymers mainly refer to long-chain polysaccharides with large molecular weight. Fulvic compounds are recalcitrant fulvic acid and humic acid. Flexible biopolymers include proteins and some loose compounds with a molecular weight below 1000 Da (Mohammad et al. 2015, Tang et al. 2011). Typically, polysaccharides are linear or rod-like macromolecules which are weakly negatively charged at neutral pH. Alginate is a hydrophilic polysaccharide with an extended coil conformation. The corresponding molecular weight ranges from 200 to 2000 kDa. The charge density of alginate can reach 6 meq/g due to the deprotonation of carboxylic functional groups (Tang et al. 2011). In this research, alginate is selected as the model organic foulant to mimic the extracellular polymeric substrate (EPS) in the municipal wastewater.

Humic acid is formed by the decomposition of heterogeneous and refractory polymeric organic compounds (Buffle et al. 1998). The molecular weight of humic acid ranges from a few kDa to a few hundred kDa. Due to the deprotonation of carboxylic and phenolic functional groups, it is negatively charged over a wide range of pH (Ritchie and Perdue 2003, Tang et al. 2007b). Unlike polysaccharides and humic acid, which have a flexible size, a specific protein corresponds to a defined molecular weight.

Besides, due to the co-existence of the negatively charged carboxylic groups and positively charged amine groups, protein displays amphoteric charge properties. Their charge properties change with pH, and the critical pH of a specific protein is determined by the respective isoelectric points (pH_{IEP}) (Tang et al. 2011).

2) Mechanisms of organic fouling

Organic fouling is mainly caused by the deposition of organic foulants on the membrane surface (Tang et al. 2011). The hydrophobic fraction of organic foulants dramatically decreases permeate productivity (Kochkodan and Hilal 2015). Main mechanisms contributing to the deposition are adsorption and gel layer formation (Lee et al. 2013, Mohammad et al. 2015, Wang et al. 2014). Adsorption is specific colloid-colloid and colloid-membrane interactions. With the presence of Ca^{2+}, the negatively charged alginate molecules might be neutralised and coiled, and be adsorbed to the membrane surface (Li et al. 2020, You et al. 2020). It can be explained by the Derjaguin-Landau-Verwey-Overbeek (DLVO) theory (Deraguin and Landau 1941, Verwey et al. 1948). DLVO theory indicates that the interaction energy of colloids-charged surface is determined by the total energy of van der Waals (VDW) interaction and electrical double layer (EDL) interaction. Both energies increase as the decrease of the distance between colloid and charged surface. The total interaction experiences attraction and repulsion as the separation distance decay. Such a phenomenon occurs on negatively charged NF membrane surface and improves the retention of negatively charged multivalent salts. However, a high concentration of cations in the feedwater will cause EDL compression and reduce the repulsive interaction between negatively charged colloid and NF membrane. The corresponding colloidal fouling is enhanced. The deposited fouling layer acts as a barrier which increases the total hydraulic resistance (Tang et al. 2007a).

Moreover, the gel-like fouling layer formed by the cross-linking between multivalent ions and long-chain alginate molecules enhances membrane fouling (Lee et al. 2006a, Wang et al. 2014). It is known as calcium bridging, and it has been confirmed by atomic force microscopy (AFM) measurement (Lee et al. 2006b). Hence, the exclusive property of alginate leads to an increased fouling propensity of it compared to humic acid and protein at higher ionic strength (Buffle et al. 1998, Tang et al. 2011). Besides, the gel-like layer improves concentration polarisation via a cake-enhanced osmotic pressure (CEOP). The porous fouling layer formed at the membrane surface traps the solutes and inhibits the back diffusion of solutes. Furthermore, it acts as a protective layer, preventing the tangential flow of the solutes. The extra gel-like layer enhances concentration polarisation and the osmotic pressure difference between the bulk and the interior of the fouling layer. This phenomenon causes an accumulation of solutes at the membrane surface and deteriorates the permeate quality (Hoek et al. 2003, Hong and Elimelech 1997).

3) Factors affecting organic fouling

Organic fouling on NF membranes is complicated and involves collaborations between various foulants and mechanisms. Factors contributing to membrane fouling can be classified into feedwater composition, membrane properties and

hydrodynamic conditions (Lee and Kim 2014, Tang et al. 2011, Zhang et al. 2013). Tang et al. (2007b) indicated that the increase of foulant concentration in the feed enhances concentration polarisation and foulant deposition at the membrane surface. A high concentration of salt compresses EDL and decays the stability of the colloids. It increases the collision frequency and the attachment of foulants to the membrane (Li et al. 2011). Calcium ion has a stronger interaction with alginate than other multivalent cations, and an increased concentration of calcium ion in the feedwater enhances calcium bridging (Lee et al. 2006a). Besides, pH and foulant type influence membrane fouling as well (Tang et al. 2011).

Membrane surface properties such as the functional groups of the membrane, the morphology of membrane (i.e. surface roughness) and hydrophobicity contribute to membrane fouling. Surface charge (zeta potential) influences membrane fouling by affecting the interaction energy with charged foulants (Tang et al. 2011). Li et al. (2019) proposed that an increase of surface roughness decreased the adhesion of alginate to the membrane. Moreover, it is noteworthy that the adhesive foulants might alter membrane properties in terms of surface charge and hydrophobicity, and accordingly changes the separation mechanism of the membrane. Agenson et al. (2007) stated that foulants were retained by size exclusion. Whereas, the retention of large solute by a pre-fouled membrane was mainly caused by adsorption.

Meanwhile, hydrodynamic conditions contribute to membrane fouling. Permeate flux plays a crucial role in membrane fouling in two aspects. Firstly, the increase of permeate flux increases the probability and frequency of collision between foulants and membrane. Secondly, an enhanced permeate flux introduces a greater hydrodynamic drag force to the solute, which increases membrane fouling. A higher TMP increases permeate flux, and an increase of crossflow velocity decreases the propensity of foulant deposition. Additionally, temperature, recovery factors, membrane modules and the design of spacer affect membrane fouling as well (Tang et al. 2011).

2.2.2. Biofouling

Biofouling is caused by biologically active organisms, such as microorganisms (Kochkodan and Hilal 2015). It indicates an irreversible adhesion of bacteria to the membrane surface and a subsequent bacterial multiplication with the nutrients presented in the feedwater. Eventually, it results in the formation of biofilm on the membrane surface (Garrett et al. 2008). It mainly occurs in RO desalination. Due to the possibility of the growth, multiplication and relocation of microorganisms, biofouling is intrinsically more complex than other types of membrane fouling. Apart from the adverse effects mentioned before, biofouling has additional unfavourable impacts including, 1) reducing the lifespan of biodegradable polymeric membranes, and 2) threatening human health with the accumulation of pathogens on the membrane surface (Kochkodan and Hilal 2015).

1) Mechanisms of biofouling

Biofouling is mainly attributed to the presence of microorganisms in the feedwater. Baker and Dudley (1998) indicated that bacteria and other microorganisms presented in most kinds of waters and are inherently capable of colonizing on any surface due to survival instincts. Biofouling mainly consists of four stages, including, 1) transportation, deposition, and adhesion of microorganisms to a surface, 2) production of exopolymer, 3) cell growth and proliferation and 4) cells dispersion from the biofilm matrix (Kochkodan and Hilal 2015, Matin et al. 2011). The adhesive ability of cells to the membrane surface is a decisive factor in the initial stage of the formation of biofilm (Matin et al. 2011). Generally, the colonisation of microorganisms on a surface results in the formation of an adhesive layer, known as a biofilm.

Biofilm composes microorganisms which are embedded in extracellular polymeric substances (EPS). EPS is bacterial originated macromolecules which consist of polysaccharides, proteins, glycoproteins, lipoproteins. Hence, it performs amphiphilic properties (Kochkodan and Hilal 2015). EPS in biofilm improves the adhesion of microorganisms to the membrane surface. The adhesion of microorganisms is greatly influenced by hydrophobic interactions, including, hydrogen bonding, London-van der Waals attractions, and electrostatic interactions (Kochkodan and Hilal 2015, Matin et al. 2011). The adhesion of biofilm to the membrane improves the hydrophilicity of the membrane surface (Matin et al. 2011, Neu and Marshall 1990). Moreover, EPS enhances the antimicrobial resistance by impeding the diffusion of antibiotics through the biofilm (Matin et al. 2011).

Biofouling is responsible for the reduction of salt retention attributing to the biofilm-enhanced osmotic pressure (BEOP) (Matin et al. 2011). EBOP hampers the back-diffusion of solutes and contributes up to 70% of TMP increase in a constant flux filtration process (Herzberg and Elimelech 2007). Biofouling induces biodegradation of polymeric membranes, which decreases salt rejection chronically (Matin et al. 2011). The kinetics of biofouling-caused flux decline usually comprises two stages: an initial rapid decline followed by gradual decay. The attachment and multiplication of cells in the early stage results in the initial rapid decline. The equilibrium between the growth of biofilm and the detachment of biofilm leads to the gradual decay. In this phase, the membrane surface is masked by biofilm (Kochkodan and Hilal 2015, Matin et al. 2011).

2) Factors affecting biofouling

Factors that affect biofouling can be categorised into membrane surface properties, species of microorganism, feedwater composition, and operational conditions. It is suggested that a hydrophilic membrane is less susceptible to biofouling due to the reduced adhesive interaction between microorganisms and membrane. A thin water boundary was formed on a hydrophilic surface with the surrounding water molecules via hydrogen bonds. This layer reduces the propensity of adsorption or adhesion of hydrophobic foulants to the membrane surface (Kochkodan and Hilal 2015).

Zeta potential is usually an indicator of surface charge of membrane. Most membranes are negatively charged. In the case of feedwater containing charged foulants,

membrane surface charge plays a critical role in membrane fouling. The leading theory (DLVO theory) involved has been explained in *Section 2.2.1*. Moreover, the charge properties of the membrane surface can be affected by the pH of feedwater. For a negatively charged surface, an increase of pH will increase the density of negatively charged groups (Kochkodan and Hilal 2015). Besides, as mentioned above, a rougher surface is less susceptible to colloidal fouling (*Section 2.2.1*). Similar results were observed for biofouling (Knoell et al. 1999, Peng et al. 2004). However, Pasmore et al. (2001) proposed that a rougher membrane slightly increased the accumulation of biofilm. A possible explanation is that a rougher surface decreases hydraulic shear in some areas, which increases the propensity cell attachment to the membrane surface.

The properties of microorganism contribute critically to the property of biofilm (Kochkodan and Hilal 2015). Herzberg and Elimelech (2007) proposed that the EPS excreted by live cells provided higher hydraulic resistance to permeate flux, which had a similar effect as alginate. On the other hand, the cake deposition formed by dead cells are porous and contribute slightly to permeate flux decline. In addition, some species of microorganisms show nonselective tendency to adhere to all kinds of surface, while others take a longer time to attach to specific surfaces (Kochkodan and Hilal 2015). Moreover, the attachment of cells can be influenced by hydrodynamic conditions and feedwater composition. A turbulent flow generates a higher shear force which decreases the deposition of cells. Feedwater composition influences the growth and multiplication of microorganisms. For a developing biofilm, an adequate supply of biodegradable nutrients in the feedwater improves the growth of biofilm (Al-Amoudi 2010). Baker and Dudley (1998) also suggested that the growth rate of biofilm was influenced by the nutrient ratio, such as carbon, nitrogen, and phosphate, temperature, redox potential, and pH.

2.2.3. Multi-Component Fouling

Membrane fouling is a complicated process which involves multiple interactions. In the practical operation, several types of foulants will present in the feedwater, and various fouling mechanisms will occur in a membrane filtration process. Sometimes, a type of foulant will have different roles in different fouling processes. For example, the organic foulants retained by membrane might act as a nutrient source for the microorganisms that attached to the membrane surface (Mohammad et al. 2015). In some cases, the presence of a kind of foulant might mitigate a certain type of fouling. Tu et al. (2011) reported that membrane pre-fouled by humic acid showed an enhancement of rejection of boron due to the increased electrostatic repulsive interaction between the negatively charged humic substance and boron. Chang et al. (2012) stated that humic acid and calcium ion introduced a cake deposited on the membrane surface, which improved the retention of small neutral charged solutes due to the cake-enhanced concentration polarisation.

2.3. FOULING MITIGATION OF NANOFILTRATION MEMBRANE

Membrane fouling negatively affects the treatment process. Fouling mitigation is necessary for the practical application of the membrane process. Generally, fouling

mitigation consists of physical cleaning and chemical cleaning (Wang et al. 2014, Zhao et al. 2000). Physical cleaning aims at removing the loosely attached foulants, also known as, reversible foulant. Fouling attributed to colloidal organic matters is more tenacious and hydraulically irreversible, which is mainly mitigated by chemical cleaning (Fujioka et al. 2014, Wang et al. 2014). Besides, feedwater pre-treatment and membrane modification are proposed to diminish membrane fouling and improve membrane performance (Anantharaman et al. 2020, Zhao and Yu 2015). In practical operation, various cleaning approaches are collaborated to increase cleaning efficiency. Regarding diverse types of membrane and foulant, it is challenging to find a proper strategy to maintain the permeate flux of a system without compromising the foulants rejection and membrane quality over a certain period (Matin et al. 2011).

Physical cleaning efficiently removes the reversible foulants. Periodical backwash and forward flush are common ways to restore permeability. Physical cleaning prevents a large amount of chemical dosage and subsequent chemical treatment. However, backwash is considered impractical due to the low permeability of the NF membrane. Forward flush is inefficient for the removal of the gel-like fouling layer formed by colloidal organic compounds (Chang and Judd 2002, Huang et al. 2008, Soesanto et al. 2019). Regarding the factors affecting membrane fouling and fouling mechanisms that were illustrated in *Section 2.2*, the major fouling mitigation strategies for NF membrane are classified into feedwater pre-treatment, surface modification and chemical cleaning.

2.3.1. Feedwater Pre-treatment

Due to the exceptional rejection property of NF membrane, high-quality feedwater is required to maintain a stable long-term performance. Pre-treatment modifies physical, chemical, and/or biological properties of feedwater which decreases the propensity of membrane fouling and extends the lifetime of the membrane. Feedwater pre-treatment is mainly categorised into coagulation and filtration, adsorption, and chemical agent addition.

1) Coagulation and low-pressure membrane filtration

Soluble particulates and colloids are the typical causes of irreversible fouling in the NF process. These tiny particles are evenly distributed in an aqueous environment. The stability of the system is ensured by the electrostatic repulsive interactions among these negatively charged matters. Coagulation is a process that the addition of positively charged coagulants destabilise and aggregate the negatively charged particles and form macro flocs. There are mainly two types of coagulants: 1) inorganic salts such as ferric chloride ($FeCl_3$) and aluminium sulfate ($Al_2(SO_4)_3$); 2) cationic organic macromolecules with low molecular weight. The inorganic coagulants accumulate particles by charge neutralisation and sweep flocculation. Whereas, organic coagulants interact with particles through adsorption and bridging effect. According to the literature, inorganic iron or aluminium salts are more frequently used in coagulation than organic coagulants. Followed by an MF/UF process, the flocs and aggregations are removed from the feedwater (Zhao and Yu 2015).

Low-pressure membrane filtration pre-treatment successfully diminishes irreversible membrane fouling, which further reduces the frequency of chemical cleaning, and improves the long-term performance of the NF process. Regarding the increasingly stringent regulation and the decrease of operating cost of the membrane process, MF/UF is widely applied before NF/RO process to improve the feedwater quality. NF process is also considered as an alternative pre-treatment for a RO process. Among these pre-treatment process, UF is probably the optimal choice which balances the productivity of permeate and membrane fouling mitigation. MF is generally applied to remove large particles and generate higher permeate production.

Moreover, low-pressure membrane filtration efficiently reduces biofouling in subsequent membrane process by removing the microorganisms and biodegradable organic compounds from the feedwater to inhibit the adhesion and growth of biofilm. However, the hydrophobic materials and cellular or extracellular polymer substrates in the feedwater will cause fouling in the MF/UF process, which declines the permeate productivity and deteriorates the permeate quality. Coagulation combines with membrane filtration effectively enhance the removal of small particles and reduce the formation of a cake layer on the NF membrane (Zhao and Yu 2015).

2) Adsorption

Activated carbon adsorption aims at removing the soluble non-polar organic materials, such as natural organic matter (NOM), in the feedwater. These matters are potential nutrients for the growth of biofilm, which cause biofouling in an NF process. In the pre-treatment of feedwater with a low concentration of organic materials, activated carbon adsorption is proposed as a well-established strategy to efficiently uptake the hydrophobic organic compounds in the feedwater. However, the low adsorption capacity and adsorption kinetic of commercially available activated carbon hinder its application in the pre-treatment of feedwater with high organic loading. Moreover, activated carbon mainly remove organic compounds that are soluble in water (Zhao and Yu 2015).

3) Chemical agent addition

Apart from coagulation, filtration and adsorption, membrane fouling can be mitigated by adjusting the chemical composition of the feedwater. For example, the addition of an antibacterial chemical enhances the antimicrobial capacity of the feedwater and reduces biofouling. As mentioned in *Section 2.2.2*, the presence of microorganisms and nutrients are the principal promoters of the formation of biofilm. Coagulation, filtration and absorption effectively remove bacteria and nutritious materials from the feedwater (Kochkodan and Hilal 2015). However, such pre-treatments hardly reach a complete removal of foulants. Chemical agents are proposed to enhance the antimicrobial capacity of the feedwater. Addition of strong oxidants such as chlorine (Cl_2), sodium hypochlorite (NaClO), monochloramine (NH_2Cl), chlorine dioxide (ClO_2) and ozone (O_3) and ultraviolet (UV) disinfection efficiently improve bacterial lysis (Matin et al. 2011, Zhao and Yu 2015). Cl_2 and NaClO present high antimicrobial activity. However, membranes composed of aromatic polyamide are Cl_2 sensitive, and the residual Cl_2 should be removed by activated carbon filter or sodium bisulfite

($NaHSO_3$) (Zhao and Yu 2015). NH_2Cl and ClO_2 are less detrimental to membrane integrity, whereas they are less anti-bacterial effective and more expensive. Ozone and UV might cause damage to the membrane surface and lack residual antibacterial effect. However, the generated disinfection by-products (DBPs) are carcinogenic and mutagenic.

2.3.2. Membrane Modification

Membrane surface modification is a common way to produce a membrane with the desired properties. As mentioned in *Section 2.2*, membrane surface properties have notable effects on altering the membrane fouling propensity. Membrane modification tailors the hydrophilicity, roughness, functional groups and zeta potential of membranes which improves the anti-fouling capacity of the membrane (Chu et al. 2016, Soesanto et al. 2019, Sun et al. 2018, van der Bruggen et al. 2003, Zhao and Yu 2015). Biofouling can also be mitigated via membrane modification to enhance anti-adhesion and antimicrobial properties of the membrane (Kochkodan and Hilal 2015, Li et al. 2006, Liu et al. 2010). Additionally, several researchers suggested that membrane pre-coated by reactive nanoparticles performed anti-fouling and self-cleaning properties with the presence of H_2O_2 via *in situ* generation of reactive oxygen species (ROS) (Hong and He 2014, Madaeni and Ghaemi 2007, Sun et al. 2018).

General modification approaches are surface coating, surface grafting, incorporation of hydrophilic monomers, incorporation with inorganic particles and modification with zwitterionic materials (Zhao and Yu 2015). Membrane coating demonstrates deposition of a dynamic layer to a conventional membrane (Anantharaman et al. 2020). Different from other surface modification strategies, the dynamic membrane is deposited on the membrane surface via physical interactions such as van der Waals attraction, hydrogen bond, or/and electrostatic interaction. Hence, the pre-coated layer might diminish after cyclic fouling/cleaning process (Zhao and Yu 2015). Anantharaman et al. (2020) summarised three main factors affecting the properties of the dynamic membrane, including, the properties of the material of dynamic membrane, the properties of the pristine membrane and the hydrodynamic conditions of the pre-coating process. Firstly, increasing the concentration of the material of the dynamic membrane in the feed generates a thicker and grater mass of dynamic membrane. Besides, the size of particles deposited on the membrane is usually smaller than the average particle size in the bulk suspension. This phenomenon is attributed to the smaller particles have a higher tendency to deposit, which results in an extra resistance on the pristine membrane. It will increase the mechanical strength of the consequent dynamic membrane. Secondly, a rougher and mechanically more robust pristine membrane improves the retention and deposition of the dynamic membrane. Lastly, hydrodynamic conditions such as crossflow velocity and TMP significantly affect the deposition of the dynamic membrane. A lower crossflow velocity yields a thicker dynamic membrane due to the lower shear force at the vicinity of the membrane. However, a crossflow velocity below a certain extent will increase the nonuniformity of the deposited dynamic membrane (Pan et al. 2015). On the other hand, a greater TMP introduces a greater driving force and generates a higher

permeate flux through the pristine membrane. A corresponding greater compaction will yield a thinner dynamic membrane with greater specific mass.

Dynamic membrane slows down membrane fouling and reduces the intrusion of foulant to the pristine membrane. Flux can quickly be restored by the complete removal of the deposited layer. The used dynamic membrane can be flushed away by chemical agents, and a new dynamic membrane can be deposited on the pristine membrane. There are some other researchers committed to clean and reuse the dynamic membrane. Only a few of them succeed in achieving flux recovery as well as preserving the dynamic membrane. Two successful attempts for inorganic dynamic membrane were: 1) volatile oily foulants removed by calcination (200-400 °C) which compromised 10% of separation performance, and 2) humic acid cleaned by NaOH combined with Fenton oxidation cleaning (Anantharaman et al. 2020).

2.3.3. Chemical Cleaning

Despite feedwater pre-treatment, membrane property improvement and hydrodynamics, fouling is still inevitable due to the retention property of membrane filtration. Chemical cleaning is intended to reduce the cohesive as well as adhesive interactions between the fouling layer and the membrane. It is conducted when the permeate flux or TMP reaches the threshold value to restore the membrane performance. The objective of chemical cleaning is to remove the tenacious or hydraulically irreversible foulants that attach to the membrane surface or adsorbed in the pore.

The typical chemical agents are acids, bases, oxidants, chelating agent, surfactants, and salt solution (Lee and Elimelech 2007, Mohammad et al. 2015). Acid such as hydrochloric acid (HCl) and sulfuric acid (H_2SO_4) aims at dissolving inorganic scaling. Specifically, citric acid and oxalic acid remove metallic materials effectively by forming chelates with metal cations (i.e. iron). Alkaline solutions and oxidants cleaning aim at removing organic fouling and biofouling. Alkaline such as sodium hydroxide (NaOH) effectively disintegrates organic compounds into fine or soluble particles (Wang et al. 2014). Oxidants, such as sodium hypochlorite (NaClO) and hydrogen peroxide (H_2O_2), decompose organic macromolecules into fine and soluble particles. Despite the high oxidative activity, NaClO oxidation might potentially generate toxic by-products such as absorbable organic halogen (AOX) and trihalomethanes (THMs). Moreover, Kramer et al. (2019) reported that long-term exposure to NaClO deteriorates the glass sealing of the ceramic NF membrane.

On the other hand, H_2O_2 is preferable as a highly reactive, environmentally friendly and safe reagent (Wang et al. 2014). Fenton(like) catalyst decomposes H_2O_2 into nonselective, highly active radicals. It is further explained in *Section 2.4*. The generated radicals efficiently degrade and detach the fouling layer. A chelating agent such as ethylene diamine tetraacetic acid (EDTA) or a surfactant such as sodium dodecyl sulphate (SDS) is useful in loosening and detaching the organic foulants. Moreover, Lee and Elimelech (2007) stated that the monovalent salt solution effectively clean Ca-alginate fouled RO membrane. The proposed mechanism is elucidated in *Section 2.5*.

Despite the high effectiveness and efficiency of chemical cleaning, the disadvantages are prominent. High cleaning frequency and long cleaning duration will deteriorate the integrity and lifespan of the membrane (Wang et al. 2014). Hazardous by-products might be produced in specific processes. Overdosage of chemicals improves cleaning efficiency, yet it might cause problems in post-treatment of the cleaning solution. Moreover, off-line chemical cleaning might cause operational difficulties, and downtime would result in a reduction of filtration efficiency (Wei et al. 2011). Therefore, an appropriate selection of chemical and dosage of chemical is of great significance.

In practical application, chemical cleaning is usually collaborated with physical cleaning to achieve higher cleaning efficiency. A two-step process is involved in the detachment of the fouling layer, including, 1) chemically loosen the fouling layer, and 2) physically detach the loosely attached foulants by fluid shear. Chemical activity is the decisive step in this process since the detachment of the fouling layer can only be achieved after reducing the foulant-foulant/foulant-membrane interactions. The reduction of adhesive interactions in chemical cleaning has been confirmed by Zhao and Yu (2015).

Table 2.1: Summary of Membrane Fouling Mitigation of NF membrane (Huang et al. 2009, Zhao and Yu 2015)

Fouling mitigation strategies	Cleaning mechanism	Targeted foulant types	Advantages	Disadvantages
1. Feedwater pre-treatment				
1) Coagulation:				
Inorganic salts, i.e. $FeCl_3$ and $Al_2(SO_4)_3$	Charge neutralisation and sweep flocculation at neutral pH	Aqueous particulate and colloidal matters	An effective method to remove major membrane foulants; Formation of the porous cake layer and reduce permeate flux decline	Sensitive to coagulant type and dosage (i.e. a residual aluminium concentration above might reduce the productivity of permeate flux of subsequent membrane process)
2) Filtration:				
MF	Size exclusion	Large particulate matters and microorganisms	Higher permeate productivity	Lower contaminant removal; Membrane fouling
UF	Size exclusion	Colloids, suspended solids, and microorganisms	Perhaps the best balance between contaminant removal and permeate productivity	Membrane fouling
NF (RO pre-treatment)	Size exclusion, electrostatic repulsion	Dissolved organic matters, particulate materials, colloids, and bivalent salts	Higher contaminant removal	Lower permeate flux; Membrane fouling
Activated carbon adsorption	Adsorption	Soluble organic matters such as DOM and endocrine disrupting compounds	Well-established technology; Effectively remove trace hydrophobic organic compounds	Low adsorption capacity and low adsorption kinetic; Mainly remove soluble compounds

Table 2.1 *(continued)*

Fouling mitigation strategies	Cleaning mechanism	Targeted foulant types	Advantages	Disadvantages
3) Chemical agent addition: Biofouling mitigation:				
Cl_2, NaClO, NH_2Cl, ClO_2, O_3 and UV	Microbial lysis	microorganisms	A wide variety of disinfection strategies; Mostly effective; O_3 alleviates organic fouling in subsequent membrane process	Cl_2 deteriorates aromatic polyamide membrane; NaClO causes defects in the ceramic membrane; NH_2Cl and ClO_2 are less effective and more expensive; The formation of DBPs; UV and O_3 lack residual effect.
2. Membrane modification				
Pre-deposition of dynamic membrane	Tailoring membrane surface properties	Organic foulant and biofouling	Poor stability; Enhancement of anti-fouling; properties of the pristine membrane	Permeability decline; Poor stability; Process complexity
3. Chemical cleaning				
Acids, alkaline, oxidants, surfactants, monovalent salt solution	Break down the cohesive and adhesive interactions between the fouling layer and the membrane	Inorganic scaling, organic fouling and biofouling	Appropriate selection of cleaning agent lead to high cleaning efficiency	Inappropriate chemical selection might lead to membrane deterioration; The cleaning solution might deteriorate the environment; Overdosage of chemical might cause problems in post-treatment of cleaning solution

2.4. FENTON-BASED CLEANING ON MEMBRANE

2.4.1. Fenton Oxidation and Membrane Cleaning

Fenton reaction is one of the advanced oxidation processes (AOPs). Homogeneous Fenton oxidation indicates a redox reaction that ferrous iron (Fe^{2+}) decomposes H_2O_2 and generates reactive oxygen species (ROS) at the acidic condition. ROS, such as unselective, highly reactive hydroxyl radical (·OH), are strong oxidants which oxidise organic matters at a near-diffusion controlled rate (*Eq. (2.3)*) (Keenan et al. 2008). On the other hand, heterogeneous Fenton oxidation denotes the decomposition of H_2O_2 on the interface of the solid catalyst at acidic or even circumneutral condition (*Eq. (2.2)*) (He et al. 2016). It has gained extensive attention due to the recyclability of solid catalyst and the reduction of iron-containing sludge (He et al. 2016, Sun et al. 2018).

$$FeOCl + H_2O_2 \leftrightarrow Fe_{1-n}^{III}Fe_n^{II}OCl + \cdot OOH^- + H^+ \quad (2.1)$$

$$\equiv Fe^{II} + H_2O_2 \leftrightarrow \equiv Fe^{III}\text{-}OH + \cdot OH \quad (2.2)$$

$$\cdot OH + organic\ compounds \leftrightarrow intermediates \leftrightarrow CO_2 + H_2O \quad (2.3)$$

Fenton-based oxidative cleaning for the organic fouled membrane is considered as an environmentally friendly and efficient membrane cleaning approach. In Fenton oxidation, macro-organic compounds are decomposed into fine or soluble particles and detached from membrane pore or surface. Currently, there are few publications concerning Fenton-based cleaning for organically fouled membrane. Soesanto et al. (2019) reported a combination of alkaline and homogeneous Fenton cleaning for polymeric MF/UF membrane used in seawater pre-treatment. The membrane was cleaned by a mixture of dissolved ferrous sulfate heptahydrate ($FeSO_4{\cdot}7H_2O$) and H_2O_2 at pH 3. Sun et al. (2018) reported a heterogeneous Fenton-based cleaning for polymeric UF membrane fouled by bovine serum albumin (BSA). The iron-based catalyst was immobilised on membrane via the facile, scalable thermal-treatment process and a 5-min Fenton-based cleaning restored 70 % of water flux.

Interfacial reaction comprises four steps, including 1) transportation of H_2O_2 from the bulk to the fouling layer; 2) penetration of H_2O_2 through the fouling layer to the pre-coated catalytic layer; 3) generation of ·OH; 4) degradation of organic foulants. The rate of a heterogeneous reaction is determined by the rate of mass transfer and radical generation (He et al. 2016, Wang et al. 2014). Additionally, the cleaning efficiency depends on the detachment rate of fouling layer. Different from homogeneous Fenton reaction, heterogeneous Fenton reaction initially degrades organic foulants attached to the vicinity of catalyst, which effectively reduces the adhesive interaction between the fouling layer and the catalytic layer and efficiently detaches the fouling layer.

2.4.2. Iron Oxychloride (FeOCl)—A Fenton-like Catalyst

Iron-based catalysts are preferable due to the high catalytic activity, accessibility, recyclability and low toxicity (He et al. 2016). Iron oxychloride (FeOCl) is a novel, heterogeneous Fenton-like catalyst that performs exceptional Fenton activity and durability in a cyclic process. Yang et al. (2013) owned the outstanding performance of FeOCl to its unique structural configuration and self-redox property. FeOCl is

nanoplates or nanosheets which stack together due to van der Waals force and electrostatic interactions. The weak interactions between layers make it an excellent host for intercalation reaction.

Additionally, it is proven that a significant number of unsaturated iron atoms were exposed at the polar surface of FeOCl nanoplate. In the meantime, the active sites on the polar surface, mainly hydroxyl groups, involves in processes such as dissolution, complexation, and anions adsorption. On the other hand, FeOCl displays a unique redox cycle of iron. It displays a strong oxidizing property. With the adsorption of intercalated organic molecules and H_2O_2, the viable electron transfer from H_2O_2 to FeOCl, which results in an *in situ* partial reduction of iron ($Fe^{III} \rightarrow Fe^{II}$) (*Eq. (2.1)*). The Fe^{II} is responsible for the decomposition of H_2O_2 (*Eq. (2.2)*). The generated radicals effectively degrade the foulants adhered to FeOCl and the detachment of organic foulants lead to the restore of the chemical state of FeOCl ($Fe^{II} \rightarrow Fe^{III}$).

Currently, FeOCl nanoplate/nanosheet is commercially unavailable, and it is mostly synthesised in the lab. Two-dimensional metal oxides were produced by rapid thermal annealing of the corresponding metal hydrous chloride. FeOCl was synthesised by iron chloride hexahydrate ($FeCl_3 \cdot 6H_2O$), and the chemical reaction equation is listed in *Eq. (2.4)* (Sun et al. 2018, Zhang et al. 2017, Zhao et al. 2016). Sun et al. (2018) immobilised FeOCl on polymeric UF membranes via thermal annealing, which generated a uniformly distributed catalytic layer on the pristine membrane surface. They also stated that the fabricated FeOCl layer improved the hydrophilicity of the membrane, which reduced the susceptibility to hydrophobic organic fouling.

$$FeCl_3 \cdot 6H_2O \rightarrow FeOCl + 2HCl + 5H_2O \quad (2.4)$$

2.4.3. Factors Affecting Fenton Activity

Generally, four factors would affect the activity of heterogeneous Fenton reaction, including, pH, H_2O_2 concentration, catalyst loading, and radical scavenger. As mentioned in *Section 2.4.1*, homogeneous Fenton reaction is sensitive to pH, and it performs the highest activity in a narrow pH range (pH 2.5-3.5). However, for heterogeneous Fenton reaction, it achieves high efficiency in a broad pH range, from 3.0 to 9.0. Although the increase of pH decreased the organic degradation in the initial phase, a thorough degradation could be reached in a certain period (Yang et al. 2013). Meanwhile, ·OH shows a reduced oxidation potential at higher pH (Babuponnusami and Muthukumar 2014). Fenton activity can be improved by increasing the concentration of H_2O_2, which accelerates the generation of ·OH and, subsequently, intensifies the oxidative degradation of organic molecules (Yang et al. 2013). However, it is also reported that overdosage of H_2O_2 might scavenge the generation of ROS (He et al. 2016). The loading of nano-catalyst remarkably influences the generation rate of radicals. A low loading of catalyst might lead to non-radical oxidation between the absorbed H_2O_2 and the absorbed organic foulants (He et al. 2016). In addition, some inorganic ions such as chloride ions, bicarbonate and carbonate would compete for radicals. They are known as radical scavengers. Among which, Cl^- plays a significant role at low pH (pH 1-2.5) (*Eq. (2.5)*), while, bicarbonate and carbonate are more competitive as the pH increased (*Eqs. (2.6)-(2.7)*) (He et al. 2016, Kiwi et al. 2000). Yang

et al. (2013) and Zhang et al. (2017) both reported FeOCl preserved a high Fenton activity and chemical property after 4 or 5 successive cycles.

$$Cl^- + \cdot OH \rightarrow \cdot ClOH^- \quad (2.5)$$

$$k = 8.9 \times 10^7\ (M \cdot s)^{-1}, pH = 1 - 2.5$$

$$HCO_3^- + \cdot OH \rightarrow \cdot CO_3^- + H_2O \quad (2.6)$$

$$CO_3^{2-} + \cdot OH \rightarrow \cdot CO_3^- + OH^- \quad (2.7)$$

2.5. NaCl PRE-TREATMENT

Sodium alginate is the model organic foulant in this study. The presence of calcium ions enhances the interactions between the coil-like alginate long-chains and the ceramic membrane and, hence, forms a tenacious, compact gel-like layer on the membrane surface (Li et al. 2011). Preliminary experiments regarding the Fenton-based cleaning for Ca-alginate fouled FeOCl immobilised ceramic NF membrane in our lab revealed that the compact gel-like layer retarded the diffusion of H_2O_2 to the catalytic layer and impeded the generation of ·OH. Lee and Elimelech (2007) suggested that the presence of Na^+ in bulk swelled the gel-like fouling layer by introducing an osmotic pressure difference between the bulk solution and the interior of the fouling layer. The hydrophilic alginate facilitated the diffusion of Na^+ into the fouling layer. Na^+ exchanged the bonded Ca^{2+} and relaxed the fouling layer. They proposed a complete removal of the fouling layer by a NaCl forward flush. However, according to the previous experiments in our lab, NaCl soaking only achieved partial removal of the fouling layer. Furthermore, the presence of NaCl improved the efficiency of Fenton-based cleaning. The hypothetical mechanism of the synergistic effect is displayed in *Figure 2.1*.

Inspired by these statements, the addition of NaCl in Fenton-based cleaning was proposed to improve the relaxation of the fouling layer. Thus, the catalytic sites on the FeOCl layer were exposed, and the diffusion rate of H_2O_2 was increased. The generated hydroxyl radicals would subsequently degrade the foulants that attached to the FeOCl layer and release the blocked pores. According to the abovementioned researches, a turbulent flow improves the efficiency of NaCl treatment. Moreover, the synergistic effect of NaCl treatment and Fenton-based cleaning at various conditions was not thoroughly investigated. Hence, it is meaningful to explore the factors that affect the efficiency of NaCl treatment and the synergistic effect of NaCl and Fenton oxidation.

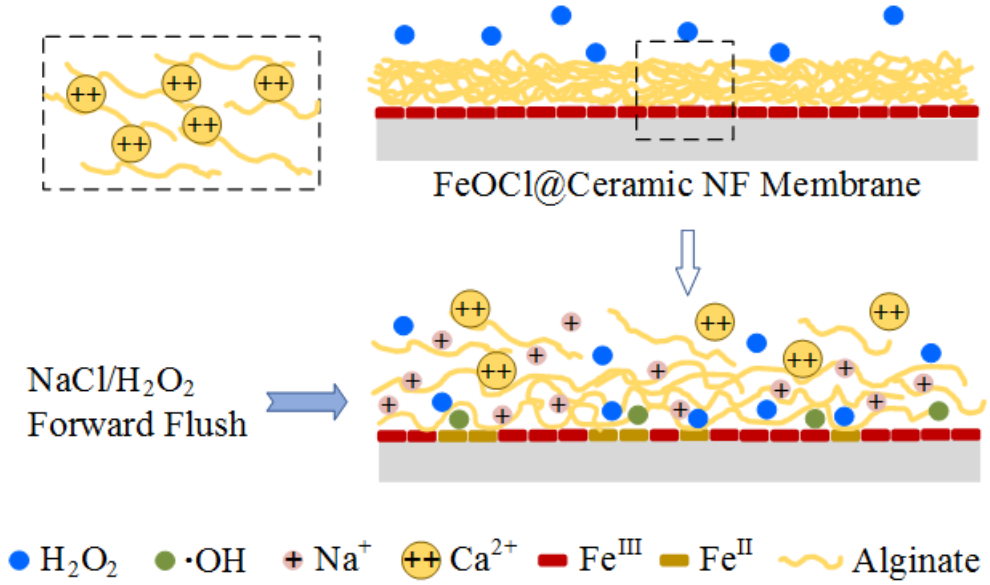

Figure 2.1: Hypothetical mechanism of synergistic cleaning by NaCl and Fenton (Adapted from Lee and Elimelech (2007))

3 MATERIALS AND METHODS

3.1. MATERIALS

Iron(III) chloride hexahydrate ($FeCl_3 \cdot 6H_2O$; ≥99% purity; solid), Methylene blue (powder), tert-butanol ($C_4H_{10}O$; ≥99% purity), oxalic acid ($C_2H_2O_4$; ≥99% purity; powder), poly(ethylene glycol) (PEG, 1000 Da), sodium alginate (Na-alginate), sodium chloride (NaCl) and sodium bicarbonate ($NaHCO_3$) were purchased from Sigma-Aldrich, Germany. Calcium chloride dihydrate ($CaCl_2 \cdot 2H_2O$) and hydrogen peroxide (H_2O_2; 30%) were purchased from Merck KGaA, Germany. Iron oxychloride (FeOCl) powder applied in this research was prepared in the lab, and the detailed synthetic conditions were elucidated in *Section 3.2.1*. The decolouration of methylene blue indicated the Fenton activity of the as-prepared FeOCl catalyst. tert-Butanol acted as a radical scavenger in Fenton reaction. PEG filtration was used to determine membrane defect. Na-alginate was the model organic foulant that represented EPS in organically loaded wastewater. The chemical composition of Na-alginate was $(C_6H_7NaO_6)_n$, and the chemical structure of it is displayed in *Figure A.1*.

In addition, iron test kit (100796) was purchased from Merck KGaA, Germany. Photometer NOVA 60 A Spectroquant® (109752) was also purchased from Merck KGaA and used for the determination of iron concentration. GENESYS™ 10S UV-Vis spectrophotometer purchased from ThermoFisher scientific was used to determine the absorbance of methylene blue solution. The 0.45 µm disposable syringe filters (CHROMAFIL® Xtra PE-45/25) were purchased from MACHEREY-NAGEL, Germany.

Filtration experiments were conducted using tubular ceramic nanofiltration (NF) membranes which were purchased from Inopor GmbH, Germany. The ceramic NF membrane comprises titanium dioxide (TiO_2), zirconium dioxide (ZrO_2) and aluminium oxide (Al_2O_3) acting as an active layer, intermediate layer, and support layer, correspondingly. Each ceramic NF membrane has one channel and the inner and outer diameters are 7 mm and 10 mm, respectively. The mean pore size of these membranes is 0.9 nm, and the active filtration area is 0.00163 m^2. The actual membrane defect was detected, as mentioned in *Section 3.2.4*.

3.2. METHODS

Figure 3.1 illustrates the overall experimental design of this research. It consists of three sections complying with the three stages, which were: 1) synthesis of FeOCl, 2) pre-coating of FeOCl, and 3) membrane cleaning.

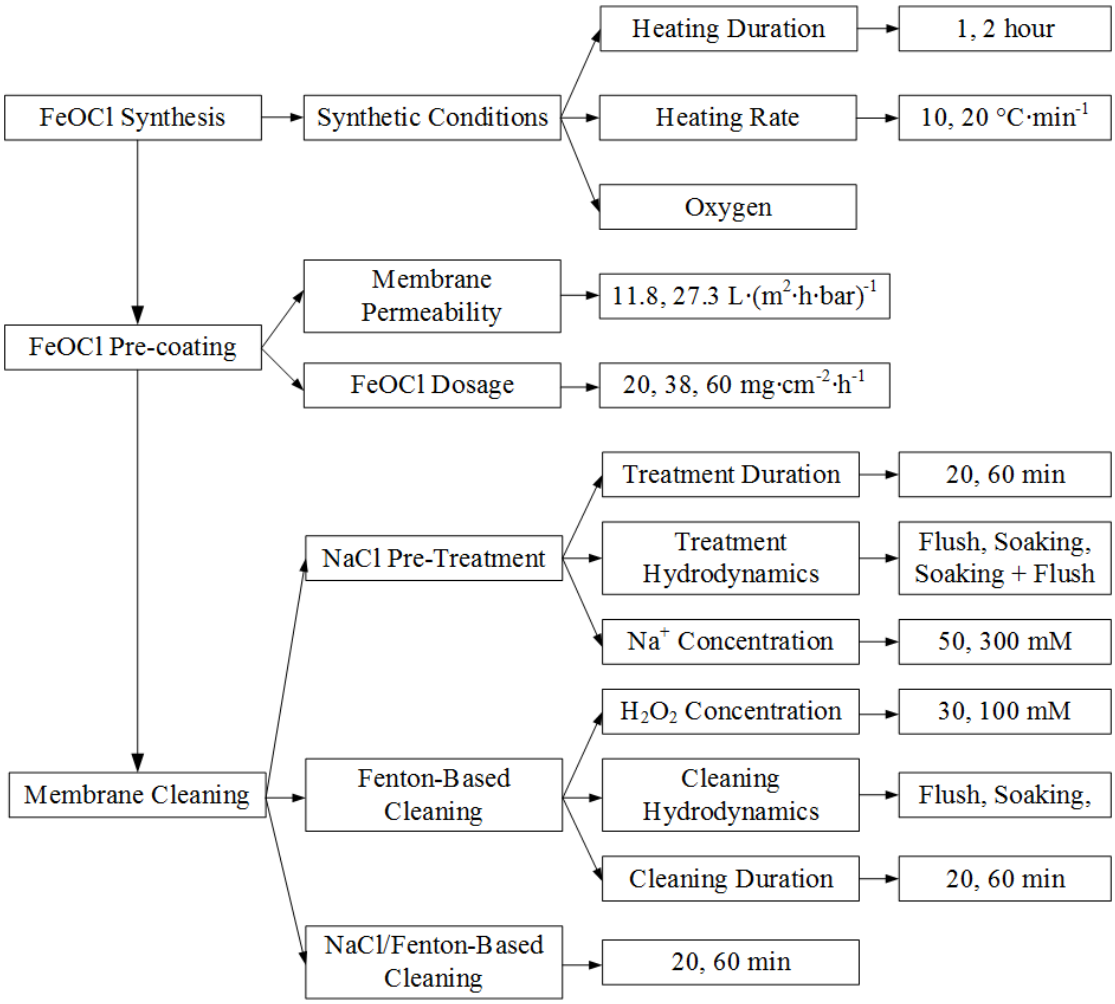

Figure 3.1: Flowchart of general experiment design.

3.2.1. Synthesis of FeOCl

This section complies with *Stage I*, which aims at synthesising FeOCl with high Fenton activity. The concerning synthetic condition was heating rate and heating duration. Regarding some publications (Sun et al. 2018, Zhang et al. 2017), the heating rate and heating time were set to be 20 °C·min^{-1} and 1 hour, respectively. In FeOCl synthesis, 10 g of $FeCl_3 \cdot 6H_2O$ powder, as the precursor, was put in a crucible. The precursor was heated at a rate of 20 °C·min^{-1} and maintained at 220 °C for 1 hour. The theoretical reaction equation was presented in *Eq. (2.4)*. The resulting product was naturally cooled to room temperature and manually grinded into small particles. The crystalline composition of the as-prepared FeOCl was characterised by X-ray diffraction (XRD) (X-ray facilities group, Faculty of 3ME, TU Delft). The product was analysed between 10° and 110° with a scan step of 0.3°·min^{-1} operating at 45 kV and 40 mA using Ca Kα radiation. The morphology and particle size of the synthesised FeOCl was determined by scanning electron microscopy (SEM) analysis (Faculty of Applied Science, TU Delft).

Batch experiments were conducted to determine the Fenton activity of the as-prepared product. The decolouration rate of methylene blue was measured by UV-vis spectrophotometry. It acted as an indicator to quantify the catalytic activity of the

synthesised FeOCl catalyst. The experiments were performed in duplicate. For each test, 100 mg FeOCl was dispersed in 100 mL demineralised water (1 g FeOCl·L^{-1}) by a 5-min sonication. Subsequently, 2 mL, 250 mg·L^{-1} methylene blue solution (5 mg·L^{-1}) was added to the solution, and the pH was adjusted to 3.3 by 1 M HCl. The system was continuously mixed by a magnetic stirrer, and the decolouration was initiated by dosing 0.3 mL H_2O_2 to the solution (30 mM). Aliquots (10 mL) of the reaction mixture were taken at 0, 1, 10, and 60 min after the beginning of the experiment. All samples were passed through 0.45 µm filters right after sampling. To inhibit the continuous degradation of methylene blue by the potentially dissolved ferric iron (Fe^{3+}), 0.1 mL 1 M tert-butanol solution (10 mM) was added to the samples. The absorbances of the samples were measured by a UV-Vis spectrophotometer at 660 nm. The decolouration rate was calculated by *Eq. (3.1)*.

$$\alpha_d = \frac{A_t}{A_0} \times 100\% \tag{3.1}$$

where a_d is the ratio of the absorbance of the sample taken at a specific time to the initial absorbance (%), A_t is the absorbance of the sample taken at sampling time t (A), where t is 1, 10, 60 min, in this case, and A_o is the initial absorbance of the sample taken at 0 min (A).

3.2.2. Preparation of FeOCl Suspension and Model Fouling Solution

The FeOCl suspension was prepared by dispersing 4 g of the as-prepared FeOCl catalyst in 1 L of demineralised water by a 10-min sonication as well as a 30-min stirring at 200 RPM. The system was settled for 10 min, and the precipitation was removed to improve the size uniformity of the particles in the suspension. The pH of the as-prepared suspension was around 3.20 at room temperature (around 20 °C). The suspension was continuously stirred at 200 RPM and was ready for pre-coating.

Artificial fouling solution comprised manufactured sodium alginate (Na-alginate) was used as model foulant to mimic EPS in municipal sewage. The total volume of the fouling solution was approximately 30 L, and the concentration was 0.8 g·L^{-1}. Sodium (5 mM) and calcium (3 mM) ions, were introduced, as mentioned in *Section 2.2.1*, to form interchain via charge screening and calcium bridging. The fouling solution was continuously stirring to avoid aggregation. The pH of the fouling solution was adjusted to 7 by 1 M HCl or 1 M NaOH. The organic loading of the artificial fouling solution was higher compared to practical municipal sewage to accelerate membrane fouling.

3.2.3. Ceramic Nanofiltration System

The filtration setup included: 1) fouling solution tank, 2) demineralised water and PEG solution tank; 3) FeOCl suspension vessel; 4) peristaltic dosing pump; 5) feed pump; 6) crossflow membrane module; 7) permeate collection vessel weighed by a scale which was interfaced with a computer; 8) computer that controlled the crossflow velocity and TMP via OSMO system; 9) recirculated pump for membrane cleaning; 10) cleaning solution vessel. The schematic experimental setup is illustrated in *Figure 3.2*. Overhead propeller stirrers were applied for the fouling solution and the FeOCl

suspension to avoid particle sedimentation or agglomeration. In the Ca-alginate fouling experiment and PEG filtration experiment, the generated concentrate was recirculated to the corresponding feed tank. In membrane cleaning experiment, the cleaning solution was recirculated to the cleaning solution vessel. In other cases, the concentrate was discharged into the sewer system. The permeate flux of the ceramic NF membrane was calculated based on the produced permeate volume, filtration time, and membrane active area.

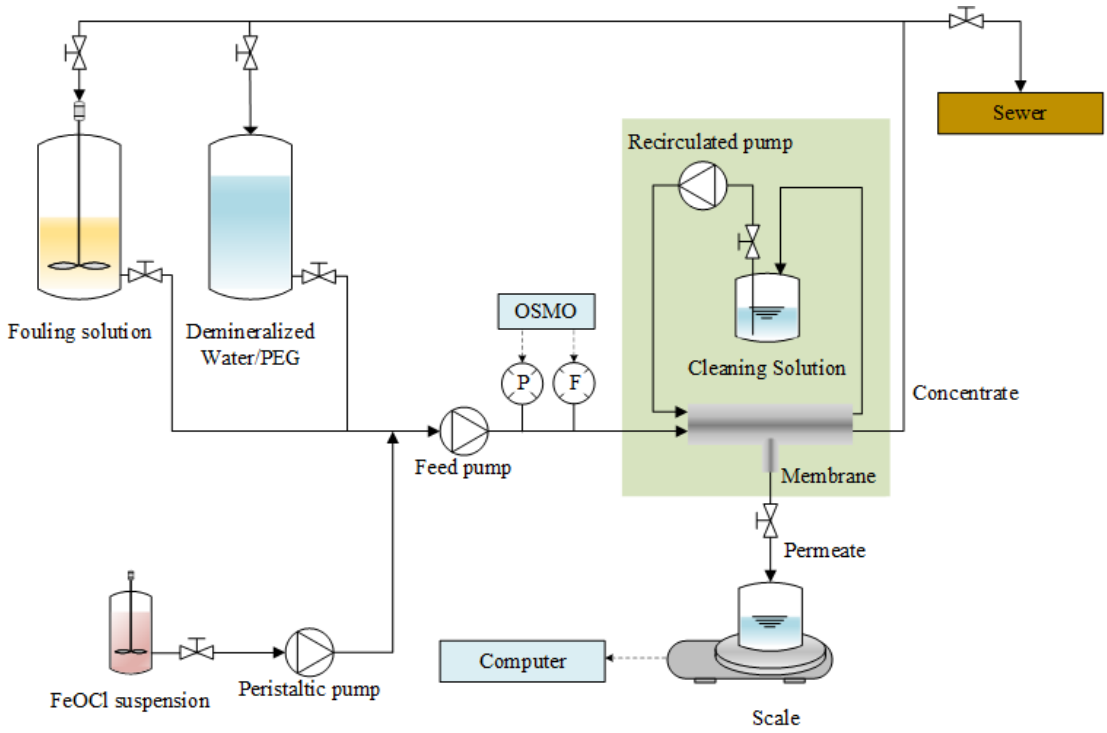

Figure 3.2: Experimental apparatus: The green box was the experimental configuration for membrane cleaning. During Ca-alginate fouling and PEG filtration, the concentrate was recirculated to the feed tank. In water flux test and FeOCl pre-coating, the concentrate was discharged into the sewer system.

3.2.4. Membrane Defect Detection

Usually, the quality of the membrane is determined by measuring the corresponding hydraulic permeability, molecular weight cut-off (MWCO), and defect. Size exclusion method is one of the most common ways to test membrane quality, and it is usually conducted by different size of polyethylene glycol (PEG). Due to the limitation of time and experimental equipment, only the hydraulic permeability and membrane defect were measured in this case. The hydraulic permeability of the membrane was determined by demineralised water filtration. Subsequently, a solution comprised 1000 Da PEG was fed to the membrane and membrane defect was determined by the percentage of the 1000 Da PEG that passed through the membrane. The measurement of the concentration of PEG was simplified via total organic carbon (TOC) analysis. According to the supplier, the MWCO of the applied membrane was 450 Da. The molecular weight of PEG used in this case is more than double compared with the MWCO of the membrane, and it is assumed to be entirely rejected by the membrane

(Kramer et al. 2019). All filtration experiments were conducted by constant pressure filtration at 3 bars. The 1000 Da PEG solution (1.2 g PEG·L^{-1}) was recirculated at 3 bars for around 30 min, and the permeate flux was recorded continuously. Detailed filtration conditions are listed in *Table B.3*. Feed and permeate were collected after obtaining a stable permeate flux. Retention of 1000 Da PEG can be determined by measuring the TOC of the collected feed and permeate samples, and yields the defects of the membrane (*Eqs. (3.2)-(3.3)*) (Kramer et al. 2019).

$$R_{PEG,1000Da} = 100\% - \frac{C_p}{C_f} \times 100\% \tag{3.2}$$

$$Defects = 100\% - R_{PEG,1000Da} \tag{3.3}$$

where $R_{PEG,\ 1000Da}$ denotes the retention of the largest PEG molecule, in this case, 1000 Da, by the membrane (%), C_p and C_f denote the TOC of PEG in the permeate and feed samples (mg C·L^{-1}), respectively, and *Defect* denotes the defect of the membrane (%).

3.2.5. FeOCl Pre-Coating

In FeOCl pre-coating, a laboratory-scale crossflow membrane filtration system, OSMO was used to deposit FeOCl to ceramic NF membranes (*Figure 3.2*). The concentration of the pre-coated material in the feed, crossflow velocity, and TMP affect the loading and efficiency of the pre-coating. Among them, the impact of concentration in pre-coating is dominant and is further discussed in *Section 4.2.2* (Anantharaman et al. 2020). A higher crossflow velocity generates a thinner pre-coated layer, whereas an overly low crossflow velocity results in nonuniformity of the pre-coated layer. Additionally, a high crossflow velocity increases the shear force at the vicinity of the membrane, which narrows the size distribution and decreases the size of the deposited particles (Anantharaman et al. 2020). It is consistent with the previous findings in our lab. Hence, a laminar crossflow (21.7 cm·s^{-1}) that minimised the flush away of FeOCl yet increased the uniformity of the pre-coated layer was applied. Moreover, a greater TMP results in a compact pre-coated layer with an increased specific loading due to the enhancement of drag force. However, the thickness of the pre-coated layer might be reduced attributed to the greater compaction (Lee et al. 1999). Thus, in this research, most pre-coating experiments were conducted at above 10 bars to improve the loading and durability of the pre-coated layer. Moreover, identical permeate production was controlled by adjusting TMP or filtration duration to ensure the comparability of the results. Detailed experimental conditions of this stage are tabulated in *Table B.2*.

In this case, FeOCl pre-coating was conducted by one-pass filtration to ensure the consistency of the property of the FeOCl suspension and the comparability of the results. The filtration protocol consisted of an initial baseline performance assessment, FeOCl pre-coating, and a second baseline performance assessment. The FeOCl suspension was dosed to the main feed stream by a peristaltic pump (*Section 3.2.2*). Subsequently, FeOCl pre-coated ceramic NF membrane was generated, indicating the deposition of FeOCl on the ceramic NF membrane. Fenton-based cleaning was catalysed by the FeOCl layer; thus, not only the Fenton activity of the catalyst but also the loading and uniformity of the pre-coated catalytic layer influenced the overall cleaning efficiency. In this stage, the effects of membrane permeability and dosage of

FeOCl suspension on the iron loading were explored to improve the pre-coating efficiency. The iron loading was quantified by recirculating 200 mL, 1 g·L^{-1} oxalic acid solution through the FeOCl pre-coated ceramic NF membrane (*Table B.3(5)*) to dissolve the pre-coated FeOCl from the membrane. The corresponding dissolved iron concentration was measured spectrophotometrically by iron test kits (100796) and spectrometer (NOVA 60 A Spectroquant®, 109752). Prior to the measurement, the samples were passed through 0.45 µm filters. In order to avoid human and accidental errors, duplications were conducted.

The pre-coating efficiency (α_c) is determined by *Eq. (3.4)*.

$$\alpha_c = \frac{M_a}{M_t} = \frac{C_{Fe\_OA} \times V_{OA}}{C_{Fe\_feed} \times V_p} \times 100\% = \frac{C_{Fe\_OA} \times V_{OA}}{C_{Fe\_feed} \times A_m \times \int_0^t J\, dt} \times 100\% \quad (3.4)$$

where a_c is the percentage of the mass of FeOCl deposited on the membrane surface compared to that was transported to the membrane (%), M_a and M_t are the actual and theoretical loading of FeOCl (mg), C_{Fe_OA} and C_{Fe_feed} are the iron concentration in the oxalic acid solution and the feed (mg·L^{-1}), V_{OA} is the volume of the oxalic acid solution, which is 200 mL, in this case, A_m is the active filtration area of the ceramic NF membrane (m^2), J is the permeate flux during the pre-coating (L·m^{-2}·h^{-1}), and t is the pre-coating time (h). In *Section 4.2.1*, the FeOCl concentration in the concentrate instead of that in the feed was used due to simplification. Theoretically, the iron loading is calculated by the iron concentration in the feed. Due to the high retention of FeOCl by NF membrane and easy accessibility of the concentrate, iron concentration in the concentrate was used as an alternative of the iron concentration in the feed.

From this stage, an optimal pre-coating condition was determined by achieving a proper iron loading with a relatively low iron loss in the concentrate. The thickness and uniformity of the FeOCl layer were characterised by SEM analysis (Faculty of Applied Science, TU Delft). The phase composition and spatial distribution of elements of the cross-section of a FeOCl pre-coated ceramic NF membrane were characterised by energy-dispersive X-ray spectroscopy (EDS) (Faculty of Applied Science, TU Delft). All the samples were dried for more than 24 h before the analysis. Microscopy required a breakage of the membrane; hence, one membrane pre-coated at the optimal condition was characterised by SEM and EDS analysis.

3.2.6. Membrane Fouling

Membrane fouling experiments were also conducted via the OSMO system (*Figure 3.2*). The filtration protocol for membrane fouling consisted of a water flux assessment of the pristine membrane, FeOCl pre-coating, a water flux assessment after pre-coating as the initial baseline, Ca-alginate fouling, membrane cleaning, and a water flux assessment after membrane cleaning as the second baseline. The membrane cleaning process is elaborated in *Section 3.2.7*. Permeate flux was affected by temperature; thus, temperature correction was necessary for flux adjustment (*Eqs. (3.5)-(3.6)*) (Mulder 2012). The operational conditions for the initial water flux test and the first and second baseline assessments were identical (*Table B.3(1)*). Hence the flux decline (*Eq. (3.7)*) and flux recovery (*Eq. (3.8)*) could be determined by comparing the measured water fluxes.

$$J_{20°C} = J \cdot e^{-0.0239 \cdot (T-20)} \quad (3.5)$$

$$L_{20°C} = \frac{J_{20°C}}{\Delta P} \quad (3.6)$$

where $J_{20°C}$ and $L_{20°C}$ are the temperature-corrected permeate flux and permeability at 20 °C ($L \cdot (m^2 \cdot h)^{-1}$ and $L \cdot (m^2 \cdot h \cdot bar)^{-1}$), T is the temperature recorded in the process (°C), J is the permeate flux recorded in the process ($L \cdot (m^2 \cdot h)^{-1}$), and ΔP is the operating TMP of the process (bar). Permeate fluxes and permeabilities were corrected to 20 °C.

$$Flux\ decline = \frac{J_{ini} - J_{end}}{J_{ini}} \times 100\% \quad (3.7)$$

where *Flux decline* denotes the decline of water flux due to pre-coating experiment or fouling experiment (%), and J_{ini} and J_{end} denote the pure water flux prior to the test and the flux at the end of the test, respectively ($L \cdot (m^2 \cdot h)^{-1}$).

All filtration experiments were conducted by a constant pressure system at room temperature. Ca-alginate fouling was performed at a turbulent condition at 3 bars to mitigate membrane fouling *(Table B.3(4)*). Comparable amounts of permeate were generated in each fouling process to ensure the comparability of the results. The top surfaces and cross-sections of a Ca-alginate fouled FeOCl pre-coated ceramic NF membrane was characterised by SEM analysis (Faculty of Applied Science, TU Delft). The thickness of the fouling layer at different locations was identified. Besides, it might reveal the interaction between the Ca-alginate fouling layer and the FeOCl pre-coated ceramic NF membrane.

3.2.7. Membrane Cleaning

In *Stage III*, NaCl pre-treatment, Fenton-based cleaning and NaCl/Fenton synergistic cleaning were performed on Ca-alginate fouled FeOCl pre-coated ceramic NF membrane. As mentioned in *Section 2.5*, the efficiency of NaCl pre-treatment was evaluated by flux recovery. The experimental setup of the membrane cleaning experiment was displayed in the green box of *Figure 3.2*. The efficiencies of NaCl pre-treatment under different chemical (Na^+ concentration) and physical (forward flush mode, soaking mode, and cleaning duration) conditions were determined. No permeate was generated during the forward flush, and no pH adjustment was conducted in NaCl pre-treatment. Detailed experimental conditions for NaCl pre-treatment are tabulated in *Table B.4*. The efficiencies of Fenton-based cleaning were evaluated at various chemical (chemical composition of the cleaning solution and H_2O_2 concentration) and physical (forward flush mode, soaking mode, and cleaning duration) conditions. In these experiments, the pH of the cleaning solution was adjusted to 3.3. The synergistic effect between NaCl and Fenton oxidation was evaluated by comparing the cleaning efficiencies of membrane cleaned by the mixture of $NaCl/H_2O_2$ solution. The contribution of hydroxyl radicals was evaluated by measuring the Fenton-based cleaning efficiencies with the presence of tert-butanol. The additional ·OH scavenger might diminish the radical effect on foulant degradation (He et al. 2016). Detailed membrane cleaning conditions are tabulated in *Table B.5*. Due to time limitation, the experiments in this stage were conducted once.

The pure water flux recovery of membrane cleaning is calculated by *Eq. (3.8)*.

$$Flux\ recovery = \frac{J_c - J_f}{J_{ini} - J_f} \times 100\% \quad (3.8)$$

where *Flux recovery* is the pure water flux recovery after cleaning (%), J_{ini} is the pure water flux of FeOCl pre-coated ceramic NF membrane prior to fouling ($L \cdot (m^2 \cdot h)^{-1}$), J_f is the flux after fouling ($L \cdot (m^2 \cdot h)^{-1}$), and J_c is the pure water flux after membrane cleaning ($L \cdot (m^2 \cdot h)^{-1}$).

4 RESULTS AND DISCUSSIONS

4.1. RESULTS OF FeOCl SYNTHESIS

In this stage, the effects of heating duration, heating rate, and the participation of oxygen on the catalytic activity of the as-synthesised FeOCl were investigated. A synthetic condition produced a highly active catalyst was explored to improve the efficiency of the subsequent Fenton-based cleaning. The influence of chloride ions on Fenton activity was quantified to evaluate the feasibility of the proposed NaCl/Fenton-based cleaning.

4.1.1. Effect of Synthetic Conditions

Firstly, the effect of heating duration on the Fenton activity of FeOCl catalysts was explored. Inspired by preliminary experiments in our lab, two batches of $FeCl_3 \cdot 6H_2O$ were subsequently heated in an oven at a heating rate of 10 °C·min^{-1} to 220 °C for 1 and 2 hours, respectively. Detailed experimental conditions are tabulated in *Table B.1(1&2)*. The corresponding products were cooled to ambient temperature and manually grinded into powder. The Fenton activity of the as-synthesised FeOCl was determined according to the Fenton-based decolouration rate of methylene blue.

The Fenton-based decolouration catalysed by FeOCl synthesised at various conditions is depicted in *Figure 4.1*. The Fenton activity of FeOCl sintered for 1 hour was higher than that sintered for 2 hours. Zhang et al. (2017) stated that a certain amount of iron hydroxides was generated during the heating process. Hence, the synthesised product was a complex comprising of FeOCl and iron hydroxide. They also reported that the FeOCl content reduced along with the increase of heating duration owing to the transformation of FeOCl to iron hydroxides. In this research, the impurity of the product was visualised by the black surface (*Figure C.1(a)*). The FeOCl content affected the Fenton activity of the product from two aspects. Firstly, FeOCl performed a superior H_2O_2 decomposition capacity among a variety of iron-containing catalysts (Yang et al. 2013). A reduction of FeOCl content reduced the catalytic activity of the product. Secondly, the efficiency of a heterogeneous Fenton oxidation depended on the overall surface area of the catalyst (He et al. 2016). As explained in *Section 2.4.2*, the amount of adsorption site was positively correlated to the surface area of the FeOCl nanoparticles. An improvement of adsorption accelerated the generation of ·OH radicals and enhanced decolouration. The surface area of FeOCl nanoparticles was greater than the surface area of iron hydroxide nanoparticles (Zhang et al. 2017). Therefore, an extension of heating duration reduced the FeOCl content in the as-synthesised catalyst, which correspondingly reduced the Fenton activity and surface area of the catalyst and resulted in a lower decolouration rate. Nevertheless, preliminary experiments in our lab showed that an overly short heating duration led to a structurally unstable product. The research of Zhang et al. (2017) also revealed that a short thermal treatment process introduced many iron ions that would be crystallised during the extension of calcination. Hence, one-hour was selected to generate a product with a stable structure and high FeOCl content.

Secondly, the influence of the heating rate was determined. Zhao et al. (2016) reported that a rapid heating process drove the exfoliation of the layered metal hydrous chloride crystal to generate the corresponding two-dimensional (2D) metal oxychlorides nanosheets. Zhang et al. (2017) stated a successful production of highly reactive FeOCl nanosheets from $FeCl_3 \cdot 6H_2O$ by rapid thermal annealing. An increased heating rate resulted in a reduction of the thickness of the synthesised FeOCl nanosheet as well as an enhancement of Fenton activity. Inspired by these researches, the heating rate was increased from 10 °C·min^{-1} to 20 °C·min^{-1}. Detailed experimental conditions are tabulated in *Table B.1(1&3)*. However, the results showed that the Fenton activity of FeOCl synthesised at a heating rate of 20 °C·min^{-1} was only two-third of the Fenton activity of FeOCl synthesised at a heating rate of 10 °C·min^{-1} (*Figure 4.1*). According to *Eq. (2.4)*, oxygen did not participate in the synthesis of FeOCl, whereas the crucible was open in the experiments mentioned above. The excess oxygen might improve the formation of impurities and contribute to the reduction of FeOCl content. In a thermal process with a greater heating rate, the exfoliation of the layered $FeCl_3 \cdot 6H_2O$ might be enhanced, and the overall surface area of the intermediate might be increased. In an open crucible, the batch with a larger overall surface area was more reactive with oxygen. Hence, a more rapid heating process in an open crucible resulted in a product with decreased FeOCl content and lower Fenton activity.

Lastly, the participation of oxygen was investigated. Alumina boat capped on a crucible was used to eliminate the participation of oxygen (*Figure C.1(e)*). FeOCl, which was synthesised in an alumina capped crucible with a heating rate of 20 °C·min^{-1} to 220 °C for 1 hour, performed a 98% decolouration of methylene blue in 1 hour (*Table B.1(4) and Figure 4.1*). The elimination of oxygen in FeOCl synthesis was an essential factor that improved the catalytic activity of the synthesised catalyst. XRD analysis was conducted to characterise the crystalline structure of the product that performed the highest activity (*Figure 4.2*). The measured XRD pattern of the product was displayed in black. Background subtraction and small displacement correction were conducted. The intensity scales were plotted in square root to better display the small peaks. The coloured sticks presented the peak positions and intensities of the possibly presented crystalline phase in the sample (ICDD pdf4 database). The synthesised FeOCl presented complex diffraction peaks, which matched with that of standard FeOCl and standard iron chloride hydrate ($FeCl_2 \cdot 4H_2O$). The result confirmed successful synthesis of a product with high FeOCl content. Due to a lack of pre-treatment of the synthesised product, a small amount of $FeCl_2 \cdot 4H_2O$ was presented as an impurity. Regarding the high catalytic activity, FeOCl synthesised in an alumina capped crucible with a heating rate of 20 °C·min^{-1} to 220 °C for 1 hour was applied in the following experiments.

The SEM analysis was conducted to reveal the morphology of the synthesised FeOCl. It was a lath-like particle with a few micrometres in length and around one µm in width (*Figure 4.6(b)*). The size of the synthesised FeOCl particles in bulk might be larger than that was deposited on the membrane (Anantharaman et al. 2020). Herein, the morphology of the FeOCl particles was different from literature which proposed plate-

like or granular FeOCl nanoparticles (Sun et al. 2018, Yang et al. 2013, Zhang et al. 2017).

Despite various synthetic conditions, similar patterns of decolouration curve were observed. Methylene blue underwent a highly efficient decolouration in the first minute and followed by a pattern similar to adsorption. The most reactive FeOCl presented the most rapid decolouration in the first minute. The outstanding initial decolouration rate was performed prominently for FeOCl synthesised at 20 °C·min^{-1} (alumina capped crucible). Over 80% of methylene blue was degraded in the first minute (*Figure 4.1*). The blank experiment (*Table B.1(7)*) demonstrated the adsorption of methylene blue by FeOCl particles. As mentioned in *Section 2.4.2*, in a heterogeneous Fenton reaction, the adsorption of organic molecules to the catalyst is the rate-determining process (Zhang et al. 2017). The low initial adsorption rate (~1%) yet high initial decolouration rate (> 80%) might be attributed to the efficient homogeneous Fenton oxidation induced by surface leached iron. Hartmann et al. (2010) proposed that 50 to 80 mg·L^{-1} of iron ions could initiate a homogenous Fenton reaction. Whereas, Kwan et al. (2002) reported that 0.34 mg·L^{-1} of leached ferric ion could already start a homogeneous Fenton reaction. In this case, Fenton oxidation was performed in acidic condition and around 50 mg·L^{-1} of iron ions leached from the complex of FeOCl and $FeCl_2{\cdot}4H_2O$. The leached iron ions might be depleted in the first minute, which induced homogeneous Fenton reaction and contributed significantly to the decolouration of methylene blue. The following slow decolouration corresponded to the blank adsorption curve might indicate a heterogeneous Fenton reaction induced by FeOCl particles.

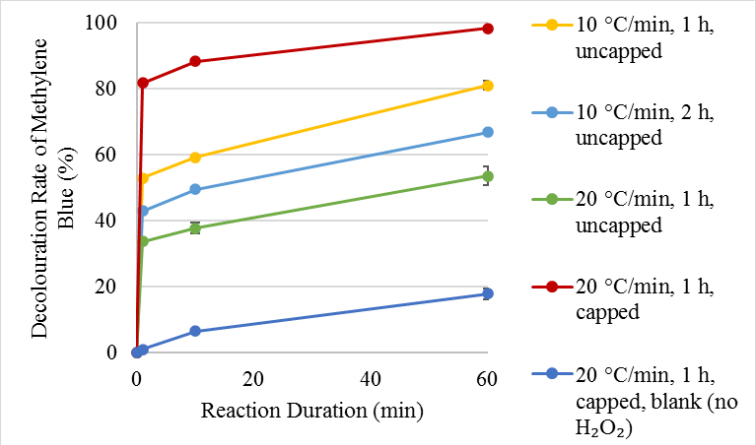

Figure 4.1: Effect of synthetic conditions on the Fenton activity of the synthesised FeOCl. Synthetic conditions: heating rate: 10 and 20 °C·min^{-1}, respectively, calcination temperature: 220 °C, calcination duration: 1 and 2 hours, respectively. The elimination of oxygen was conducted by capping the crucible with an alumina boat (*Figure C.1(e)*). Fenton activity test conditions: methylene blue concentration: 5 mg·L^{-1}, pH = 3.3, H_2O_2 concentration: 30 mM. The blank measured the adsorption of methylene blue by FeOCl synthesised at the heating rate of 20 °C·min^{-1} for 1 hour without the addition of H_2O_2.

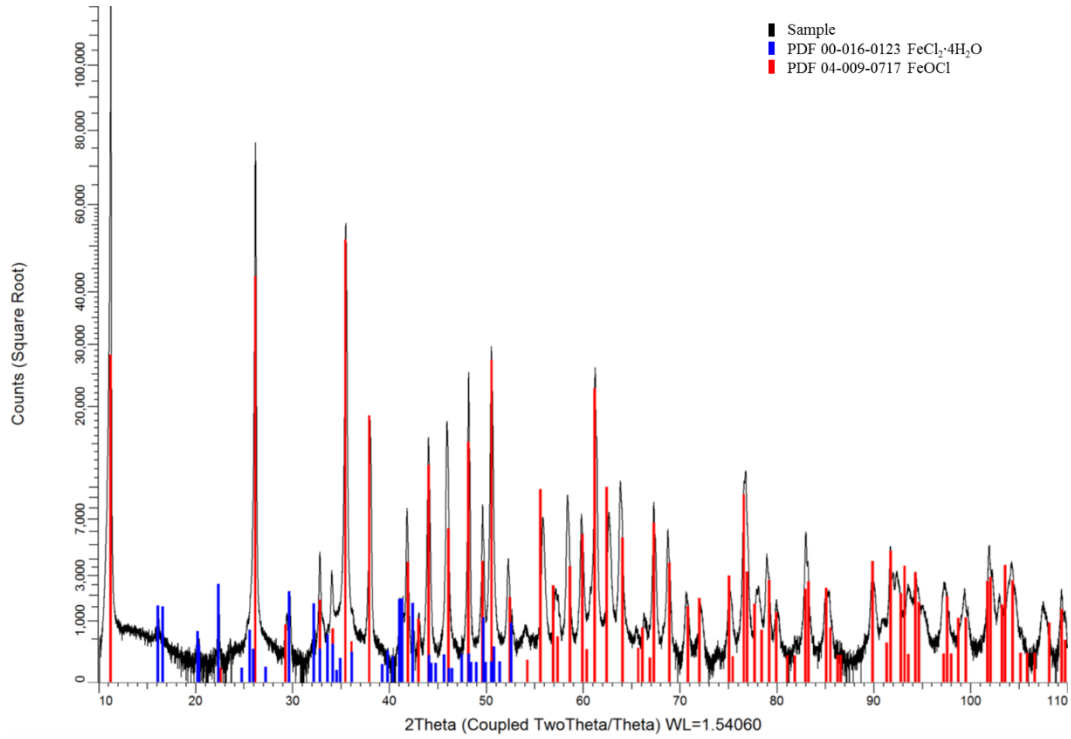

Figure 4.2: XRD pattern of the as-synthesised FeOCl. Background subtraction and small displacement correction were conducted. The intensity scales were plotted in square root to better display the small peaks.

4.1.2. Effect of Chloride Ions

The effect of Cl^- on FeOCl catalysed Fenton reaction was determined by dosing a certain amount of NaCl to the reaction system. The most reactive FeOCl was used. Detailed experimental conditions are tabulated in *Table B.1(4-6)*. Similar decolouration patterns were observed among different dosage of NaCl. The effect of Cl^- on the Fenton oxidative decolouration of methylene blue is plotted in *Figure 4.3*. Although the addition of Cl^- slightly decreased the decolouration rate in the whole process, a 70% decolouration was achieved in the first minute, and a 90% decolouration was accomplished in one hour (*Figure 4.3*). The effect of high concentration of Cl^- on FeOCl catalysed decolouration was examined by increasing the Cl^- dosage from 50 mM to 300 mM. The six-fold concentrated Cl^- solution did not show a retardance on the Fenton oxidation of methylene blue. This finding was consistent with previous researches which stated that the inhibitory effect of Cl^- was mainly observed at low pH (pH 1-2.5) and the hindrance of Cl^- can be diminished by bringing the pH up to 3 (He et al. 2016, Machulek Jr et al. 2007).

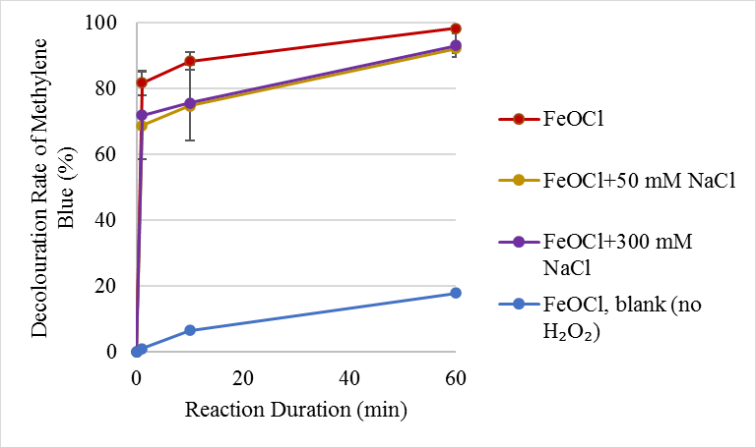

Figure 4.3: Effect of chloride ion on the Fenton activity of the synthesised FeOCl. Synthetic conditions: heating rate: 20 °C·min^{-1}, calcination temperature: 220 °C, calcination duration: 1 hour. All used FeOCl was synthesised in a capped crucible to eliminate the participation of oxygen. Fenton reaction conditions: methylene blue concentration: 5 mg·L^{-1}, pH=3.3, H_2O_2 concentration: 30 mM. The blank measured the adsorption of methylene blue by FeOCl without the addition of H_2O_2.

4.2. RESULTS OF FeOCl PRE-COATING

A highly reactive Fenton-like catalyst was obtained in *Section 4.1*. Fenton-based cleaning was performed on the pre-coated FeOCl layer on a ceramic NF membrane. Thus, not only the activity of the catalyst but also the loading and uniformity of the pre-coated catalytic layer influenced the overall cleaning efficiency. In this stage, the effects of membrane permeability and FeOCl dosage on the iron loading were explored to improve the pre-coating efficiency. The measured pH of the bulk FeOCl suspension was around 3.1 at room temperature (around 20 °C), and the measured iron particle concentration was 643 mg Fe·L^{-1}. Due to the small amount of impurity in the as-prepared catalyst (*Section 4.1.1*), the corresponding concentration was represented in terms of iron concentration.

4.2.1. Effect of Pristine Membrane Permeability

Ceramic NF membranes with relatively low and high permeability, 12 and 27 L·(m^2·h·bar)$^{-1}$, respectively, were used to investigate the effect of pristine membrane permeability on the iron loading. Pre-coating was conducted at constant TMP, and an identical amount of permeate was generated by adjusting TMP to ensure the comparability of the results. Iron loading and pre-coating efficiency are plotted in *Figure 4.4*. For low- and high-permeability membrane, comparable loading and pre-coating efficiency were obtained. In both conditions, around 0.13 mg·cm^{-2} of iron was deposited on the ceramic NF membrane, and around 0.17 mg·cm^{-2} of iron was lost in the concentrate (*Figure 4.4(a)*). The specific iron loading is the total iron loading divided by the membrane area (16.3 cm^2). The iron loading largely relied on the permeate flux, and crossflow velocity (Anantharaman et al., 2020), which determined the mass transported to the membrane surface (nominal FeOCl loading) and the mass

swept away from the membrane (FeOCl loss), respectively. In this case, identical permeate production and crossflow velocity were conducted; hence, comparable iron loading and pre-coating efficiency were achieved. The results revealed that in a pre-coating conducted by pressure-driven filtration, the loading of the targeted material could be accustomed by the productivity of permeate. The amount of permeate can be controlled by adjusting TMP or filtration duration.

The pre-coating on the low-permeability membrane was faintly more efficient than that on the high-permeability membrane (*Figure 4.4(b)*). The corresponding pre-coating efficiencies were 45.76% and 40.90%, respectively. This result was likely due to the much higher applied TMP (20 bars) for the low-permeability membrane compared to that for the high-permeability membrane (10 bars), which contributed to a thinner yet denser pre-coated layer with a higher specific mass (Anantharaman et al. 2020). It was consistent with the slightly higher iron loading on the low-permeability membrane compared to that on the high-permeability membrane (*Figure 4.4(a)*). It was noticed for both cases that more than half of the feeding FeOCl was lost in the pre-coating process. It was ascribed to the one-pass filtration applied in this research. In the pre-deposition process, FeOCl particles were physically stacked and compacted by the TMP with no chemical bonding formed. Hence, the catalytic layer was only formed by van der Waals and electrostatic interactions. Moreover, iron loss (caused by back-diffusion) and iron deposition (caused by permeation) might reach a dynamic equilibrium after a particular pre-coating duration, which might impede the growth of iron loading (Anantharaman et al. 2020).

The reduction of permeability in the pre-coating process is listed in *Figure 4.4(c)*. The flux behaviour of pre-coating is depicted in *Figure D.1(a)*. A higher TMP led to a lower permeability decline, which contradicted the finding summarised by Anantharaman et al. (2020). It might be due to the disparity of membrane permeability or the potential defects for high-permeability membranes. Conclusively, the FeOCl layer introduced a minor extra resistance to the membrane and hardly deteriorated the membrane permeability. This result was likely to be attributed to that the size of the FeOCl particles (a few micrometres in length and one μm in width (*Figure 4.6(b)*) was much larger than the pore of ceramic NF membrane (0.9 nm, supplied by the manufacturer). The consequent cake deposition of FeOCl was expected to provide abundant porous channels for water permeation, which maintained the membrane permeability.

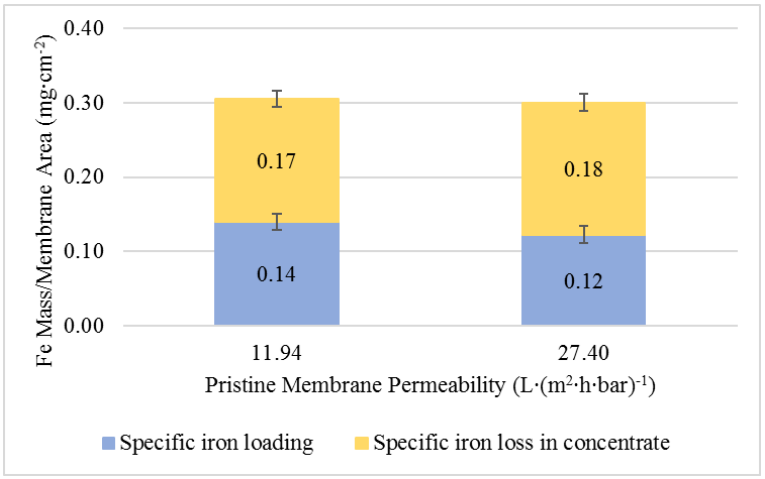

(a)

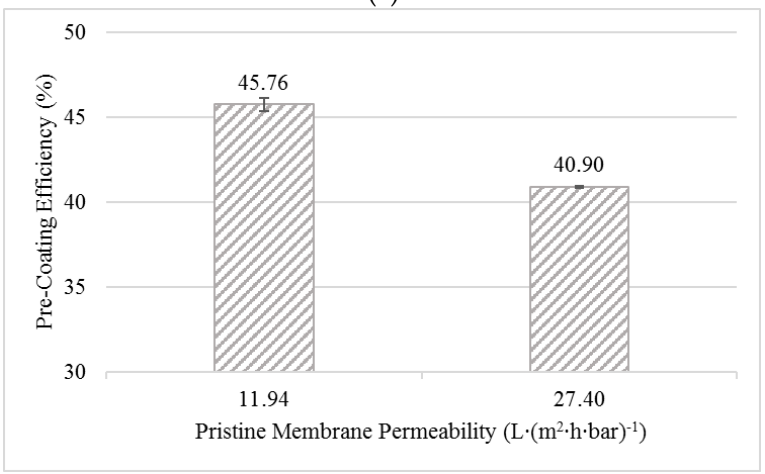

(b)

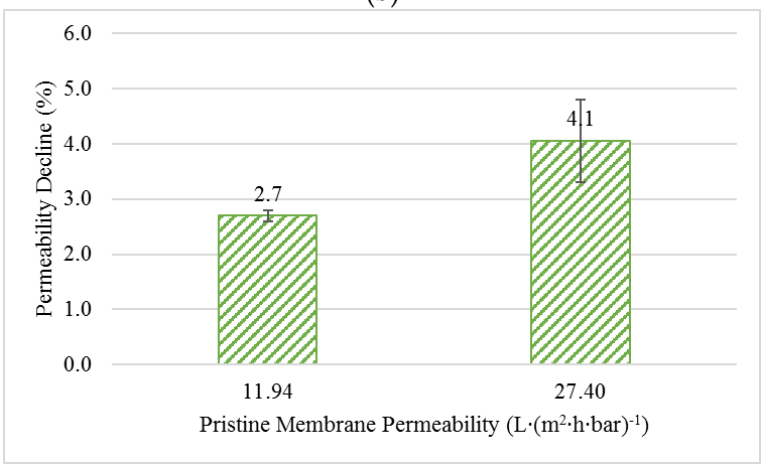

(c)

Figure 4.4: Influence of pristine membrane permeability on FeOCl pre-coating: (a) the specific mass of iron deposition and lost in pre-coating, (b) pre-coating efficiency, and (c) permeability decline. The specific mass was the iron mass divided by the membrane area (16.3 cm^2). Conditions for pre-coating experiment: iron concentration in concentrate: 22.78 mg $Fe \cdot L^{-1}$, crossflow velocity: 0.22 $m \cdot s^{-1}$, pre-coating duration: 30 min. Pre-coating efficiencies were calculated based on *Eq.* (3.4).

4.2.2. Effect of FeOCl Concentration

The impact of the feeding concentration of FeOCl on iron loading was researched in this section. The pre-coating duration was shortened to 10 min due to the time limitation. All the pre-coating experiments in this section were performed on the same membrane with a relatively low permeability (11.6-13.4 $L\cdot(m^2\cdot h\cdot bar)^{-1}$). FeOCl suspension was dosed to the mainstream by a peristaltic pump. The concentration of FeOCl in the concentrate was linearly correlated to the dosage of FeOCl suspension (*Figure D.2*) ($y=0.2262x-0.5972$, $R^2=0.9885$).

The effect of FeOCl concentration on iron loading and pre-coating efficiency and the corresponding permeability decline are plotted in *Figure 4.5*. It can be seen that the specific iron loading was linearly correlated to the FeOCl concentration ($y=0.0036x+0.0017$, $R^2=0.9944$) (*Figure 4.5(a)*). An increased FeOCl concentration improved the iron deposition and accelerated the formation of the FeOCl layer. This result was in accordance with previous findings summarised by Anantharaman et al. (2020). They concluded that the feeding concentration of the pre-coated material had a positive relationship with the loading of the pre-coated layer. Additionally, they proposed that the increase in feeding concentration enhanced the mechanical strength of the pre-coated layer.

Due to the shortening of pre-coating duration and the resulting insufficient mixing, the measured iron concentration in the concentrate was less than that in *Section 4.2.1*. The consequent pre-coating efficiency calculated by iron concentration in the concentrate exceeded 100% (*Eq. (3.4)*). It was assumed that a larger percentage of FeOCl in the feed was deposited on the membrane at the initial stage of pre-coating (Anantharaman et al. 2020). It might enlarge the difference between the iron concentration in the concentrate and that in the feed. Hence, the pre-coating efficiency of this stage was calculated by the theoretical iron concentration in the feed. The corresponding pre-coating efficiency against various FeOCl concentration is plotted in *Figure 4.5(b)*. The increase in feeding concentration of FeOCl improved the pre-coating efficiency. The ratio of three different FeOCl dosage was 1.0 : 1.9 : 3.0, and the corresponding ratio of the pre-coating efficiency was 1.0 : 1.0 : 1.1. A more considerable improvement of pre-coating efficiency (from 39.19% to 42.68%) was observed by increasing the FeOCl dosage from 38 to 60 $mg\cdot cm^{-2}\cdot h^{-1}$.

The decreased membrane permeability under different FeOCl dosage is displayed in *Figure 4.5(c)*. The flux behaviour of the pre-coating process is displayed in *Figure D.1(b)*. The permeabilities of membranes decreased with the increase of the dosage of FeOCl. This result was consistent with the suggestion of Anantharaman et al. (2020) which indicated that an increased feeding concentration introduced a greater extra resistance to the membrane. The permeability decline was comparable to that in *Section 4.2.1*. This was attributed to the shortening of the pre-coating duration, which reduced the compaction of the pre-coated layer. Compaction contributed to extra resistance and a permeability decline (Anantharaman et al. 2020). The corresponding ratio of permeability decline to three FeOCl dosage was 1 : 1.1 : 1.6. Membrane experienced 46% of permeability decline by increasing FeOCl dosage from 38 to 60 $mg\cdot cm^{-2}\cdot h^{-1}$.

Figure 4.6 displays SEM images of the top surface and cross-section of pristine ceramic NF membrane, FeOCl pre-coated ceramic NF membrane, and Ca-alginate fouled FeOCl pre-coated ceramic NF membrane. Lath-like FeOCl particles with around 10 µm in length and around 1 µm in width were observed at the top surface of the FeOCl pre-coated ceramic NF membrane. The FeOCl particles were much larger than the pore of ceramic NF membrane (0.9 nm), and hence, a cake layer with randomly dispersed pores (around 1 µm) was observed on the membrane surface. Yang et al. (2013) reported that flat-like FeOCl particles with 0.3-10 µm in length, and 100-300 nm in thickness were successfully synthesised by conventional chemical-vapour transition method. Zhang et al. (2017) stated a synthesis of FeOCl nanosheets with a thickness of 15-20 nm via a facile, rapid thermal annealing method. Sun et al. (2018) applied a facile and scalable thermal-treatment method to immobilise the catalytic FeOCl on a PVDF UF membrane and observed granular FeOCl particles with 1-5 nm in diameter. They ascribed the unique morphology of the FeOCl particles to the pre-coating of $FeCl_3$ to the membrane.

The cross-sections of a FeOCl pre-coated ceramic NF membrane at different locations are displayed in *Figure D.3(a&b)*. Uneven distribution of FeOCl was observed in a horizontal tubular membrane, resulting in FeOCl layer with a thickness of 4.97 µm and 7.35 µm at different locations on a membrane. The nonuniformity of the FeOCl layer might be due to gravity and/or the relatively low crossflow velocity (21.7 $cm \cdot s^{-1}$, laminar flow) applied in the experiments which resulted in a decrease of the thickness of the pre-coated layer from the bottom to the top in a tubular membrane (Pan et al. 2015). The pre-coated layer increased the surface roughness of the membrane (*Figure 4.6(a&b)*), which might increase the fouling susceptibility of the membrane (Zhao and Yu 2015). The EDS analysis reveals the phase composition and spatial distribution of the cross-section of a FeOCl pre-coated ceramic NF membrane (*Figure 4.7*). The atomic-level elemental mapping confirmed the composition of the pre-coated layer, which was FeOCl.

In conclusion, a low feeding concentration decreased the iron loading on the membrane. A high feeding concentration and/or a low crossflow velocity increased the nonuniformity of the pre-coated FeOCl layer. Regarding the scarcity of the synthesised FeOCl catalyst, a FeOCl dosage of 38 $mg \cdot cm^{-2} \cdot h^{-1}$ was conducted in the following pre-coating experiments. The pre-coating was conducted in 30 min to avoid uneven distribution of FeOCl particles in the system.

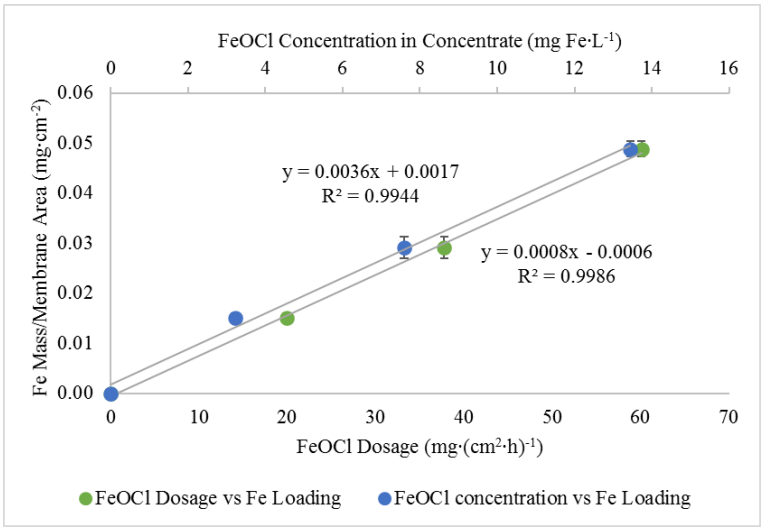

(a)

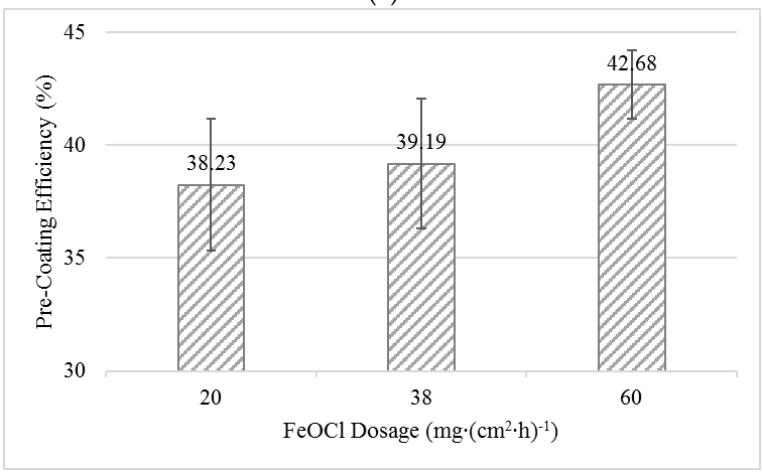

(b)

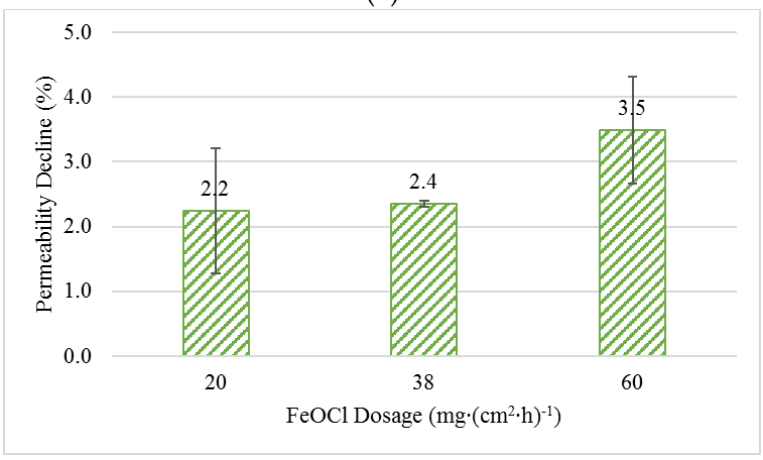

(c)

Figure 4.5: Influence of dosage of FeOCl on the iron loading on the membrane: (a) iron loading, (b) pre-coating efficiency, and (c) permeability decline. Pre-coating conditions: FeOCl suspension: 643 mg Fe·L^{-1}, crossflow velocity: 0.22 m·s^{-1}, duration: 10 min. Pre-coating efficiencies were calculated based on *Eq. (3.4)*. Due to the short pre-coating duration, the calculated feeding concentrations rather than the measured concentrations of the concentrate were used to calculate the pre-coating efficiencies.

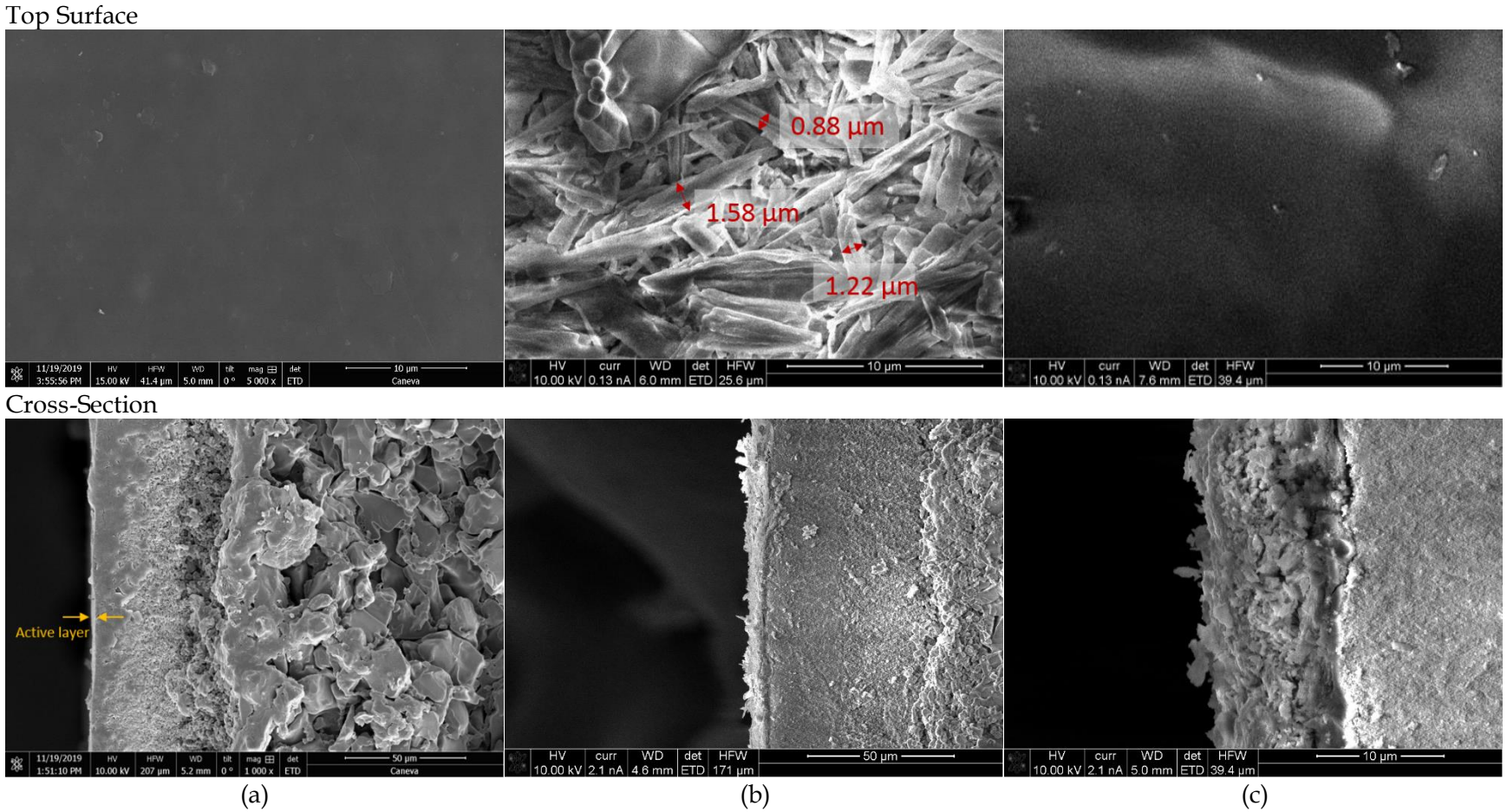

Figure 4.6: SEM images depicting the top surfaces and cross-sections of the membrane: (a) pristine ceramic NF membrane, (b) FeOCl pre-coated ceramic NF membrane, and (c) Ca-alginate fouled FeOCl pre-coated ceramic NF membrane.

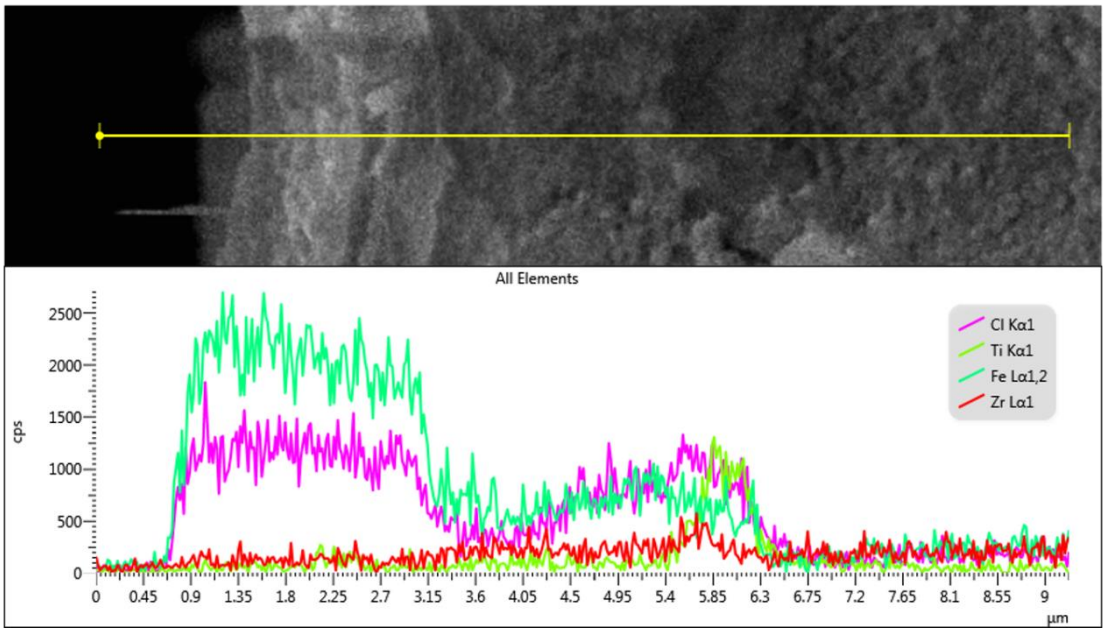

Figure 4.7: EDS analysis: the cross-section of a FeOCl pre-coated ceramic NF membrane.

4.3. RESULTS OF MEMBRANE CLEANING

In this stage, NaCl treatment and FeOCl catalysed Fenton oxidation were applied to clean Ca-alginate fouled FeOCl pre-coated ceramic NF membranes. The cleaning efficiency was determined according to the recovered demineralised water flux after cleaning. The cleaning efficiencies of only NaCl pre-treatment and only Fenton-based cleaning were investigated individually. The synergistic effect between NaCl and Fenton-based cleaning was examined by cleaning the Ca-alginate fouled membrane with a mixture of NaCl and H_2O_2. The effects of cleaning duration, cleaning hydrodynamic conditions, and chemical concentration on cleaning efficiency were studied. The corresponding underlying cleaning mechanisms were explored.

Prior to membrane cleaning, the characterisation of a Ca-alginate fouled FeOCl pre-coated ceramic NF membrane was conducted by SEM analysis (*Figure 4.6(c)*). The top surface of a Ca-alginate fouled membrane demonstrated a compact gel-like fouling layer on the membrane. Similar to the thickness of the FeOCl layer, the thickness of the fouling layer varies according to different locations in the tubular membrane (*Figure D.3(c&d)*). The thickness of the fouling layer ranged from 2.50 µm to 8.23 µm. It might also be ascribed to gravity and the crossflow velocity (86.6 $cm \cdot s^{-1}$, turbulent flow) applied in the fouling process (Pan et al. 2015).

4.3.1. NaCl Pre-Treatment: Effect of Treatment Conditions

The presence of Ca^{2+} in alginate solution enhanced membrane fouling by forming membrane-Ca-alginate and alginate-Ca-alginate interchain (Li et al. 2020, You et al. 2020). A resulting compact gel-like layer was formed on the membrane, which caused a decline of membrane permeability (Mohammad et al. 2015, Wang et al. 2014).

Moreover, according to the previous experiments in our lab, the gel-like layer impeded the diffusion of cleaning chemicals and, consequently, reduced the cleaning efficiency (*Figure 2.1*). Lee and Elimelech (2007) confirmed the swelling of the fouling layer by NaCl induced Na-Ca ion exchange. Preliminary experiments in our lab confirmed that NaCl soaking recovered part of the permeate flux of a Ca-alginate fouled FeOCl pre-coated ceramic NF membrane. Though in those cases, FeOCl layer was chemically immobilised on the ceramic NF membrane by thermal treatment.

In this section, NaCl treatments were performed on Ca-alginate fouled FeOCl pre-coated ceramic NF membranes. FeOCl was pre-coated to the membrane surface via a pressure-driven crossflow filtration. Different from the previous experiments, in this study, a physically deposited porous FeOCl layer was pre-coated to the membrane surface. The effects of cleaning hydrodynamics, cleaning duration and Na^+ concentration were investigated. The catalytic durability of FeOCl was confirmed by Yang et al. (2013) and Zhang et al. (2017). The mechanical durability of the pre-coated FeOCl layer was evaluated by measuring the iron detachment during NaCl pre-treatment. For a membrane with defect, the potential blocking or adsorption of foulants to the cracks increases the difficulties of foulant detachment and, consequently, decreases the NaCl treatment efficiency. In this section, membrane defect was not detected; however, 16 out of 17 experiments were conducted by one membrane. Hence, the experimental results were regarded as comparable. Moreover, the experiments in this stage were conducted at around 20°C. However, the exact temperature was not recorded. Thus, the flux recovery was calculated by raw recorded flux without temperature correction.

1) Effect of Treatment Duration

In this section, three kinds of hydrodynamic conditions were conducted, which were 1) soaking + forward flush, 2) soaking, and 3) forward flush. One cycle of NaCl treatment was 20 min. The applied Na^+ concentration was 50 mM. Detailed experimental conditions are tabulated in *Table B.4(1-3)*. The influence of duration was examined by applying one and three cycles of NaCl treatment under three hydrodynamic conditions. The treatment efficiencies were quantified by flux recovery (*Eq. (3.8)*). The effects of hydrodynamic conditions and treatment duration on cleaning efficiency are displayed in *Figure 4.8*. The forward flush mode recovered the most permeability in both one and three cycles of NaCl treatment. Soaking was the most inefficient cleaning mode among the three. It could be seen that in the forward flush, flux recovery was mainly achieved in the first cycle, and the increase of treatment duration had a slight effect on the enhancement of flux recovery. A similar finding was noticed in the soaking + forward flush mode, although it was less efficient than the forward flush mode. Whereas, in the soaking mode, the cleaning efficiency improved noticeably from 12.36% to 32.09% along with the increase of treatment duration from 20 min to 60 min.

The high cleaning efficiency of forward flush was attributed to the collaboration between ion exchange and turbulent flow. In a flush condition, Na-Ca ion exchange was enhanced by the turbulent flow, which improved the diffusion of Na^+ into the foulant (Lee and Elimelech 2007). The breakage of calcium bridge and the swelling of

the gel-like fouling layer was accelerated. Meanwhile, the relaxed foulants were removed by the forward flush. The detachment of foulant resulted in a decrease in the thickness of the fouling layer, which might decrease the diffusion distance of Na^+. Ion exchange and the subsequent fouling layer swelling was further promoted.

On the other hand, in a soaking mode, the high concentration of Na^+ caused the swelling of the fouling layer (Lee and Elimelech 2007). Nevertheless, further relaxation might be retarded by the long diffusion distance from the bulk to the interior of the fouling layer. A detachment of the fouling layer hardly occurred in a soaking mode. The subsequent recovered flux test was conducted at 3 bars, maintaining the consistency with the determination of the initial baseline. The relaxed fouling layer might be recompacted during the flux check, resulting in low cleaning efficiency. It was consistent with the moderate cleaning efficiency of soaking + forward flush mode. The fouling layer was relaxed during the 15-min soaking, and the swelled fouling layer was removed in the 5-min forward flush. Hence, compared to the forward flush mode, the fouling layer detachment in this mode was retarded during the 15-min soaking. Whereas, with the 5-min forward, the flux recovery of this mode surpassed that of the soaking mode.

Different from the finding of Lee and Elimelech (2007), which proposed a complete flux recovery by 15-min salt cleaning, NaCl treatment had a limited cleaning efficiency in this case. The limitation was visibly observed in the soaking + forward flush mode and the only forward flush mode. The cleaning efficiency was prominent in the first cycle, followed by a slight improvement by further prolonging the treatment duration. Firstly, 800 $mg \cdot L^{-1}$ alginate solution was applied in this case, which was much higher than that applied in their case (20 $mg \cdot L^{-1}$). It might lead to a much greater fouling extent in this case, which retarded the diffusion of Na^+. Secondly, it might be ascribed to the limited effect of forward flush on the removal of irreversible fouling layer, which contributed remarkably to the flux decline in a membrane process. Na-Ca ion exchange reduced the cross-linking density and restored the long-chain alginate molecules in the gel-like layer, which caused the swelling of the network (Lee and Elimelech 2007). It might be able to swell the irreversible fouling layer. Fouling layer swelling was observed by visual inspection after NaCl pre-treatment. The visualised swelling was prominent on membrane treated by soaking since the relaxed foulant was not removed by a turbulent flow. However, regarding the much greater fouling extent in this case, the treatment process might be prolonged excessively to achieve a complete swelling of the fouling layer.

The FeOCl detachment in NaCl pre-treatment is displayed in *Figure F.1*. A maximum iron leaching in a 1- hour forward flush was 0.25$mg \cdot L^{-1}$. The reduction of turbulent flow reduced the shear force that was exerted on the FeOCl layer, resulting in a decline of iron leaching. In the one-hour soaking, the iron leaching was 0.07 $mg \cdot L^{-1}$. NaCl pre-treatment had a limited effect on the leaching of FeOCl, which caused a maximum of 3.21% (wt%) of iron leaching in a one-hour forward flush. However, it might affect Fenton-based cleaning. As mentioned in *Section 4.1.1*, the iron concentration to initiate a homogeneous Fenton oxidation is difficult to determine, and a small amount of leached iron might have a substantial effect on starting a homogeneous Fenton

oxidation. On the other hand, in all hydrodynamic modes, the iron leaching increased with the extension of treatment duration, which shared a similar tendency with the treatment efficiency. A possible explanation was that as the treatment progressed, the fouling layer swelled greater, and more FeOCl sites were exposed to the cleaning solution. Thus, it resulted in a higher propensity of iron leaching.

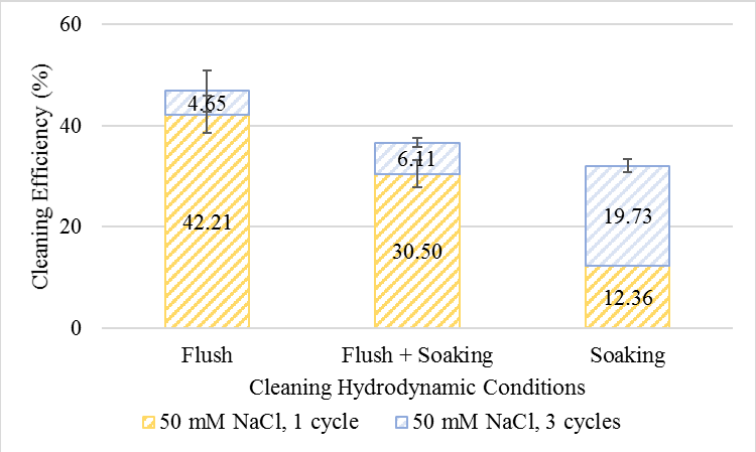

Figure 4.8: Effect of cleaning hydrodynamic conditions and cleaning duration on NaCl treatment. Three cycles of cleaning were performed for each hydrodynamic condition. Each cycle of cleaning included "flush 20 min", "soaking 15 min + flush 5 min", and "soaking 20 min", respectively. Fouling and cleaning conditions are listed in *Table B.2* and *Table B.3(1-3)*. No permeation was generated during the forward flush, and no pH adjustment was conducted in NaCl treatment. The fouling extent was controlled by generating a comparable amount of permeate (around 20 mL).

2) Effect of Na^+ Concentration

NaCl treatments with 50 mM and 300 mM NaCl solution were conducted for three hydrodynamic conditions, including 1) soaking + forward flush, 2) soaking, and 3) forward flush. In this section, only one cycle of treatment (20 min) was conducted. Detailed experimental conditions are tabulated in *Table B.4(4-6)*. The effects of Na^+ concentration on treatment efficiency in different hydrodynamic conditions are displayed in *Figure 4.9*. For all hydrodynamic conditions, the increase of Na^+ concentration improved the flux recovery. A higher concentration of Na^+ enlarged the difference of the osmotic pressure between the bulk and the interior of the fouling layer (Lee and Elimelech 2007). The osmotic pressure drove a greater Na^+ diffusion and improved the Na-Ca ion exchange. Therefore, the relaxation of the fouling layer was promoted, and higher cleaning efficiencies were achieved.

However, the extent of the improvements was different according to different applied hydrodynamic conditions. The increased Na^+ concentration had the least effect on the forward flush mode, which increased the cleaning efficiency from 42.21% to 51.14%. It could be ascribed to that the effect of a turbulent flow surpassed the effect of the increase of Na^+ concentration (Lee and Elimelech 2007), which indicated that the rate of mass transfer of Na^+ was controlled by the turbulent flow rather than the

concentration of Na^+. In the three hydrodynamic conditions, the greater the participation of forward flush, the lower the impact of the increase of Na^+ concentration. The high concentration of NaCl noticeably improved the flux recovery of the soaking mode from 12.36% to 35.17%. The flux recovery of one-cycle 300 mM NaCl soaking even transcended the flux recovery of three-cycle 50 mM NaCl soaking. The result indicated that in the soaking mode, the treatment efficiency was stoichiometrically related to the Na^+ concentration (Lee and Elimelech 2007). A similar finding was observed in the soaking + forward flush mode, where the flux recovery of 300 mM NaCl treated for one cycle surpassed that of 50 mM NaCl treated for three cycles.

The influence of Na^+ concentration on FeOCl detachment was examined, and the results are showed in *Figure F.2*. Despite a slight increase of iron leaching compared to *Figure F.1*, for a 20-min forward flush, the resulting iron leaching was less than 2%, and the increase of Na^+ concentration did not deteriorate the iron leaching. It was noteworthy that a high concentration of salt solution has adverse environmental impacts, and it might cause problems in the subsequent treatment process. Hence, a less concentrated salt solution was desired.

Conclusively, a 20-min of forward flush by 50 mM NaCl solution was the most efficient condition resulting in an effective cleaning and acceptably low iron leaching for Ca-alginate fouled FeOCl pre-coated ceramic NF membrane. The hydrodynamic condition was the predominant factor among the three. Compared to a forward flush mode, the increase of Na^+ concentration or treatment duration had a greater improvement of the cleaning efficiency of a soaking mode. However, the improvement was limited by the ineffective removal of the irreversible fouling layer. NaCl treatment merely detached FeOCl from the pre-coated layer. Moreover, the consequent saline water after NaCl treatment needed to be treated before discharge.

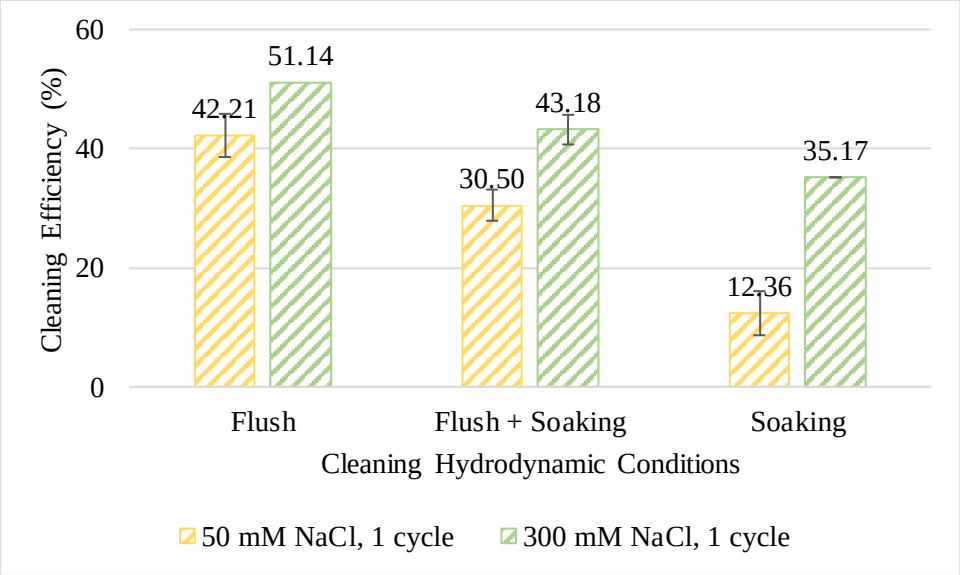

Figure 4.9: Effect of cleaning hydrodynamic conditions and Na^+ concentration on NaCl treatment. Fouling and cleaning conditions are listed in *Table B.2* and *Table B.3(4-6)*. All experiments were performed in duplicate except "300 mM

NaCl flush 1 cycle". The fouling extent was controlled by generating a comparable amount of permeate (around 20 mL).

4.3.2. Fenton-Based Cleaning: Effect of Cleaning Conditions

In this section, FeOCl catalysed Fenton oxidation was conducted to clean the Ca-alginate fouled FeOCl pre-coated ceramic NF membrane. The influences of cleaning duration, cleaning hydrodynamics, and H_2O_2 concentration on the cleaning efficiency were investigated. Demineralised water flux was tested after the pre-coating and served as a baseline for the flux normalisation. Membrane fouling was accelerated by feeding fouling solution with high organic loading. Fouling experiments were conducted at constant TMP, and the fouling extent was controlled by adjusting the filtration duration to generate comparable amounts of permeate (14 mL). Demineralised water flux was tested after cleaning to determine the flux recovery of the cleaning.

The effects of various conditions on the cleaning efficiency are displayed in *Figure 4.10*. A high concentration of H_2O_2 was used to improve the diffusion of H_2O_2 and subsequently improved Fenton-based cleaning efficiency. Forward flush was proposed to effectively increase the diffusion of chemicals and detach the swelled fouling layer (*Section 4.3.1*). The one-hour forward flush by 100 mM H_2O_2 restored permeability completely (*Figure 4.10(a)*). Although the cleaning efficiency exceeded 100%, the recovered flux was below the pristine permeate flux before pre-coating. The exceeding flux recovery was due to the detachment of FeOCl. The complete removal of the fouling layer fully exposed the FeOCl layer. Moreover, the acidic condition (pH 3.3) enhanced the leaching of iron. Hence, it led to greater FeOCl leaching compared to NaCl pre-treatment, which was conducted at neutral pH (*Section 4.3.1*). Fenton-based cleaning demonstrated an efficient removal of the gel-like fouling layer. Possible explanations and underlying mechanisms are further discussed in *Section 4.3.3*.

A soaking mode and a reduction of H_2O_2 concentration were applied subsequently to examine the effects of the hydrodynamic condition and chemical concentration, respectively. 5-min demineralised water forward flush was conducted after the 60-min soaking by 100 mM H_2O_2 to detach the swelled fouling layer. The applied crossflow velocity (46.5 $cm \cdot s^{-1}$) could generate a turbulent flow in the tube and remove the swelled fouling layer. Despite a slight decrease, the cleaning efficiencies for both conditions surpassed 95% (*Figure 4.10(a)*). These findings implied that the effects of the hydrodynamic condition and H_2O_2 concentration were overwhelmed by the long cleaning duration. The effects of the hydrodynamic condition and chemical concentration should be further examined in a shortened cleaning.

Hence, the influence of cleaning duration was explored by shortening the cleaning duration to 20 min. Compared to the efficiency of a 60-min forward flush by 100 mM H_2O_2, the consequent cleaning efficiency exhibited a remarkable reduction, decreasing from 112% to 67% (*Figure 4.10(a)*). The result indicated the fact that in this case, cleaning duration was the dominant factor to the cleaning efficiency. *Section 4.1.1* displayed an efficient Fenton oxidative decolouration in the first minute and followed

by slow adsorption. The high initial efficiency was due to the efficient mass transfer in batch reactions and the potential homogeneous Fenton oxidation induced by heterogeneous Fenton oxidation. However, in membrane cleaning, the mass transfer of H_2O_2 and the possible iron leaching were impeded by the gel-like fouling layer. Therefore, cleaning duration became the dominant factor, because the increase of cleaning duration further improved the diffusion of H_2O_2 and enhanced Fenton-based cleaning.

An initial plummet of flux (40-60%) was observed in all Ca-alginate fouling experiments conducted on FeOCl pre-coated ceramic NF membrane (*Figure 4.10(b), Figure 4.11(a) and Figure 4.12(a&b)*). Four speculations were proposed to be responsible for this phenomenon. Firstly, membrane fouling might be exacerbated by the electrostatic adhesion between the positively charged FeOCl layer and the negatively charged Ca-alginate fouling layer (Tang et al. 2011, Zhang et al. 2017). Besides, the pre-coated FeOCl layer was formed by pre-filtration, and the catalytic nanosheets were stacked via van der Waals and electrostatic interactions. A porous deposited layer was observed in *Figure 4.6(b),* and Ca-alginate was a structurally flexible macromolecule. In the fouling experiment, the Ca-alginate molecules might be partially pressed into the gaps in the FeOCl layer and block the water channels. Hence, Ca-alginate fouling on pristine membranes was performed to evaluate the effect of the FeOCl pre-coated layer on the initial flux drop. Nonetheless, still, 50-60% of flux decline was observed at the beginning of the fouling *Figure G.1*.

Secondly, the overly high concentration of Ca-alginate solution might further increase membrane fouling in the initial stage. As mentioned above, in this research, the organic loading of the fouling solution was increased to accelerate membrane fouling. Several pieces of research concerning membrane fouling by a high concentration of alginate solution experienced similar severe initial flux decline. García-Molina et al. (2006) reported a 50% of initial flux decline for alginic acid fouled polymeric UF membrane by increasing the concentration of fouling solution from 0.3 $g \cdot L^{-1}$ to 3 $g \cdot L^{-1}$. Hashino et al. (2011) stated that 50 $mg \cdot L^{-1}$ of alginate solution resulted in a 40% of initial flux drop for polymeric MF/UF membrane. De Angelis et al. (2013) suggested a 65% of initial flux decline by 10 $mg \cdot L^{-1}$ of alginate solution in a dead-end filtration for iron oxide pre-coated ceramic UF membrane. Both García-Molina et al. (2006) and De Angelis et al. (2013) ascribed the initial flux sharp drop to concentration polarization and consequent rapid formation of gel-like fouling layer at the beginning, which decreased permeate flux remarkably. Contradictory, Lee and Elimelech (2007) published a much less initial flux decline (around 10%) in a crossflow filtration of 20 $mg \cdot L^{-1}$ Ca-alginate solution conducted on polymeric RO membranes. Kramer et al. (2020) also reported a continuous and slow decrease of permeate flux along with the Ca-alginate fouling. However, in that case, a much larger ceramic NF membrane (length: 1200 mm; effective area: 0.25 m^2) with 19 channels was applied. Besides, the initial water flux was not indicated in that research.

Thirdly, the initial flux drop might be due to the superior fouling capacity of alginate. Different from humic acid or protein such as bovine serum albumin (BSA), alginate is a long-chain macromolecule, and the addition of Ca^{2+} further enhances membrane

fouling by cross-linking (You et al. 2020). Hashino et al. (2011) suggested that alginate caused a greater initial flux decline and more severe membrane fouling compared to BSA or humic acid. Lastly, a membrane with 50-60% of defects might cause a sharp initial flux decline in a fouling process. However, according to *Figure E.1(b)*, the defect of the applied membrane was 4.69%, which would not cause a 50-60% of initial flux decline.

Conclusively, Fenton-based cleaning efficiently recovered membrane permeability in one hour. However, the sharp drop of flux at the beginning was a critical problem that deteriorated the efficiency of membrane filtration. It might be attributed to the severe fouling property of alginate and the high concentration solution applied in this research. Further experiments are needed to investigate the cause of the initial flux decline. If it is ascribed to the high feeding concentration, in practical application, the applied feeding solution is much less concentrated compared to that in the lab, which will lead to a continuous and slow decline along with the fouling duration. However, if the flux decline is attributed to the pre-coated FeOCl layer, Fenton-based cleaning induced by the pre-coated FeOCl layer might not be applicable for gel-like fouling for ceramic NF membrane.

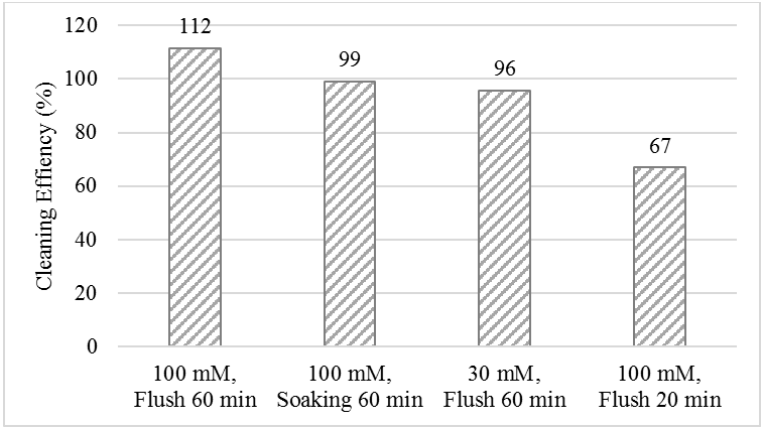

(a)

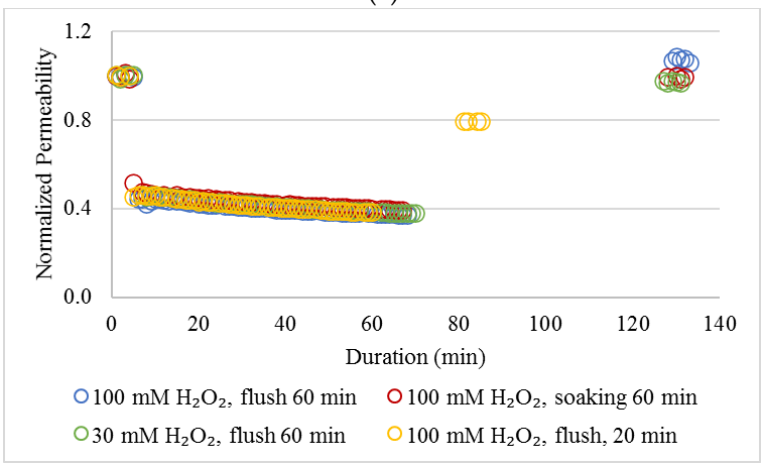

(b)

Figure 4.10: Effect of cleaning conditions on Fenton-based cleaning efficiency: (a) cleaning efficiency and (b) flux behaviour during fouling/cleaning experiments. Detailed fouling and cleaning conditions are listed in *Table*

B.3(4&5) and *Table B.5(1-3&5)*. The fouling extent was controlled by generating a comparable amount of permeate (14 mL). No permeation was generated during the forward flush.

4.3.3. Underlying Mechanisms of Fenton-Based Cleaning

According to the results in *Section 4.3.2*, Fenton-based cleaning displayed a high cleaning efficiency in the removal of the Ca-alginate fouling layer. In this section, the underlying mechanisms of efficient and effective Fenton-based cleaning are discussed. Firstly, Fenton oxidation was determined by the addition of tert-butanol, an ·OH scavenger, to quantify the participation of ·OH (He et al. 2016). A concentration ratio of H_2O_2 : tert-butanol = 3 : 1 was applied to obtain an excess dosage of radical scavenger (Xu et al. 2012). The results are plotted in *Figure 4.11*. A decrease in Fenton-based cleaning efficiency was observed with the presence of radical scavenger (*Figure 4.11(b)*). The participation of hydroxyl radical in the degradation of organic foulant was confirmed. For the 20-min cleaning, the effect of tert-butanol on ·OH scavenging can be quantified by excluding the hydrodynamic effect. The hydrodynamic effect was determined by the cleaning efficiency of demineralised water forward flush. The addition of 100 mM H_2O_2 contributed to 40% of the overall cleaning efficiency. The addition of 33 mM tert-butanol resulted in a 20% reduction on the cleaning efficiency excluding the hydrodynamic condition.

The results mentioned above quantified a 20% of ·OH effect in Fenton-based cleaning. Regarding the overdosage of H_2O_2, the participation of ·OH was less than expected. The low ·OH effect might be due to the hindrance of the diffusion of tert-butanol by the gel-like fouling layer. Hydroxyl radical has an extremely short half-life, which is the order of a few nanoseconds, and it corresponds to a migration distance of several micrometres. Despite an exceptional scavenging effect of tert-butanol, it primarily relies on the availability of ·OH. The molecular weight of tert-butanol is twice as much as that of H_2O_2. Moreover, as an organic molecule, tert-butanol molecules experienced more considerable difficulties in the diffusion into the fouling layer compared to H_2O_2 molecules. The fouling layer was at the vicinity of the FeOCl layer as well as the generated ·OH. Whereas, the accessibility of tert-butanol to the generated ·OH was hindered. Hence, the scavenging effect might be retarded stoichiometrically due to the insufficiency of tert-butanol.

In contrast to previous experiments in our lab, Fenton-based cleaning performed a high efficiency in the removal of the gel-like fouling layer. Several possible explanations were proposed for this finding. Firstly, homogeneous Fenton reaction induced by surface-leached iron was observed in heterogeneous Fenton reaction (He et al. 2016). In many circumstances, heterogeneous and homogeneous Fenton reaction co-existed in a heterogeneous system. In this case, the acidic cleaning solution (pH=3.3) and the turbulent flow potentially increase the leaching of iron. The iron leaching after cleaning was around 0.1 mg $Fe{\cdot}L^{-1}$, and the FeOCl detachment rate was around 0.6%. The iron leaching was below the reported value, which was 0.34 mg $Fe{\cdot}L^{-1}$ (Kwan et al. 2002). However, it is difficult to determine the iron concentration that could initiate a homogeneous Fenton reaction, and it is challenging to quantify the contribution of the potential homogeneous Fenton oxidation in Fenton-based cleaning.

Secondly, the possibility of the direct oxidation of alginate by H_2O_2 was considered despite the superior oxidative capacity of ·OH among various oxidants. It is a nonselective oxidant which achieved the oxidation of organic compounds at near-diffusion controlled rates (Keenan et al. 2008). Direct oxidation of BSA by H_2O_2 was reported (Zhou et al. 2017); however, the applied concentration was over ten times higher than that in this research. Thirdly, the fouling duration in this research was less than half of the fouling duration of the previous experiments performed in our lab (Kramer et al. 2020). It might lead to insufficient fouling and result in a thinner gel-like fouling layer, which reduced the hindrance of the diffusion of H_2O_2. Lastly, De Angelis and de Cortalezzi (2016) proposed a porous and hydrophilic fouling layer was formed by Ca-alginate, which had a lower impact on the retardance of the diffusion of H_2O_2.

Overall, heterogeneous Fenton reaction is a very complex process involving various interactions among solid-phase catalyst, H_2O_2, organic compounds, ROS, intermediates, and by-products. A Fenton-based cleaning, excluding the participation of ·OH, was challenging to present. According to the results and discussions mentioned above, it can be assumed that Fenton oxidation played an essential role in restoring the permeate flux of the Ca-alginate fouled FeOCl pre-coated ceramic NF membrane. Both heterogeneous and homogeneous Fenton oxidation might contribute to the efficient cleaning yet, the individual contribution might be challenging to quantify.

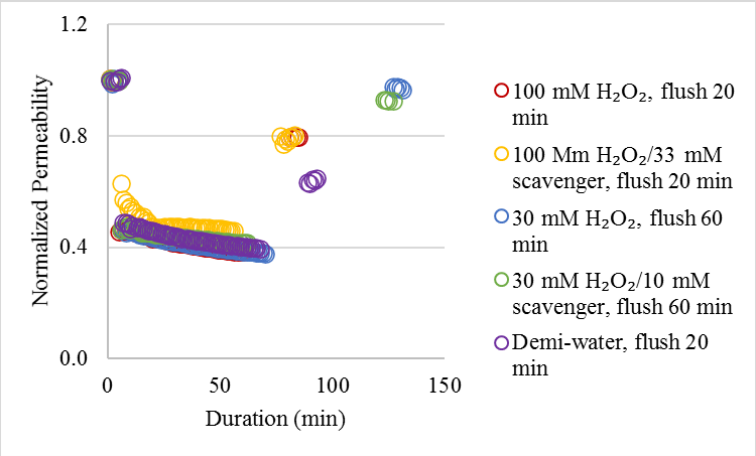

(a)

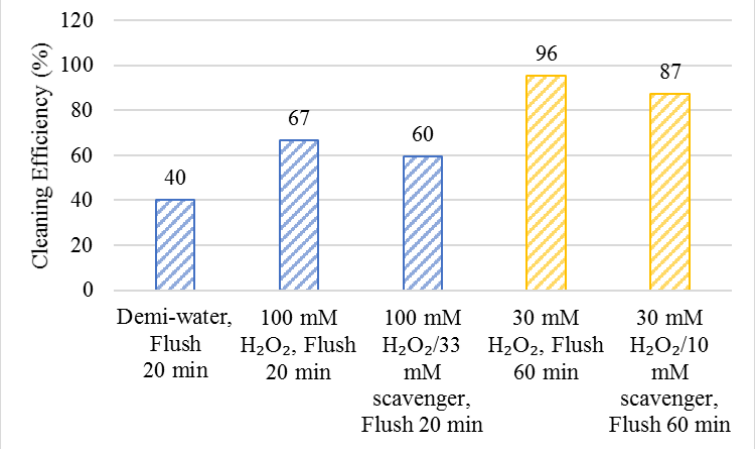

(b)

Figure 4.11: Effect of hydroxyl radical on the Fenton-based cleaning: (a) flux behaviour during fouling/cleaning experiments and (b) cleaning efficiency. Detailed fouling and cleaning conditions are listed in *Table B.3(4&5)* and *Table B.5(3-6&11)*. The fouling extent was controlled by generating a comparable amount of permeate (14 mL). No permeation was generated during the forward flush.

4.3.4. Synergistic Effect of NaCl treatment and Fenton-Based Cleaning

Individual effects of NaCl pre-treatment and Fenton-based cleaning were investigated in *Section 4.3.2* and *Section 4.3.3*. As mentioned in *Section 2.5* and *Section 4.3.1*, Na-Ca ion-exchange swelled the fouling layer, which might potentially improve the efficiency of Fenton-based cleaning. The synergistic effect between NaCl induced ion exchange, and Fenton oxidation was explored by cleaning the Ca-alginate fouled ceramic NF membranes with a mixture of NaCl and H_2O_2 at pH 3.3. Membrane cleaning by NaCl, H_2O_2 and NaCl/H_2O_2 were conducted at the identical condition to ensure the comparability of the results. The corresponding flux behaviour and cleaning efficiency are illustrated in *Figure 4.12*. As discussed in *Section 4.3.2*, a 60-min forward flush by 100 mM H_2O_2 achieved a complete flux recovery. An addition of 50 mM NaCl to the Fenton-based cleaning system slightly decreased Fenton-based cleaning efficiency (*Figure 4.12(c)*). In accordance with the results in *Section 4.3.1*, a 60-min forward flush by 50 mM NaCl solution at pH 3.3 only restored 42% of membrane permeability (*Figure 4.12(c)*). It can be ascribed to the inefficiency in the removal of irreversible fouling layer by NaCl forward flush. For both cases involving Fenton-based cleaning, the cleaning efficiency surpassed 100% due to iron leaching (*Section 4.3.2*). The difference between the efficiency of Fenton-based cleaning and NaCl/Fenton-based cleaning was difficult to be quantified, and the synergistic effects of NaCl and H_2O_2 were hard to determine.

Therefore, similar experiments were performed in a shorter cleaning duration, 20 min. The cleaning efficiency decreased along with the reduction of cleaning duration. In a 20-min forward flush, the efficiency of NaCl/Fenton-based cleaning was comparable with that of Fenton-based cleaning, which was 64% and 67%, respectively (*Figure 4.12(c)*). The results indicated that the addition of NaCl to Fenton-based cleaning did not improve Fenton-based cleaning efficiency. However, according to the previous experiment in our lab, Fenton-based cleaning performed in a soaking mode was improved by the addition of NaCl. A possible explanation was that the effect of hydrodynamics on the promotion of H_2O_2 diffusion surpassed the effect of fouling layer swelling induced by NaCl treatment on that. Additionally, the hydrophilic property of alginate improved the diffusion of H_2O_2 (De Angelis and de Cortalezzi 2016). With the enhancement of the diffusion of H_2O_2, the decomposition of H_2O_2 and the generation of ·OH was improved. Subsequently, a highly efficient Fenton oxidative cleaning was achieved. Moreover, the addition of NaCl slightly decreased Fenton-based cleaning efficiency. This finding was consistent with the results displayed in *Section 4.1.2*, where the addition of 50 mM NaCl in the batch Fenton reaction decreased the decolouration rate of methylene blue. Regarding the prominent hydrodynamic effect, it was assumed that the synergistic effect might predominate in a soaking mode

where the mass transfer of H_2O_2 was retarded by the fouling layer. In that case, Na-Ca ion exchange might predominantly improve the diffusion of H_2O_2 by swelling the fouling layer.

It was noticed that a 20-min NaCl forward flush was more efficient than a 60-min NaCl forward flush (*Figure 4.12(c)*). A possible explanation was that the 60-min experiment was conducted after a fouling/cleaning experiment. Due to the time limitation and the low iron leaching (around 3.2%), FeOCl pre-coating was not performed before the fouling experiment. It was the only case that pre-coating was not conducted before the membrane fouling/cleaning experiment. In this case, the FeOCl layer was thinner, rougher, and mechanically more robust because of the detachment of the loosely attached FeOCl in the previous cleaning process. It might lead to a lower iron leaching and enhance the adhesive interaction between the FeOCl layer and fouling layer, which, subsequently, reduced the cleaning efficiency.

Although no synergistic effect was observed between NaCl and Fenton oxidation, Fenton-based cleaning efficiently and effectively recovered the permeability for Ca-alginate fouled ceramic NF membrane. The cause of the initial flux decline in fouling process required further investigation. If the pre-coated FeOCl layer were confirmed not to damage membrane productivity, Fenton-based cleaning could provide mild yet efficient cleaning for gel-like fouling layer without deterioration of membrane quality. The absence of NaCl reduces the operating complexity concerning the post-treatment of the consequent saline water. Besides, the potential adverse impacts on the environment would be reduced.

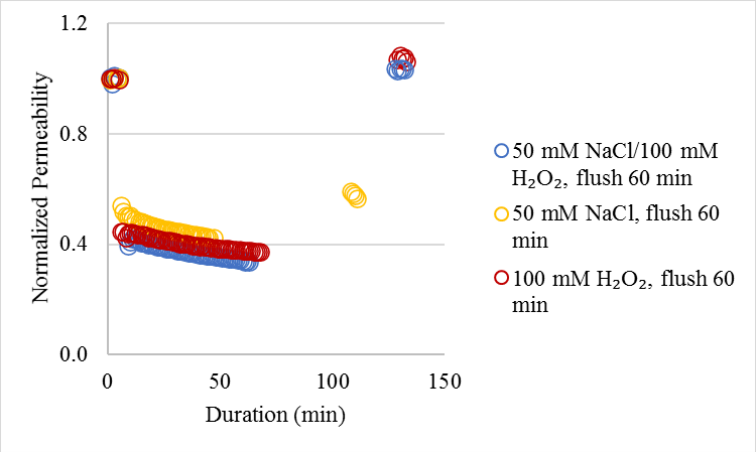

(a)

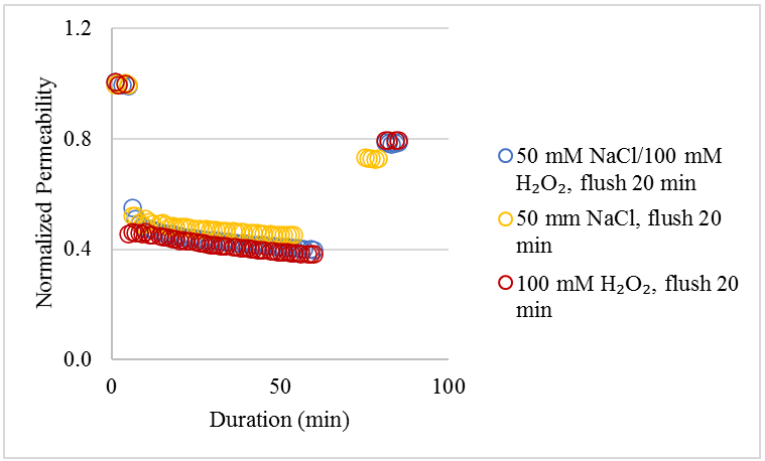

(b)

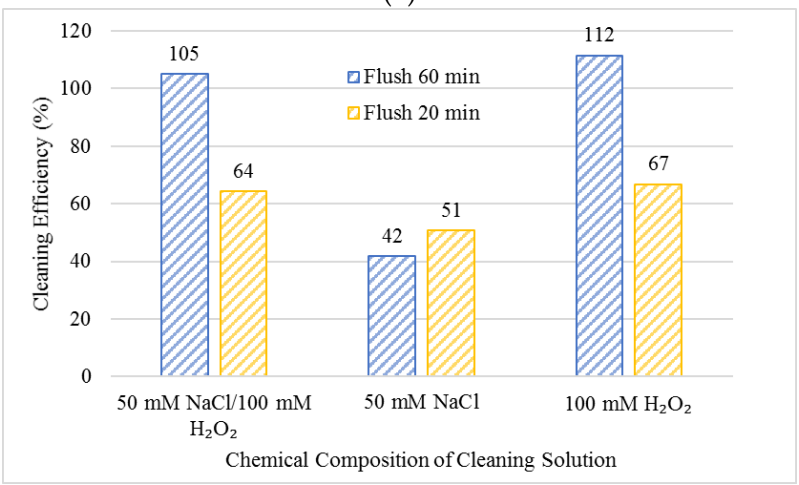

(c)

Figure 4.12: Synergistic effect of NaCl treatment and Fenton-based cleaning: (a) flush behaviour of 20 min synergistic cleaning, (b) flush behaviour of 60 min synergistic cleaning, and (c) cleaning efficiency 20 and 60 min cleaning. Detailed fouling and cleaning conditions are listed in *Table B.3(4&5)* and *Table B.5(1,3,7-10)*. The fouling extent was controlled by generating a comparable amount of permeate (14 mL). No permeation was generated during the forward flush.

5 RESEARCH LIMITATIONS AND OUTLOOK

According to the abovementioned experiments, several limitations of this research are listed in this section. The corresponding recommendations are proposed to improve further experiments.

5.1. FeOCl PRE-COATING

In this research, FeOCl catalysed Fenton-based cleaning was performed on Ca-alginate fouled ceramic NF membrane. The catalytic FeOCl layer was deposited to ceramic NF membrane by one-pass pressure-driven filtration. Firstly, it is of considerable significance to determine the cause of the initial flux drop in the fouling process. If it is attributed to the pre-coated FeOCl layer, alternative pre-coating or membrane cleaning strategies should be explored. For example, the immobilisation of FeOCl on the membrane can be researched (Sun et al. 2018). In that case, the stability of the FeOCl layer is enhanced by forming chemical bonds with ceramic membrane and the uniformity of the FeOCl layer is improved without influencing by gravity. The low iron leaching and durability of the immobilised FeOCl layer in cyclic fouling/cleaning process are confirmed (Sun et al. 2018). However, compared to pressure-driven filtration, it might alter the particle size and morphology of the FeOCl particle and further affect the properties (i.e. surface roughness and porosity) of the pre-coated layer. The FeOCl-foulant interaction might be altered, and the fouling behaviour and cleaning efficiency might be affected. Thus, further research is needed to reveal the effect of the immobilisation of FeOCl layer on ceramic NF membrane. Moreover, regarding the practical application of the Fenton-based cleaning on tubular ceramic membranes, studies on multi-tube modules are imperative (Anantharaman et al. 2020).

5.2. NaCl PRE-TREATMENT

As mention in *Section 4.3.1*, in NaCl pre-treatment, the defect of the used membrane was unknown, and the process temperature was not recorded. In a filtration process, foulant might pass through the membrane through the defect and deteriorate the quality of the permeate. Preference paths might be generated in defects which might increase the measured permeate flux. Moreover, foulant might be absorbed to the cracks or block the cracks during fouling experiment. The foulant trapped within the crack is hardly removed by NaCl treatment or turbulent flow. The potential defect decreases the reliability of the result (Kramer et al. 2019). On the other hand, temperature influences the permeation and accordingly, the measured flux and flux recovery (Mulder 2012). Hence, it is essential to quantify the defect of the membrane and record the process temperature to generate flux recovery, which represents the actual cleaning efficiency. Regarding the reliability of the result, membrane MWCO and defect should be determined by a single filtration of a mixture of PEG molecules with different molecular weights, and the feed and permeate samples should be analysed by high-performance liquid chromatography (HPLC) (Kramer et al. 2019).

According to the study of Lee and Elimelech (2007), the cleaning mechanism of NaCl treatment was attributed to Na-Ca ion exchange and fouling layer swelling. However, in this research, the proposed mechanism was not confirmed experimentally. In a further experiment, the Ca^{2+} detachment in the cleaning solution can be measured to prove the ion exchange (Lee and Elimelech 2007). Regarding the difficulty of measuring a trace amount of Ca^{2+}, an alternative batch experiment is proposed. NaCl solution can be fed to a column of Ca-alginate gel beads, and the Ca^{2+} concentration in the effluent can be measured. Additionally, the fouling layer detachment can be quantified by TOC analysis or measuring the change of viscosity of the cleaning solution before and after NaCl treatment. The difficulties lie in the dissolution of the fouling layer (Lee and Elimelech 2007). Lastly, the swelling of the fouling layer can be quantified by atomic force microscopy (AFM) colloid probe technique to determine the intermolecular foulant-foulant or foulant-membrane adhesions (Anantharaman et al. 2020, Lee and Elimelech 2007).

5.3. FENTON-BASED CLEANING

5.3.1. Analysis of ·OH

In this research, the effect of ·OH in membrane cleaning was examined by the addition of tert-butanol. However, the scavenging effect might be impeded by the diffusion of tert-butanol. The quantification of ·OH effect might be less representative of the actual situation. Moreover, for the 100 mM Fenton-based cleaning, a large amount of tert-butanol solution was added to the cleaning solution. Fenton-based cleaning is a complex process which involved various interactions. The addition of a high concentration of tert-butanol might introduce unknown effects on the cleaning process. Additional approaches such as electron spin resonance (ESR) spectra could serve as an alternative method to quantify the generation of ·OH by FeOCl pre-coated ceramic NF membrane (Sun et al. 2018).

5.3.2. FeOCl-Foulant Interaction

The interaction between the FeOCl layer and the fouling layer was unclear. Assumptions were proposed according to the results. As assumed in *Section 4.3.2*, the FeOCl layer was physically stacked by van der Waals and electrostatic interaction, and the flexible long-chain alginate might be pressed into the porous FeOCl layer which increased the difficulties in membrane cleaning. The electrostatic interactions between FeOCl and fouling layer further improve the adhesion of them (Tang et al. 2011, Zhang et al. 2017). In this case, the properties of FeOCl layer such as the loading, thickness, coverage, and surface roughness might affect the FeOCl-foulant interaction. It is meaningful to conduct further experiments to explore this interaction, i.e. AFM analysis (Anantharaman et al. 2020). Moreover, the effects of FeOCl-foulant interaction on cleaning efficiency required further investigation.

5.3.3. Chemical Composition of Cleaning Solution

In the membrane cleaning process, the vital effects of the hydrodynamic condition and cleaning duration on cleaning efficiency have been exposed (*Section 4.3.2*). However,

the effects of pH and H_2O_2 concentration were uncertain. Fenton-based cleaning was performed at acidic condition (pH 3.3). However, one of the advantages of FeOCl as a Fenton-like catalyst is its exceptional activity in a broad pH range (Sun et al. 2018, Zhang et al. 2017). It is suggested that in the following research, FeOCl catalysed Fenton-based cleaning can be conducted for organic fouled membrane at circumneutral pH to eliminate the addition of acid and reduce iron leaching (Sun et al. 2018). On the other hand, compared to the 60-min forward flush by 100 mM H_2O_2, the 60-min forward flush by 30 mM H_2O_2 performed efficient cleaning as well. Whereas, due to the time limitation, cleaning efficiency conducted at a lower H_2O_2 concentration was not systematically investigated. In practical application, a decreased concentration is preferred if the cleaning efficiency can be maintained. In further research, it is meaningful to investigate the cleaning efficiencies for Fenton-based cleaning performed at circumneutral pH and lower H_2O_2 concentration.

5.4. SYNERGISTIC EFFECT OF NaCl AND FENTON CLEANING

Several experiments were conducted to explore the synergistic effect of NaCl and Fenton-based cleaning. The results disagreed with previous results obtained from our lab, which indicated a synergistic effect between Fenton oxidation and NaCl induced ion exchange in a soaking mode. Both turbulent flow and Na-Ca ion exchange were proposed to improve the Fenton-based cleaning (Lee and Elimelech 2007). It was assumed that the synergistic effect was influenced by the hydrodynamic condition, and the contribution of hydrodynamics to the synergy remained unclear. Thus, it is interesting to conduct further experiments to quantify the synergistic effects at different hydrodynamic conditions.

6 CONCLUSIONS

6.1. OVERALL DISCUSSION FOR RESULTS OF RESEARCH QUESTIONS

The proposed research questions can be answered according to the conducted experiments as listed below.

i. **What are the main factors affecting the pre-coating (i.e., iron loading) of FeOCl catalysts on top of ceramic NF membrane by the pressure-driven pre-filtration method?**

It was found that the iron loading on a ceramic NF membrane depended on the productivity of permeate, and the dosage of FeOCl. The iron loading was linearly related to the dosage of FeOCl. With identical permeate production, crossflow velocity, and FeOCl dosage, comparable iron loading and pre-coating efficiency could be obtained for membrane with different permeability.

ii. **What are the efficiency, influencing factors and mechanisms of using the NaCl pre-treatment and FeOCl catalysed Fenton oxidation for cleaning gel-like fouling of ceramic NF membrane?**

In NaCl pre-treatment, it was found that a 20-min forward flush by 50 mM NaCl for a Ca-alginate fouled FeOCl pre-coated ceramic NF membrane achieved a maximum of 42% of flux recovery. Among various cleaning conditions, hydrodynamic condition (turbulent forward flush/soaking) was the main factor that influenced the efficiency of NaCl pre-treatment. The effect of cleaning duration (20 min/60 min) and Na^+ concentration (50 mM/300 mM) was much less prominent. Moreover, NaCl pre-treatment was inefficient in the removal of the irreversible fouling layer.

In Fenton-based cleaning, cleaning duration was the vital factor that affected the cleaning efficiency. Despite various H_2O_2 concentration (100 mM/30 mM) and hydrodynamic condition (turbulent forward flush/soaking), a 60-min Fenton-based cleaning achieved almost full flux recovery. However, the cleaning efficiency decreased from 112% to 67% by reducing the cleaning duration from 60 min to 20 min. The participation of ·OH radical in the Fenton-based cleaning was confirmed by the addition of tert-butanol, an ·OH scavenger.

iii. **What are the efficiency and underlying synergistic mechanisms of the NaCl/Fenton-based cleaning for gel-like fouling on ceramic NF membrane?**

In a 60-min forward flush, the synergistic cleaning achieved a complete flux recovery. The synergistic cleaning efficiency decreased to 64% as the cleaning duration was reduced to 20 min. However, in both cases, the addition of NaCl slightly decreased Fenton-based cleaning efficiency. It might be attributed to that the effect of turbulent flow on the improvement of H_2O_2 diffusion surpassed the effect of Na-Ca ion exchange on that.

6.2. CONCLUSIONS

In this research, Ca-alginate fouling was conducted on FeOCl pre-coated ceramic NF membrane. The efficiency of NaCl pre-treatment and Fenton-based cleaning was investigated by the determination of flux recovery after cleaning. The proposed synergy between Fenton-based cleaning. Several conclusions were drawn according to the conducted experiments and were listed as followed:

1) A successful synthesis of lath-like FeOCl particles in oxygen-deficient, rapid heating process with several micrometres in length and around 1 μm in width was confirmed by SEM and XRD analyses. The synthesised FeOCl performed high Fenton activity at acidic condition, and the addition of Cl^- slightly decreased the Fenton activity.

2) In FeOCl pre-coating, the iron loading could be customised by adjusting permeate production, and FeOCl dosage. The iron loading was linearly correlated to the feeding concentration of FeOCl. The pre-coated FeOCl layer caused low permeability decline (< 4%) and the thickness of it varied from 4.97 μm to 7.35 μm according to different locations. Moreover, it is of great significance to determine the cause of the initial flux drop in the fouling process.

3) In NaCl pre-treatment, hydrodynamic condition (turbulent flow/soaking) was the critical factor that affected the cleaning efficiency compared to treatment duration or Na^+ concentration. A turbulent flow was proposed to improve the Na^+ diffusion and the fouling layer swelling. Nevertheless, NaCl treatment was inefficient in removing the irreversible fouling layer, limiting the overall treatment efficiency to below 50%.

4) Cleaning duration was the main factor that affected the efficiency of Fenton-based cleaning. A relatively longer Fenton-based cleaning improve the diffusion of H_2O_2, leading to higher cleaning efficiency. The addition of ·OH scavenger proved the participation of ·OH in the turbulent Fenton-based cleaning. However, further research is necessary to quantify the effect of ·OH in Fenton-based cleaning.

5) No remarkable synergistic effect was observed in the flush mode between NaCl and Fenton oxidation. It was proposed that the effect of hydrodynamics surpassed the effect of fouling layer swelling induced by Na-Ca ion exchange. However, further research is needed to evaluate the synergistic effect of NaCl on Fenton-based cleaning under different hydrodynamic conditions.

BIBLIOGRAPHY

Agenson, K.O., Urase, T.J.S. and Technology, P. (2007) Change in membrane performance due to organic fouling in nanofiltration (NF)/reverse osmosis (RO) applications. 55(2), 147-156.

Al-Amoudi, A.S.J.D. (2010) Factors affecting natural organic matter (NOM) and scaling fouling in NF membranes: a review. 259(1-3), 1-10.

Anantharaman, A., Chun, Y., Hua, T., Chew, J.W. and Wang, R.J.W.R. (2020) Pre-deposited dynamic membrane filtration–A review. 115558.

Ashfaq, M.Y., Al-Ghouti, M.A., Da'na, D.A., Qiblawey, H. and Zouari, N.J.S.o.T.T.E. (2020) Investigating the effect of temperature on calcium sulfate scaling of reverse osmosis membranes using FTIR, SEM-EDX and multivariate analysis. 703, 134726.

Babuponnusami, A. and Muthukumar, K.J.J.o.E.C.E. (2014) A review on Fenton and improvements to the Fenton process for wastewater treatment. 2(1), 557-572.

Baker, J. and Dudley, L.J.D. (1998) Biofouling in membrane systems—a review. 118(1-3), 81-89.

Buffle, J., Wilkinson, K.J., Stoll, S., Filella, M., Zhang, J.J.E.S. and Technology (1998) A generalized description of aquatic colloidal interactions: the three-colloidal component approach. 32(19), 2887-2899.

Chang, E.-E., Chang, Y.-C., Liang, C.-H., Huang, C.-P. and Chiang, P.-C.J.J.o.h.m. (2012) Identifying the rejection mechanism for nanofiltration membranes fouled by humic acid and calcium ions exemplified by acetaminophen, sulfamethoxazole, and triclosan. 221, 19-27.

Chang, I.-S. and Judd, S.J.J.P.B. (2002) Air sparging of a submerged MBR for municipal wastewater treatment. 37(8), 915-920.

Chu, K.H., Huang, Y., Yu, M., Her, N., Flora, J.R., Park, C.M., Kim, S., Cho, J., Yoon, Y.J.A.a.m. and interfaces (2016) Evaluation of humic acid and tannic acid fouling in graphene oxide-coated ultrafiltration membranes. 8(34), 22270-22279.

De Angelis, L. and de Cortalezzi, M.M.F.J.J.o.M.S. (2016) Improved membrane flux recovery by Fenton-type reactions. 500, 255-264.

De Angelis, L., de Cortalezzi, M.M.F.J.S. and Technology, P. (2013) Ceramic membrane filtration of organic compounds: Effect of concentration, pH, and mixtures interactions on fouling. 118, 762-775.

Deraguin, B. and Landau, L.J.A.P.U. (1941) Theory of the stability of strongly charged lyophobic sols and of the adhesion of strongly charged particles in solution of electrolytes. 14, 633-662.

Elimelech, M., Zhu, X., Childress, A.E. and Hong, S.J.J.o.m.s. (1997) Role of membrane surface morphology in colloidal fouling of cellulose acetate and composite aromatic polyamide reverse osmosis membranes. 127(1), 101-109.

Fujioka, T., Khan, S.J., McDonald, J.A., Nghiem, L.D.J.S. and Technology, P. (2014) Nanofiltration of trace organic chemicals: A comparison between ceramic and polymeric membranes. 136, 258-264.

García-Molina, V., Lyko, S., Esplugas, S., Wintgens, T. and Melin, T.J.D. (2006) Ultrafiltration of aqueous solutions containing organic polymers. 189(1-3), 110-118.

Garrett, T.R., Bhakoo, M. and Zhang, Z.J.P.i.N.S. (2008) Bacterial adhesion and biofilms on surfaces. 18(9), 1049-1056.

Hartmann, M., Kullmann, S. and Keller, H.J.J.o.M.C. (2010) Wastewater treatment with heterogeneous Fenton-type catalysts based on porous materials. 20(41), 9002-9017.

Hashino, M., Hirami, K., Katagiri, T., Kubota, N., Ohmukai, Y., Ishigami, T., Maruyama, T. and Matsuyama, H.J.J.o.m.s. (2011) Effects of three natural organic matter types on cellulose acetate butyrate microfiltration membrane fouling. 379(1-2), 233-238.

He, J., Yang, X., Men, B. and Wang, D.J.J.o.e.s. (2016) Interfacial mechanisms of heterogeneous Fenton reactions catalyzed by iron-based materials: A review. 39, 97-109.

Herzberg, M. and Elimelech, M.J.J.o.M.S. (2007) Biofouling of reverse osmosis membranes: role of biofilm-enhanced osmotic pressure. 295(1-2), 11-20.

Hilal, N., Al-Zoubi, H., Darwish, N., Mohamma, A. and Arabi, M.A.J.D. (2004) A comprehensive review of nanofiltration membranes: Treatment, pretreatment, modelling, and atomic force microscopy. 170(3), 281-308.

Hoek, E.M., Elimelech, M.J.E.s. and technology (2003) Cake-enhanced concentration polarization: a new fouling mechanism for salt-rejecting membranes. 37(24), 5581-5588.

Homayouni, A., Ehsani, M.R., Azizi, A., Yarmand, M.S. and Razavi, H. (2007) Effect of lecithin and calcium chloride solution on the microencapsulation process yield of calcium alginate beads.

Hong, J. and He, Y.J.D. (2014) Polyvinylidene fluoride ultrafiltration membrane blended with nano-ZnO particle for photo-catalysis self-cleaning. 332(1), 67-75.

Hong, S. and Elimelech, M.J.J.o.m.s. (1997) Chemical and physical aspects of natural organic matter (NOM) fouling of nanofiltration membranes. 132(2), 159-181.

Huang, H., Schwab, K., Jacangelo, J.G.J.E.s. and technology (2009) Pretreatment for low pressure membranes in water treatment: a review. 43(9), 3011-3019.

Huang, X., Wei, C.-H. and Yu, K.-C.J.J.o.m.s. (2008) Mechanism of membrane fouling control by suspended carriers in a submerged membrane bioreactor. 309(1-2), 7-16.

Keenan, C.R., Sedlak, D.L.J.E.S. and Technology (2008) Factors affecting the yield of oxidants from the reaction of nanoparticulate zero-valent iron and oxygen. 42(4), 1262-1267.

Kiwi, J., Lopez, A., Nadtochenko, V.J.E.S. and Technology (2000) Mechanism and kinetics of the OH-radical intervention during Fenton oxidation in the presence of a significant amount of radical scavenger (Cl-). 34(11), 2162-2168.

Knoell, T., Safarik, J., Cormack, T., Riley, R., Lin, S. and Ridgway, H.J.J.o.m.s. (1999) Biofouling potentials of microporous polysulfone membranes containing a sulfonated polyether-ethersulfone/polyethersulfone block copolymer: correlation of membrane surface properties with bacterial attachment. 157(1), 117-138.

Kochkodan, V. and Hilal, N.J.D. (2015) A comprehensive review on surface modified polymer membranes for biofouling mitigation. 356, 187-207.

Kramer, F., Shang, R., Rietveld, L., Heijman, S.J.S. and Technology, P. (2020) Fouling control in ceramic nanofiltration membranes during municipal sewage treatment. 237, 116373.

Kramer, F., Shang, R., Scherrenberg, S., Rietveld, L., Heijman, S.J.S. and Technology, P. (2019) Quantifying defects in ceramic tight ultra-and nanofiltration membranes and investigating their robustness. 219, 159-168.

Kwan, W.P., Voelker, B.M.J.E.s. and technology (2002) Decomposition of hydrogen peroxide and organic compounds in the presence of dissolved iron and ferrihydrite. 36(7), 1467-1476.

Lee, S.-J., Dilaver, M., Park, P.-K. and Kim, J.-H.J.J.o.M.S. (2013) Comparative analysis of fouling characteristics of ceramic and polymeric microfiltration membranes using filtration models. 432, 97-105.

Lee, S.-J. and Kim, J.-H.J.W.r. (2014) Differential natural organic matter fouling of ceramic versus polymeric ultrafiltration membranes. 48, 43-51.

Lee, S., Ang, W. and Elimelech, M.J.D. (2006a) Fouling of reverse osmosis membranes by hydrophilic organic matter: implications for water reuse. 187(1-3), 313-321.

Lee, S., Elimelech, M.J.E.s. and technology (2006b) Relating organic fouling of reverse osmosis membranes to intermolecular adhesion forces. 40(3), 980-987.

Lee, S. and Elimelech, M.J.W.r. (2007) Salt cleaning of organic-fouled reverse osmosis membranes. 41(5), 1134-1142.

Lee, S., Kim, J. and Lee, C.-H.J.J.o.m.s. (1999) Analysis of CaSO4 scale formation mechanism in various nanofiltration modules. 163(1), 63-74.

Li, B., He, X., Wang, P., Liu, Q., Qiu, W. and Ma, J.J.W.R. (2020) Opposite impacts of K+ and Ca2+ on membrane fouling by humic acid and cleaning process: Evaluation and mechanism investigation. 116006.

Li, Q. and Elimelech, M.J.E.s.t. (2004) Organic fouling and chemical cleaning of nanofiltration membranes: measurements and mechanisms. 38(17), 4683-4693.

Li, R., Lou, Y., Xu, Y., Ma, G., Liao, B.-Q., Shen, L. and Lin, H.J.C. (2019) Effects of surface morphology on alginate adhesion: molecular insights into membrane fouling based on XDLVO and DFT analysis. 233, 373-380.

Li, S., Heijman, S., Verberk, J., Le Clech, P., Lu, J., Kemperman, A.J., Amy, G.L. and Van Dijk, J.C.J.W.r. (2011) Fouling control mechanisms of demineralized water backwash: reduction of charge screening and calcium bridging effects. 45(19), 6289-6300.

Li, Z., Lee, D., Sheng, X., Cohen, R.E. and Rubner, M.F.J.L. (2006) Two-level antibacterial coating with both release-killing and contact-killing capabilities. 22(24), 9820-9823.

Lin, Y.-L., Chiou, J.-H. and Lee, C.-H.J.J.o.h.m. (2014) Effect of silica fouling on the removal of pharmaceuticals and personal care products by nanofiltration and reverse osmosis membranes. 277, 102-109.

Liu, C., Zhang, D., He, Y., Zhao, X. and Bai, R.J.J.o.M.S. (2010) Modification of membrane surface for anti-biofouling performance: Effect of anti-adhesion and anti-bacteria approaches. 346(1), 121-130.

Machulek Jr, A., Moraes, J.E., Vautier-Giongo, C., Silverio, C.A., Friedrich, L.C., Nascimento, C.A., Gonzalez, M.C., Quina, F.H.J.E.s. and technology (2007) Abatement of the inhibitory effect of chloride anions on the photo-Fenton process. 41(24), 8459-8463.

Madaeni, S. and Ghaemi, N.J.J.o.M.S. (2007) Characterization of self-cleaning RO membranes coated with TiO2 particles under UV irradiation. 303(1-2), 221-233.

Matin, A., Khan, Z., Zaidi, S. and Boyce, M.J.D. (2011) Biofouling in reverse osmosis membranes for seawater desalination: phenomena and prevention. 281, 1-16.

Mohammad, A.W., Teow, Y., Ang, W., Chung, Y., Oatley-Radcliffe, D. and Hilal, N.J.D. (2015) Nanofiltration membranes review: Recent advances and future prospects. 356, 226-254.

Mulder, M. (2012) Basic principles of membrane technology, Springer Science & Business Media.

Neu, T.R. and Marshall, K.C.J.J.o.b.a. (1990) Bacterial polymers: physicochemical aspects of their interactions at interfaces. 5(2), 107-133.

Pan, Y., Wang, W., Wang, W. and Wang, T.J.R.A. (2015) Prediction of particle deposition and layer growth in the preparation of a dynamic membrane with cross-flow microfiltration. 5(108), 89015-89024.

Pasmore, M., Todd, P., Smith, S., Baker, D., Silverstein, J., Coons, D. and Bowman, C.N.J.J.o.M.S. (2001) Effects of ultrafiltration membrane surface properties on Pseudomonas aeruginosa biofilm initiation for the purpose of reducing biofouling. 194(1), 15-32.

Peng, W., Escobar, I.C. and White, D.B.J.J.o.M.S. (2004) Effects of water chemistries and properties of membrane on the performance and fouling—a model development study. 238(1-2), 33-46.

Rietveld, L., Norton-Brandão, D., Shang, R., Van Agtmaal, J., Van Lier, J.J.W.S. and Technology (2011) Possibilities for reuse of treated domestic wastewater in The Netherlands. 64(7), 1540-1546.

Ritchie, J.D. and Perdue, E.M.J.G.e.C.A. (2003) Proton-binding study of standard and reference fulvic acids, humic acids, and natural organic matter. 67(1), 85-96.

Shams Ashaghi, K., Ebrahimi, M. and Czermak, P.J.O.E.S. (2007) Ceramic ultra-and nanofiltration membranes for oilfield produced water treatment: a mini review. 1(1).

Soesanto, J.F., Hwang, K.-J., Cheng, C.-W., Tsai, H.-Y., Huang, A., Chen, C.-H., Cheng, T.-W. and Tung, K.-L.J.J.o.M.S. (2019) Fenton oxidation-based cleaning technology for powdered activated carbon-precoated dynamic membranes used in microfiltration seawater pretreatment systems. 591, 117298.

Sun, M., Zucker, I., Davenport, D.M., Zhou, X., Qu, J., Elimelech, M.J.E.s. and technology (2018) Reactive, self-cleaning ultrafiltration membrane functionalized with iron oxychloride nanocatalysts. 52(15), 8674-8683.

Tang, C.Y., Chong, T., Fane, A.G.J.A.i.c. and science, i. (2011) Colloidal interactions and fouling of NF and RO membranes: a review. 164(1-2), 126-143.

Tang, C.Y., Kwon, Y.-N., Leckie, J.O.J.E.s. and technology (2007a) Characterization of humic acid fouled reverse osmosis and nanofiltration membranes by transmission electron microscopy and streaming potential measurements. 41(3), 942-949.

Tang, C.Y., Kwon, Y.-N. and Leckie, J.O.J.J.o.M.S. (2007b) Fouling of reverse osmosis and nanofiltration membranes by humic acid—effects of solution composition and hydrodynamic conditions. 290(1-2), 86-94.

Tu, K.L., Chivas, A.R. and Nghiem, L.D.J.D. (2011) Effects of membrane fouling and scaling on boron rejection by nanofiltration and reverse osmosis membranes. 279(1-3), 269-277.

van der Bruggen, B., Vandecasteele, C., Van Gestel, T., Doyen, W. and Leysen, R.J.E.p. (2003) A review of pressure-driven membrane processes in wastewater treatment and drinking water production. 22(1), 46-56.

van der Bruggen, B. and Vandecasteele, C.J.E.p. (2003) Removal of pollutants from surface water and groundwater by nanofiltration: overview of possible applications in the drinking water industry. 122(3), 435-445.

Verwey, E.J.W., Overbeek, J.T.G. and Van Nes, K. (1948) Theory of the stability of lyophobic colloids: the interaction of sol particles having an electric double layer, Elsevier Publishing Company.

Vrijenhoek, E.M., Hong, S. and Elimelech, M.J.J.o.m.s. (2001) Influence of membrane surface properties on initial rate of colloidal fouling of reverse osmosis and nanofiltration membranes. 188(1), 115-128.

Wang, Z., Ma, J., Tang, C.Y., Kimura, K., Wang, Q. and Han, X.J.J.o.M.S. (2014) Membrane cleaning in membrane bioreactors: a review. 468, 276-307.

Weber, R., Chmiel, H. and Mavrov, V.J.D. (2003) Characteristics and application of new ceramic nanofiltration membranes. 157(1-3), 113-125.

Wei, C.-H., Huang, X., Aim, R.B., Yamamoto, K. and Amy, G.J.W.r. (2011) Critical flux and chemical cleaning-in-place during the long-term operation of a pilot-scale submerged membrane bioreactor for municipal wastewater treatment. 45(2), 863-871.

Xu, L., Wang, J.J.E.s. and technology (2012) Magnetic nanoscaled Fe3O4/CeO2 composite as an efficient Fenton-like heterogeneous catalyst for degradation of 4-chlorophenol. 46(18), 10145-10153.

Yang, X.-j., Xu, X.-m., Xu, J. and Han, Y.-f.J.J.o.t.A.C.S. (2013) Iron oxychloride (FeOCl): an efficient Fenton-like catalyst for producing hydroxyl radicals in degradation of organic contaminants. 135(43), 16058-16061.

You, X., Teng, J., Chen, Y., Long, Y., Yu, G., Shen, L. and Lin, H.J.C. (2020) New insights into membrane fouling by alginate: Impacts of ionic strength in presence of calcium ions. 246, 125801.

Zhang, J., Liu, G., Wang, P. and Liu, S.J.N.J.o.C. (2017) Facile synthesis of FeOCl/iron hydroxide hybrid nanosheets: enhanced catalytic activity as a Fenton-like catalyst. 41(18), 10339-10346.

Zhang, X., Fan, L. and Roddick, F.A.J.J.o.m.s. (2013) Understanding the fouling of a ceramic microfiltration membrane caused by algal organic matter released from Microcystis aeruginosa. 447, 362-368.

Zhao, C., Zhang, H., Si, W. and Wu, H.J.N.c. (2016) Mass production of two-dimensional oxides by rapid heating of hydrous chlorides. 7(1), 1-8.

Zhao, D. and Yu, S.J.D.W.T. (2015) A review of recent advance in fouling mitigation of NF/RO membranes in water treatment: pretreatment, membrane modification, and chemical cleaning. 55(4), 870-891.

Zhao, Y., WU, K.-f., Wang, Z.-j., Zhao, L. and Li, S.-s.J.E.S. (2000) Fouling and cleaning of membrane–a literature review. 12(2), 241-251.

Zhou, Z., He, X., Zhou, M. and Meng, F.J.W.r. (2017) Chemically induced alterations in the characteristics of fouling-causing bio-macromolecules–Implications for the chemical cleaning of fouled membranes. 108, 115-123.

Zhu, X., Elimelech, M.J.E.s. and technology (1997) Colloidal fouling of reverse osmosis membranes: measurements and fouling mechanisms. 31(12), 3654-3662.

Appendix A: Model Foulant—Sodium Alginate

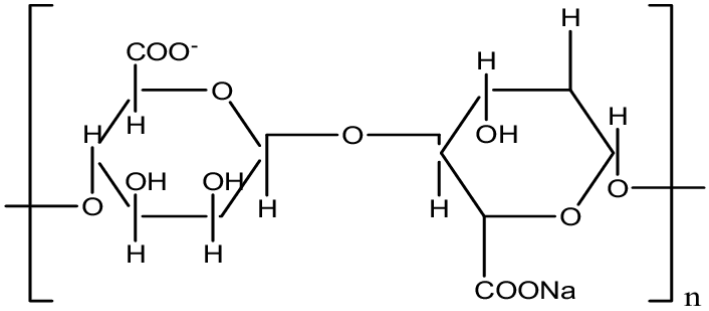

Figure A.1: Chemical structure of sodium alginate molecule (Homayouni et al. 2007)

Table A.1: Chemical composition of fouling solution.

Chemicals	Concentration	Dosage (g)
Sodium alginate	0.8 g/L	24
$CaCl_2 \cdot 2H_2O$	3 mM	13.23
NaCl	5 mM	8.77
$NaHCO_3$	1 mM	2.52

Appendix B: Detailed Experimental Conditions

Table B.1: Detailed conditions and Fenton activity test conditions for *Stage I*. In Fenton activity test, samples were taken at 0, 1, 10, and 60 min after the addition of H_2O_2. The corresponding one-hour decolouration rates were listed as well.

	FeOCl Synthesis				Fenton Activity Test		
NO.	Heating Rate (°C·min^{-1})	Temperature (°C)	Heating Duration (h)	Crucible	Chemical Dosage	Remark	60-min Decolouration Rate (%)
1)	10	220	1	Uncapped	FeOCl: 1 g·L^{-1} Methylene blue: 5 mg·L^{-1} H_2O_2: 30 mM pH: 3.3	/	81.03
2)	10	220	2			/	66.88
3)	20	220	1			/	53.60
4)	20	220	1	Capped		/	98.33
5)	20	220	1			Added 50 mM NaCl	92.20
6)	20	220	1			Added 300 mM NaCl	93.13
7)	20	220	1			No H_2O_2 addition (blank)	17.78

Table B.2: Detailed Pre-coating conditions for *Stage II*. The feeding flow and crossflow velocity were identical to that shown in *Table B.3*.

Membrane Permeability (L·(m^2·h·bar)$^{-1}$)	Feeding Flow (kg·h^{-1})	TMP (bar)	FeOCl Dosage (mg·(cm^2·h)$^{-1}$)	Concentration of Suspension (mg Fe/L)	Permeate Volume (mL)
Pristine Membrane Permeability vs Loading					
11.94	30	20	38	643	190
27.40	30	9.0	38	643	190
Dosing Rate vs Loading					
11.56-13.43	30	16.5-20	20, 38, 60	643	60

Table B.3: Detailed hydrodynamic conditions for pre-coating, fouling, and cleaning experiments. In the membrane cleaning section, the FeOCl dosage in the pre-coating was 38 mg·cm^{-2}·h^{-1}.

NO.	Process	Feeding Flow (kg·h^{-1})	Crossflow Velocity (cm·s^{-1})	TMP (bar)	Re	Remark
1)	Water Flux Test	120	86.6	3	6116	
2)	PEG Filtration	120	86.6	3	6116	Recirculation
3)	Pre-Coating	30	21.7	20	1529	FeOCl dosage: 38 mg·(cm^2·h)$^{-1}$
4)	Ca-Alginate	120	86.6	3	6116	Recirculation
5)	Membrane Cleaning	50	46.5	/	2548	Recirculation

The Reynolds number is an indicator of the flow regime which can be calculated according to *Eq. (C.1)*:

$$Re = \frac{v_c \cdot d_h}{\nu} \tag{C.1}$$

where Re denotes the Reynolds number (-), v_c denotes crossflow velocity (m·s^{-1}), d_h denotes the hydraulic diameter of the cross-section of the flow, and for tubular membrane, the hydraulic diameter is equal to the inner diameter of the membrane (m), ν denotes the kinematic viscosity of the flow, and it is $1.004 \times 10^{-6}\ \mathrm{m^2 \cdot s^{-1}}$ for water at 20 °C.

Table B.4: Detailed experiment conditions for NaCl pre-treatment. "S" and "F" denote soaking and flush, respectively. NaCl pre-treatment was conducted at ambient pH.

	NO.	Na^+ Concentration (mM)	Cleaning Condition for 1 Cycle	Cleaning Cycle
Effect of cleaning duration	1)	50	S (15 min) + F (5 min)	1 and 3 (20 and 60 min in total)
	2)		S (20min)	
	3)		F (20 min)	
Effect of Na^+ concentration	4)	50, 300	S (15 min) + F (5 min)	1 (20 min in total)
	5)		S (20min)	
	6)		F (20 min)	

Table B.5: Detailed experimental conditions and flux recoveries for membrane cleaning. For Exp.2), the cleaning solution was recirculated at a crossflow velocity less than 0.1 $cm \cdot s^{-1,}$ and the membrane was flush by demineralised water at a crossflow velocity of 46.5 $cm \cdot s^{-1}$ for 5 min prior to recovered flux test. The listed flux recovery was calculated by temperature-corrected flux.

Membrane Defect (%)	Membrane Modification	NO.	Chemical Composition of Cleaning Solution	Hydrodynamic Condition	Cleaning Duration (min)	pH	Flux Recovery (%)
4.69	FeOCl Pre-Coated Ceramic NF Membrane	1)	100 mM H_2O_2	Flush	60	3.3	112
		2)	100 mM H_2O_2	Soaking	60	3.3	99
		3)	100 mM H_2O_2	Flush	20	3.3	67
		4)	100 mM H_2O_2/33 mM tert-butanol	Flush	20	3.3	60
		5)	30 mM H_2O_2	Flush	60	3.3	96
		6)	30 mM H_2O_2/10 mM tert-butanol	Flush	60	3.3	87
		7)	50 mM NaCl/100 mM H_2O_2	Flush	60	3.3	105
		8)	50 mM NaCl	Flush	60	3.3	42
		9)	50 mM NaCl/100 mM H_2O_2	Flush	20	3.3	64
		10)	50 mM NaCl	Flush	20	3.3	51
		11)	Demineralised water	Flush	20	3.3	40

Appendix C: Pictures of FeOCl Synthesised at Different Conditions

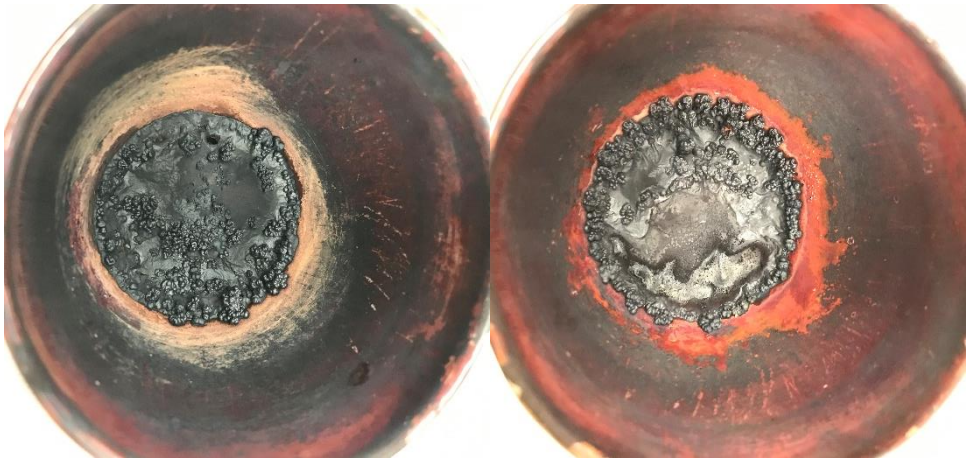

(a) 10 °C·min^{-1}, 220 °C, 1 hour, uncapped (b) 20 °C·min^{-1}, 220 °C, 1 hour, uncapped

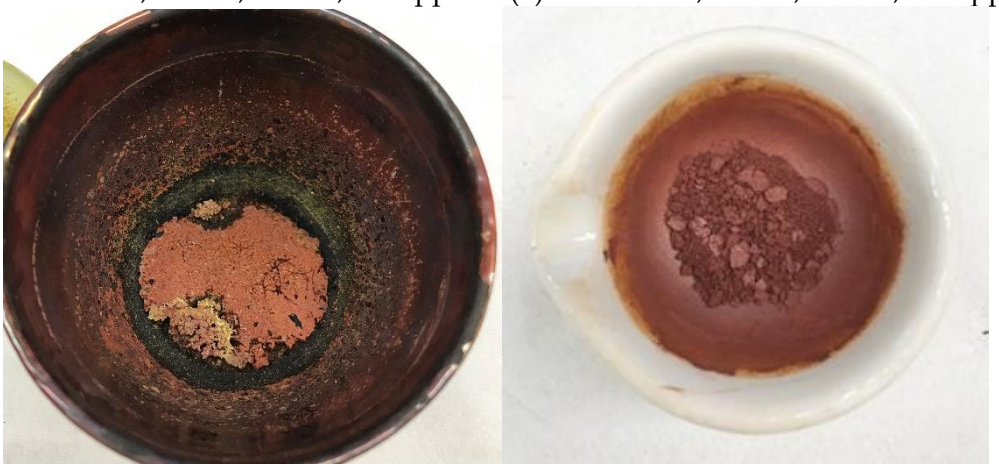

(c) 20 °C·min^{-1}, 220 °C, 1 hour, capped (d) 20 °C·min^{-1}, 220 °C, 1 hour, capped, grinded product

(e)

Figure C.1: Pictures of FeOCl synthesised at different conditions: (a), (b) and (c) synthesised product in the crucible, (d) highly active grinded FeOCl, and (e) crucible capped by alumina boat.

Appendix D: Additional Results of FeOCl Pre-Coating

Table D.1: Results of membrane permeability for *Section 4.2.1.*

Ceramic NF Membrane	Pristine Membrane Permeability ($L\cdot(m^2\cdot h\cdot bar)^{-1}$)	Pre-coated Membrane Permeability ($L\cdot(m^2\cdot h\cdot bar)^{-1}$)	Permeability Decline (%)
F5	12.15	11.84	2.6
F7	11.74	11.41	2.8
Average	11.94	11.62	2.7
F10	26.98	26.08	3.3
F11	27.83	26.49	4.8
Average	27.40	26.28	4.1

Table D.2: Results of membrane permeability for *Section 4.2.2.*

FeOCl Dosage ($mg\cdot(cm^2\cdot h)^{-1}$)	FeOCl Concentration (mg $Fe\cdot L^{-1}$)	Pristine Membrane Permeability ($L\cdot(m^2\cdot h\cdot bar)^{-1}$)	Pre-coated Membrane Permeability ($L\cdot(m^2\cdot h\cdot bar)^{-1}$)	Permeability Decline (%)
20	3.2	11.56	11.18	3.29
20	3.2	12.56	12.40	1.27
Average		12.06	11.79	2.24
38	7.6	12.13	11.84	2.39
38	7.6	13.06	12.76	2.30
Average		12.59	12.30	2.35
60	13.4	12.37	12.04	2.67
60	13.4	13.43	12.87	4.17
Average		12.90	12.45	3.49

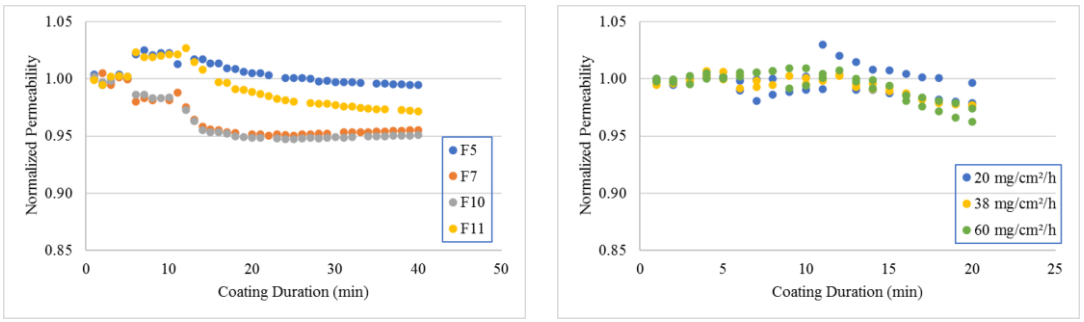

(a) (b)

Figure D.1: Flux behaviour of FeOCl pre-coating: (a) effect of membrane permeability on iron loading and (b) effect of the dosage of FeOCl on iron loading. For (a), the permeability of membrane F5, F7, F10 and F11 were 12.15, 11.74, 26.98 and 27.83 $L\cdot(m^2\cdot h\cdot bar)^{-1}$, respectively. For (b), the permeability ranged from 11.56 to 13.43 $L\cdot(m^2\cdot h\cdot bar)^{-1}$.

A linear relationship was observed between the concentration of FeOCl and the dosing rate of FeOCl suspension (y=0.2262x-0.5972, R^2=0.9885).

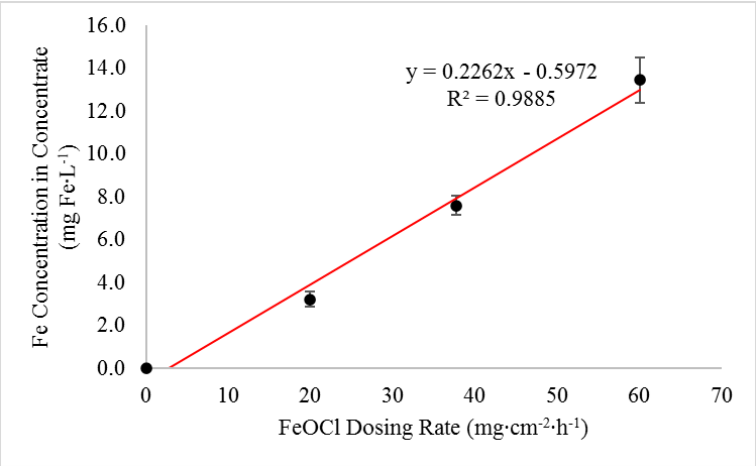

Figure D.2: Correlation between the dosage of FeOCl and the iron loading on the membrane.

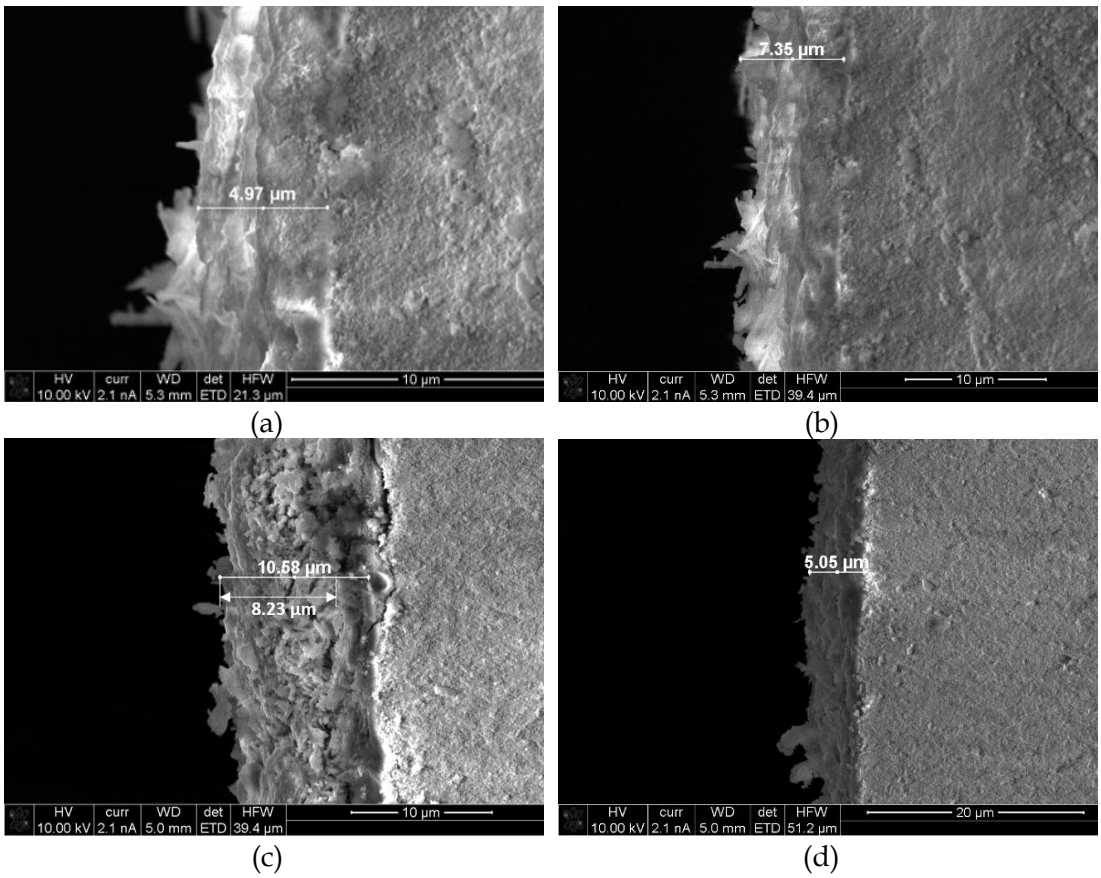

Figure D.3: Thickness of the pre-coated layer and fouling layer: SEM images of the cross-sections of (a&b): different locations of a FeOCl pre-coated ceramic NF membranes, and (c&d): different locations of a Ca-alginate fouled FeOCl pre-coated ceramic NF membrane.

Appendix E: Results of Membrane Defect Detection

In membrane defect detection, membrane compaction was performed prior to 1000 Da PEG filtration. Due to the time limitation, PEG filtration was conducted when the demineralised water flux was stabilised for 10 min. PEG filtration was conducted for 20-30 min until a steady flux was obtained. The flux behaviour was displayed in *Figure E.1(a)*. The concentrations of PEG in the feed and permeate were simply determined by TOC analysis. According to the flux behaviour and the detected defect, the qualities of these new ceramic NF membranes were disappointing. The water flux of membrane B decreased continuously in the 60 min compaction. 20% of initial flux drop was observed in the PEG filtration of membrane E. Hence, membrane A, with the least defect, was used in the most membrane cleaning experiments in this research.

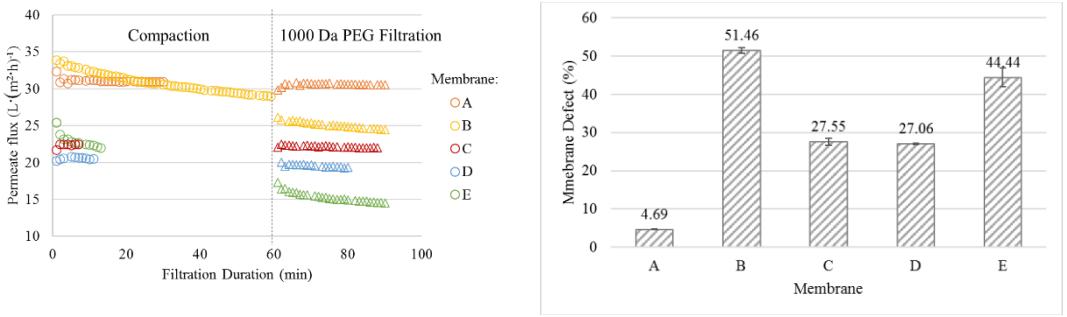

(a) (b)

Figure E.1: Membrane defect detection of five pristine membranes: (a) flux behaviour during filtration, and (b) membrane defect.

Appendix F: Iron Leaching in NaCl Pre-Treatment

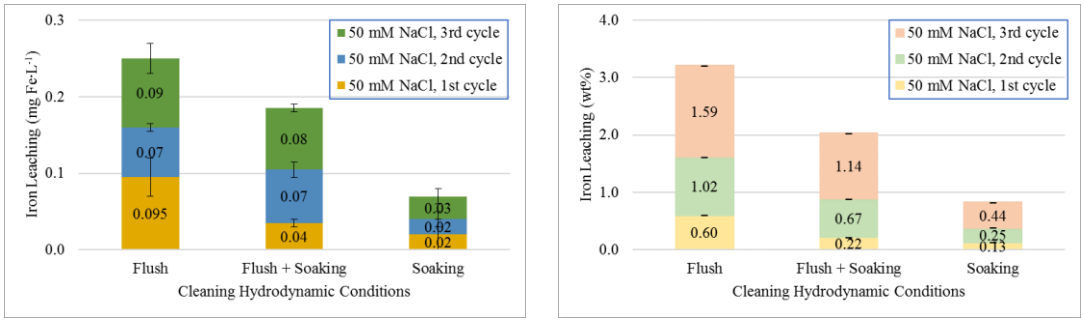

(a) (b)

Figure F.1: Effect of cleaning hydrodynamic conditions and cleaning duration on the iron leaching in NaCl pre-treatment for Ca-alginate fouled ceramic NF membrane: (a) the mass of iron leaching and (b) iron leaching percentage by weight.

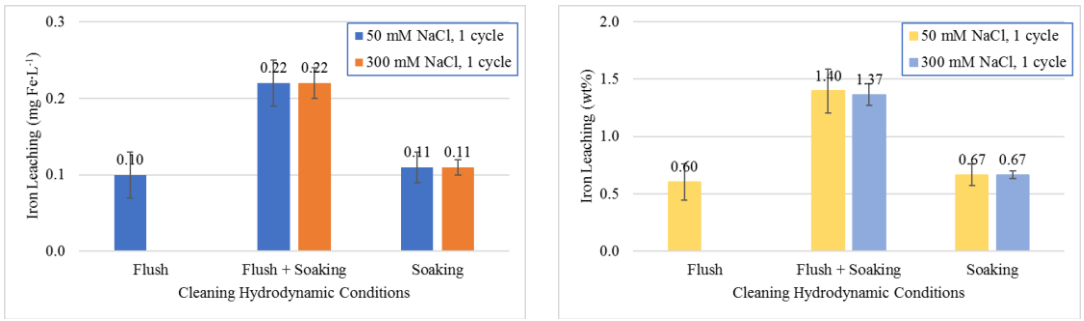

(a) (b)

Figure F.2: Effect of cleaning hydrodynamic conditions and Na^+ concentration on the iron leaching in NaCl pre-treatment for Ca-alginate fouled ceramic NF membrane: (a) the mass of iron leaching and (b) iron leaching percentage by weight.

Appendix G: Ca-Alginate Fouling on Pristine Ceramic NF Membrane

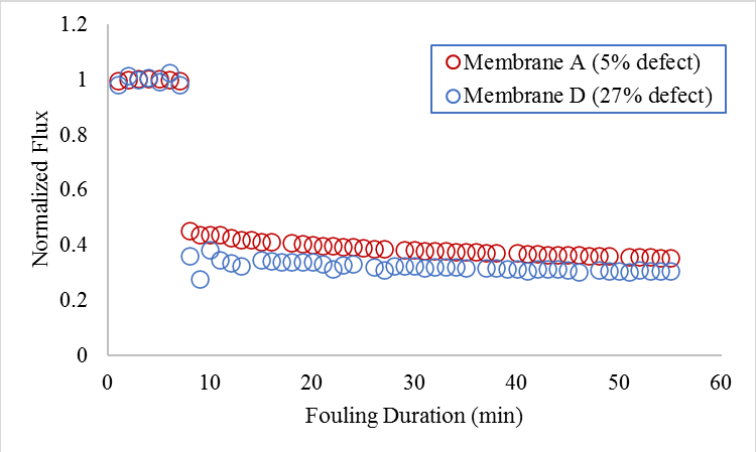

Figure G.1: Flux behaviour of Ca-alginate fouling on pristine ceramic NF membrane (the fouling of membrane A was conducted by Bin Lin, TU Delft).


TUDelft